RIGA TECHNICAL UNIVERSITY

Endija Namsone-Sīle

EFFECTIVENESS AND PRODUCTIVITY IMPROVEMENT OF CONVENTIONAL PULTRUSION PROCESSES

Doctoral Thesis

RTU Press
Riga 2025

RIGA TECHNICAL UNIVERSITY
Faculty of Civil and Mechanical Engineering
Institute of High-performance Materials and Structures

Endija Namsone-Sīle
Doctoral Student of the Study Programme "Civil Engineering"

EFFECTIVENESS AND PRODUCTIVITY IMPROVEMENT OF CONVENTIONAL PULTRUSION PROCESSES

Doctoral Thesis

Scientific Supervisor
Professor *Dr. sc. ing.*
JEVGENIJS BARKANOVS

Riga 2025

ABSTRACT

The doctoral Thesis is about the effectiveness and productivity improvement of the conventional pultrusion processes. For a better comprehension of the pultrusion process, at the beginning of the study a short review about the conventional pultrusion process, examples of numerical simulations and different approaches of optimisation is done. An effectiveness and productivity of conventional pultrusion processes, preserving the quality of pultruded profiles and reducing their cost, could be improved by the process optimization of the parameters of pultrusion process or by an application of innovative heating sources instead of electrical resistances with high heat losses.

For this reason, a new effective non-linear optimisation methodology, based on experimental design and response surface technique, has been developed. An application of this methodology with two objective functions has been successfully demonstrated for the pultrusion process producing a rod profile made of glass fibre and polyester resin. The first one describes an effectiveness of pultrusion process and minimizes an electrical energy necessary for a production of pultruded profile, while the second objective function is connected with a productivity of pultrusion process and maximises the pull speed. The generalized reduced gradient algorithm has been applied for the solution of formulated optimisation problems. New technological map of pultrusion process has been developed for a designer convenience on *Microsoft Excel* tool, allowing to define the process conditions for the fixed process parameters and to minimize the energy consumption or to maximise the pull speed.

New electro-magnetic-thermo-chemical finite element models and algorithms have been developed for a real advanced microwave assisted pultrusion process manufacturing a rod profile. To verify the results of electro-magnetic analysis obtained in finite element software *ANSYS Mechanical*, the finite element model for the same microwave assisted pultrusion process has been developed and analysed in *COMSOL Multiphysics* and no difference has been observed between both results. This talks about high reliability of the developed electro-magnetic finite element model and algorithm.

At the end of the Thesis, an evaluation of the developed microwave assisted pultrusion process in comparison with the real conventional pultrusion process has been done. The obtained results have demonstrated improvement of productivity more than 5.5 times, but effectiveness – almost until 3 times. It is necessary to note that high effectiveness and productivity of microwave assisted pultrusion processes have been obtained without their optimisation. An application of optimisation could improve these values additionally.

ANOTĀCIJA

Promocijas darbs ir par tradicionālu pultrūzijas procesu efektivitātes un produktivitātes uzlabošanu. Lai labāk tiktu izprasts pultrūzijas process, darba sākumā ir sniegts īss pārskats par tradicionālu pultrūzijas procesu, skaitlisko simulāciju piemēriem un dažādām optimizācijas pieejām. Tradicionālu pultrūzijas procesu efektivitāti un produktivitāti var uzlabot, optimizējot pultrūzijas procesa parametrus vai izmantojot inovatīvus siltuma avotus.

Darbā ir izstrādāta jauna, efektīva nelineārā optimizācijas metodoloģija, kas ir balstīta uz eksperimentu plānošanu un atbildes virsmu metodi. Metodoloģija ar divām mērķfunkcijām ir veiksmīgi pielietota pultrūzijas procesam, lai izstrādātu stieņa profilu, kas ir veidots no stikla šķiedras un poliestera sveķiem. Pirmā mērķfunkcija apraksta pultrūzijas procesa efektivitāti, vienlaicīgi samazinot pultrūdēta profila ražošanai nepieciešamo elektrisko enerģiju, turpretī, otrā funkcija raksturo pultrūzijas procesa produktivitāti un maksimāli palielina pultrūzijas procesa vilkšanas ātrumu. Optimizācijas problēmu atrisināšanai tiek izmantots vispārinātais samazināta gradienta algoritms. *Microsoft Excel* rīkā ir izstrādāta jauna, inovatīva tehnoloģiskā karte, kas ļauj definēt pultrūzijas procesa nosacījumus konstantajiem parametriem, un minimizēt enerģijas patēriņu vai palielināt vilkšanas ātrumu.

Ir izstrādāti jauni elektromagnētisko-termoķīmisko galīgo elementu modeļi un to algoritmi reālam progresīvam, mikroviļņiem veicinātu pultrūzijas procesam, kas ražo stieņa profilu. Lai pārbaudītu galīgo elementu programmatūrā *ANSYS Mechanical* iegūtos elektromagnētiskās analīzes rezultātus, programmatūrā *COMSOL Multiphysics* ir izstrādāts un analizēts galīgo elementu modelis tam pašam, ar mikroviļņiem veicinātam pultrūzijas procesam, un nav novērota nekāda atšķirība. Tas liecina par izstrādātā elektromagnētiskā galīgo elementu modeļa un algoritma augsto precizitāti.

Promocijas darba noslēgumā ir veikts izstrādātā, mikroviļņiem veicinātā pultrūzijas procesa novērtējums salīdzinājuma ar reālo, tradicionālo pultrūzijas procesu. Iegūtie rezultāti parāda, ka procesa produktivitāte ir uzlabota vairāk nekā 5,5 reizes, bet efektivitāte – gandrīz 3 reizes. Ir svarīgi atzīmēt, ka mikroviļņiem veicinātu pultrūzijas procesu augstā efektivitāte un produktivitāte ir iegūta bez procesa optimizācijas. Līdz ar to var secināt, ka optimizācijas pielietošana šīs vērtības varētu krietni uzlabot.

ACKNOWLEDGEMENTS

I would like to thank my supervisor Prof. Evgeny Barkanov for the response and support throughout the years I spent for a doctoral study and working at the Riga Technical university as Scientific assistant, and for the help on preparing my work.

I would also like to thank my colleague Dr. Pavel Akishin and also Prof. Andris Chate for their help, support, and advices.

Also, I would like to thank my family for the support of everything.

The results presented in Thesis are the part of the European Regional Development Fund (ERDF), project No. 1.1.1.1/18/A/053 “An effectiveness improvement of conventional pultrusion processes”.

TABLE OF CONTENT

INTRODUCTION

Pultrusion is a continuous process for a production of high strength fibre-reinforced polymer composite profiles with a constant cross-section. The term “pultrusion” is derived from words “pull” and “extrusion”. It is an automated and cost-effective process with minimal waste of material and requirement of labour.

Nowadays fiber reinforced composites are used widely in different lightweight structures requiring high stiffness-to-weight and strength-to-weight properties and working under high operational loads. The pultruded profiles are replacing a lot of conventional materials used in various range of industries – transportations, civil constructions, wind energy, marine and aerospace. At present pultrusion is one of the fastest increasing production processes inside the composites market. The pultrusion market is further expected to growth at a compound annual growth rate of 4.9 % from 2021 to 2028.

Although the pultrusion area demonstrates a healthy development now but a continuous increase in the cost of electricity could significantly reduce this movement or even stop it. An effectiveness and productivity of conventional pultrusion processes, preserving the quality of pultruded profiles and reducing their cost, could be improved by the process optimization of the parameters of pultrusion process or by an application of innovative heating sources instead of electrical resistances with high heat losses. For this reason, a new effective optimisation methodology, taking into account all the required parameters of the industrial pultrusion processes and ambient room temperature, and electro-magnetic-thermo-chemical finite element models and algorithms will be developed.

1. LITERATURE REVIEW

1.1. Conventional pultrusion processes

Pultrusion is a continuous process for a production of fibre-reinforced polymer composite profiles with a constant cross-section. It is an automated and cost-effective process with minimal waste of materials and requirement of labour [1]. The history of pultrusion process has begun already in the early 1950s by the first published patent in 1951, proposing a continuous production method for rod composite structures [2]. Brandt Goldsworthy was one of the first pioneers and inventors of pultrusion process with his first patented pultrusion machine in 1959 [3]. At that time machines had vertical design and mostly with intermittent pull type. Within the growing demand of pultrusion products, the industry developed significantly by improving production machines and expanding the range of resin and reinforcement used.

The conventional pultrusion process and the equipment employed are schematically represented in Figure 1.1. During this automated process, reinforced fibers are pulled through a heated die, forming them into a fibre-reinforced polymer composite product. The manufacture process can be divided into four main steps like it is presented in Figure 1.2. As the pultrusion process involves to pull the necessary raw materials through a heated die, the reinforced fibers need to be in continuous form. Therefore, mostly rolls or filament roving are used. The first step of the process is feeding these continuous roving filaments into the machinery through the preforming guides. Then the reinforced rovings go through a wet-out bath for resin impregnation. The most common is an open-resin filled bath, where rovings are guided over and under the rolls for impregnation process. After that, the reinforced fibers are pulled through a heated die, where the forming and curing of the resin are completed. Usually, along the pultrusion die are installed several heaters with different heating temperatures. When the temperature has reached the gel point, an exothermic reaction is occurred and the resin start curing (see Figure 1.3). At the end of the process a traveling automatic saw cuts the required length of composite profile.

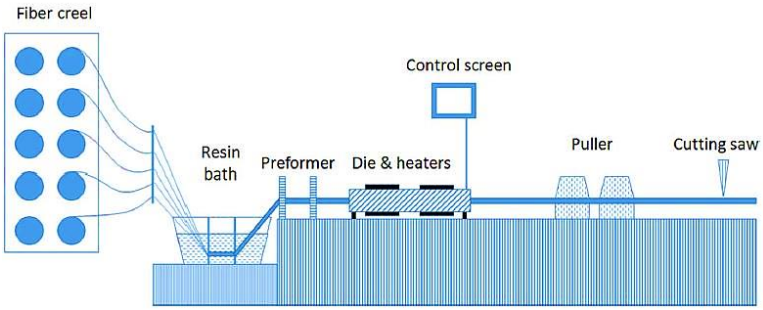

Figure 1.1. Conventional pultrusion process [1].

The pultruded composites are made of high-performance fibers and linked by a polymer matrix, which protects the composite material from the environmental influence. For the pultrusion process various forms of fibre-reinforcement are used like, unidirectional roving, continuous roving, woven fabric, and stitched fabric in order to increase the mechanical properties of composite material. The first one provides the tensile strength and Young`s modulus in the pull direction (the longitudinal direction), while others increase the strength and stiffness in the transverse direction. The most popular reinforcement for pultruded composite materials is glass fiber reinforcement due to its good mechanical properties and high affordability. During the pultrusion procedure smooth, textured or monofilament rovings are usually used.

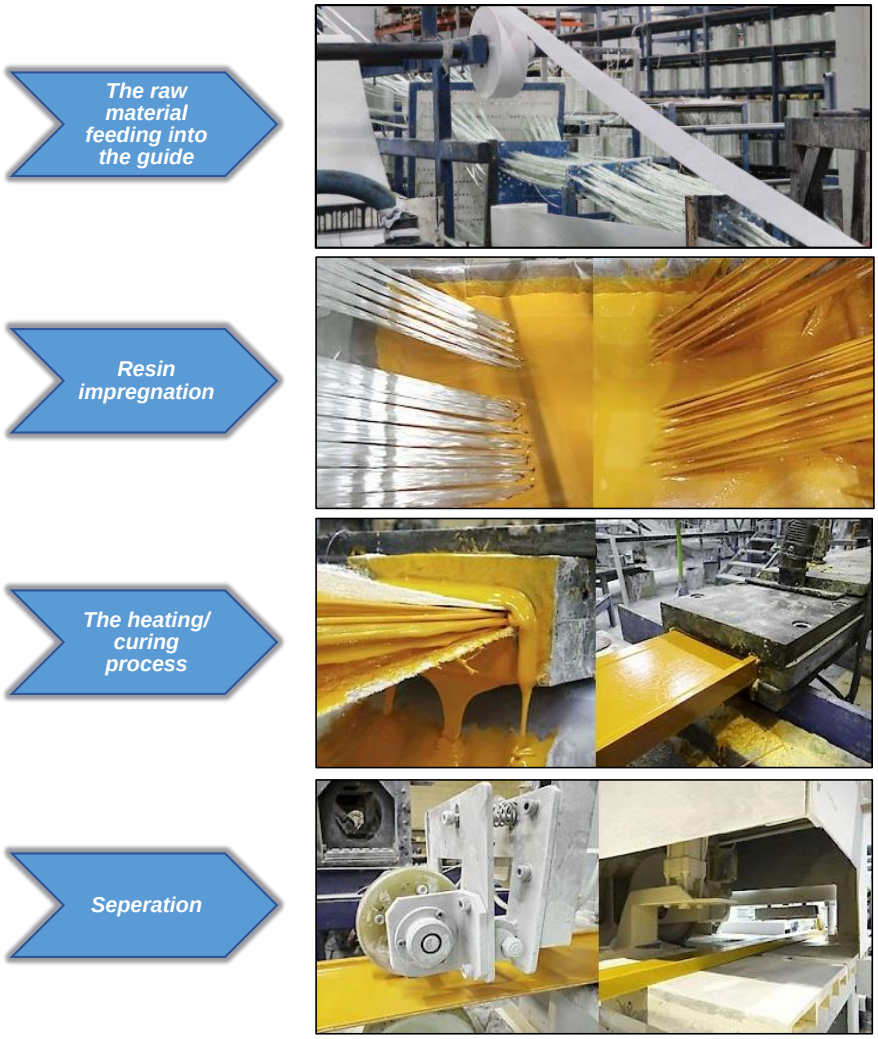

Figure 1.2. The main steps of the conventional pultrusion manufacture process [14].

The application of the monofilament rovings allows to increase the transverse strength despite the unidirectional arrangement. The typical structure of reinforcement of pultruded profile is demonstrated in Figure 1.4. During the pultrusion process a wide variety of thermoset or thermoplastic resins are used to provide the structural and thermal stability for the resulting composite material. The most commonly used thermoset resins in the pultrusion processes:

- **Epoxy resin** – due to their excellent thermo-chemical integrity, this type of resin is appropriate for reinforcing and bonding fibre-reinforcement polymer components. In addition, they have great electrical properties, corrosion resistance and they perform well in high temperatures. However, epoxy resins have high viscosity and poor UV resistance, and they also require a post-cure, which makes them hard to use.
- **Polyester resin** – due to their excellent resistance to corrosion, these resins are applied in the manufacture of products used in highly corrosive and aggressive environments, but on the other hand, polyester resins have average water-resistance and emit a lot of scent during the pultrusion process.
- **Vinyl ester resin** – this type of resin was developed in order to maximize the good properties of epoxy resins. It offers moisture resistance and corrosion resistance (especially of top-shelf), therefore is widely used in the production of marine and coastal products.
- **Polyurethane resin** – due to their excellent load-bearing properties and durability, polyurethane polymers have a wide range of applications and are used for a production of such materials that require a tougher surface.
- **Phenolic resin** – these resins are phenol-based and they cure through a condensation reaction. Phenolic resins have excellent fire resistance and thermal insulation properties, and are usually used as matrix binders or adhesives.

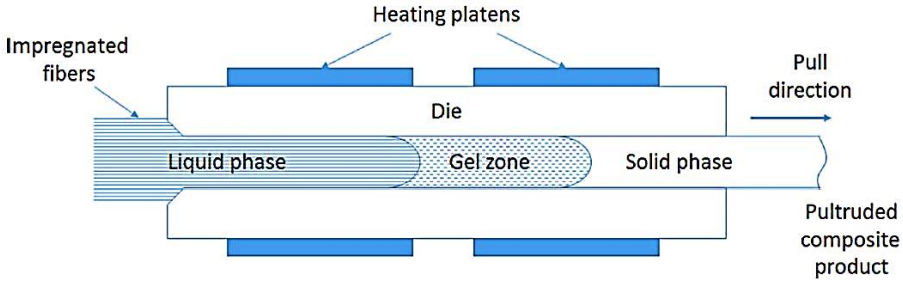

Figure 1.3. Heating section of the conventional pultrusion die [1].

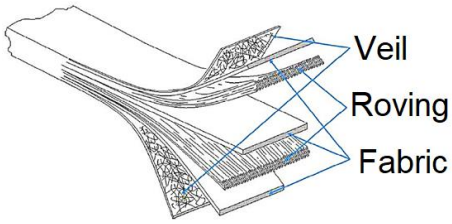

Figure 1.4. The typical structure of reinforcement for pultruded profile [1].

Figure 1.5. Different types of pultruded profiles [5].

Over the last 70 years, pultrusion has become one of the most efficient processes of manufacturing composite materials with a constant cross-section due to the ability to produce a wide range of standard pultruded cross-sectional profiles, like, rods, tubes, square-rods/bars, C-profiles, U-profiles, T-profiles, Z-profiles, corner profiles etc. (Figure 1.5) or customized special shaped profiles. The market report [6] shows that at the present time pultrusion is one of the fastest growing manufacturing processes within the composites market. Glass fiber-reinforced systems (GRP) are still the dominant material, accounting over 90 % of reinforced composites production, of which approximately 5% of total European GRP production are pultrusion processes. The pultrusion market is further expected to growth at a compound annual growth rate of 4.9 % from 2021 to 2028. The main reason for the growth of this market is the high demand for lightweight materials in different industrial sectors. Nowadays fiber reinforced composites are used widely in different lightweight structures [7]-[9] requiring high stiffness-to-weight and strength-to-weight properties and working under high operational loads [10], [11]. The application examples of pultruded profiles are given in Table 1.1 [1]. The pultruded profiles are replacing a lot of conventional materials used in various range of industries – transportations, civil constructions, wind energy, marine and aerospace. A great example is the increased use of pultruded profiles in bridge constructions, especially I-beams, due to their low maintenance requirements and the above-mentioned high strength-to-weight ratio. In a compare with metal, concrete and wood, fiberglass composite has a better strength to weight ratio. For a comparison, a profile of the same size made of glass fiber weights about 75 % less than a metal profile and 30 % less than an aluminum profile. Due to the material dielectric properties, glass fiber composite material is a nonradioactive material and can

Table 1.1.

Application examples for pultruded profiles

Application	Examples
Construction	Flooring and walling systems, fences, bridges
Application in adverse environment	Walkways, ladders, staging, fencing, stairs
Electrical applications	Cable tray support members, ladders, transmission, towers
Marine	Wastewater treatment plants
Transportation	Railways, vehicle body panels
Sport and leisure	Hockey sticks, ski poles, golf clubs, arrows, kites, sail mats

Table 1.2.

The minimal required mechanical properties for pultruded profiles according to EN 13706

Property	Unit	E17	E23
Modulus of elasticity	GPa	17	23
Tensile modulus - longitudinal	GPa	17	23
Tensile modulus - transverse	GPa	5	7
Tensile strength - longitudinal	MPa	170	240
Tensile strength - transverse	MPa	30	50

be used in specific application structures, like antenna towers or platforms and radio receivers in radio industry. Fiberglass composite products are long-lasting with no additional maintenance costs and are suitable for both, households, and urban infrastructure. COMPOR [12] is one of the largest pultrusion factories in the Baltic states, and its produced fiberglass composites are easy to install, sawed and joined during the assembly process. These profiles can be used as:

- bridge constructions – truss and cable bridges, pedestrian, and bicycle bridges;
- modular buildings – terraces and house support, hangar elements, floating houses;
- urban infrastructure – railway platforms, noise barriers, hydraulic structures, roof railings, balconies, street, and tunnel fencing.

As pultruded products have a lot of benefits that are highly competitive with the properties provided by other materials, they are now considered to be one of the highest performing composites. The application, in the construction industry of reinforcement concrete elements of pultruded rods, has significantly increased due to their high corrosion resistance. Fiberglass pultruded materials can resist both – acidic and alkaline corrosives, therefore these products are appropriate for outdoor and harsh environmental condition, and are also ideal in different construction vertical use, like handrails, guardrails, trays for cables, decks etc. In addition, pultruded composite materials are with high dimensional stability and do not change overtime, the coefficient of thermal expansion is slightly less than steel or aluminum. Therefore, it reduces the thermal transmittance of material.

The European standard “CEN-EN 13706: Reinforced Composite – Specification for Pultruded profiles” [13] regulates and sets the minimal requirements of characteristics of pultruded products, like mechanical properties, raw material content. The EN 13706 standard consists of three parts – Designation, Methods of test and general requirements and Specific requirements. The minimal required mechanical properties of pultruded composite profiles according to this standard are given in Table 1.2., where two strength

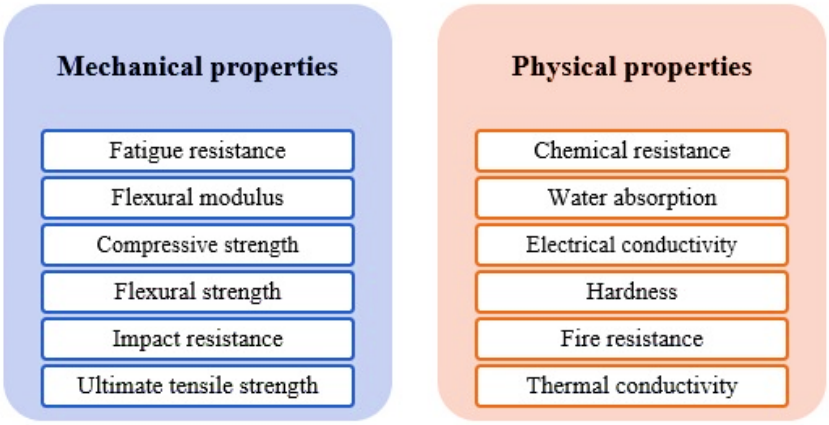

Figure 1.6. The physical and mechanical properties of pultruded profiles [14].

classes are divided: E17 - a minimal elastic modulus is 17 GPa and E23 – the modulus of elasticity is equal or greater than 23 GPa. The physical and mechanical properties of pultruded profiles are summarized in Figure 1.6.

Despite all the advantages mentioned above, the conventional pultrusion process could be seriously affected by an increase growth of electricity prices and the total costs for the heated dies could be very high. In addition, the traditional electric heaters have high heat losses and therefore, an application of innovative heating sources could significantly improve an effectiveness and productivity of the conventional pultrusion processes.

1.2. Numerical simulation of conventional pultrusion processes

To provide a better comprehension of the pultrusion processes, to support the pultrusion process control and tooling design, a lot of numerical simulations have been done in the last thirty years [15]-[17]. Many of them are related to the cure and heat transfer [18]-[22], the development of process capabilities and the pressure rise in the tapered zone of the die [23],[24] and on problems influencing the impregnation of reinforcing fibres for obtained final product with the desired mechanical properties [25]-[27].

In most of them, thermo-chemical modelling in transient and steady state analyses is executed by using the finite difference methodology [28],[29] and finite element methodology [30],[31] with the nodal control volume method. Although, the solutions of steady state pultrusion simulations with constant processing conditions are more effective, the transient analysis should be used when the composite material properties are examined in dependence on time (or temperature) and thermocouples are controlling the temperature of heaters. The curing kinetic models [32] for resins used

in pultrusion processes and describing an exothermic chemical reaction are an obligate component in numerical simulations. It is necessary to note that these models are required not only for the development of conventional pultrusion processes with electrical heaters [33] but also for the development of advanced pultrusion processes [34].

Numerical simulations for pultrusion processes are performed by using general-purpose FE software and FE codes. Mostly, these developed numerical models are closely related to the final product and used technology. For this reason, in [35] study the finite element methodologies have been applied for the simulation of pultrusion process of the C cross-section profile made of epoxy resin and fibreglass. The paper [36] represents a simulation of pultrusion process for a flat plate utilizing transient and steady-state analyses with applied three-dimensional thermochemical strategy. During this study, it was concluded that the steady state analysis is a faster approach comparing with the transient analysis in term of number of iteration loops for the convergence and the total computational time to reach the steady state. In addition, this analysis is more suitable for an optimisation process, where many design evaluations are required. The pultrusion process simulation in paper [37] has been performed for a unidirectional graphite/epoxy composite material with a circular cross-section, including processing physics, like heat transfer, chemical reactions, fluid flow and solid mechanics. Various models of different homogenization levels and different solutions schemes are proposed in [37]. In this case, using continuous and porous models, a finite element methodology (*ABAQUS*) with nodal control volume method and finite volume numerical scheme (*ANSYS CFX*) has been applied.

The analyses of pultrusion processes with a temperature control [38]-[41] is less studied. In [38] the model of unsteady-state distributions of temperature and degree of cure for a production of fibreglass-epoxy composite materials have been investigated. For the development of a numerical model, a finite difference control volume technique has been utilized. The heating zones of the die are controlled in order to maintain the prescribed temperatures – at the end of each solution time step heaters are turned on/turned off, to compensate for the pre-set temperature changes greater than 1 °C, in the places of located thermocouples. A computer simulation code has been developed in order to predict the dynamics of heat transfer in [39] for a pultrusion process of the flat plate profile. The die block and heater arrangement are also included into the heat transfer analyse, therefore, the temperature profile at the interface between the pultrusion die and the composite is provided. In the simulation code the heater power control along the heating die has been performed with three thermocouples. As the pre-set temperature has been reached, the electrical heaters are switched off and the heating process is finished. The temperature dropping is till the previously defined value when the electrical heaters are turned on again.

More complicated control of the pultrusion process has been proposed in [40] of a fibreglass-vinyl ester composite I-beam profile, using a general-purpose FE based numerical procedure. The heating system consists of four electrical heat platens on the

top and bottom of the pultrusion die surfaces, and two electrical strip heaters on the die sides. The finite element numerical procedure automatically switches the applied heating powers on or off in accordance of the temperature values at the control nodes. The predicted temperature values have been verified with the experimental results published in the literature. At the die exit a sufficient value of degree of cure has been obtained in case of controlled temperature value at 133 °C. It must be noted that without the side heaters, the curing reaction has not been activated within the pultrusion die and the obtained temperature at the die exit was under the controlled temperature value of heat platens – 123 °C.

During these numerical simulations, it has been concluded that two of pultrusion process parameters affect the degree of cure and temperature the most, like, heating temperature and pull speed. It is necessary to note that the material properties should be defined with high accuracy, as these parameters are sensitive to the activation energy and density of resin.

1.3. Optimisation of pultrusion processes

Different optimisation procedures are used to obtain a better quality of pultruded profiles and higher manufacturing rates, while ensuring reduced production costs. First optimisation problems have studied an influence of single design parameter on the quality of pultruded profiles. So, optimal die-heater temperatures have been investigated in [42] to obtain a uniformly cured C-section profile at the die exit and using a die with fixed multiple heating zones. Optimal solution has been obtained with adopted optimisation approach based on the steepest descend method. As constraints, the limiting value of the highest temperature within the composite has been considered. The same pultrusion problem has been optimised in [43] applying a hybrid approach based on genetic algorithms and simplex method. The heating platens temperatures have been used as optimisation variables, but all other parameters, such as pull speed or cooling channel temperature have been assumed as constant values.

Later an effect of two parameters: die temperature and pull speed on uniformity of the curing of thermosetting C-section profile has been investigated in [44], and in [45] taking into account pre-heating and die-cooler temperatures. In time of optimisation the finite element analysis is carried out by changing only one process parameter keeping other parameters unchanged and final solution is obtained superimposing the mathematical relationships for individual parameters. It is necessary to note that no interconnection between die temperature and pull speed has been established for the objective function in these investigations. Simulated Annealing method with constraints on minimum degree of cure at the end of process and resin degradation temperature has been successfully applied to minimise an economic objective function (the profit per unit of time) for the rod pultrusion in dependence on two parameters: pulling speed and temperature profile on the die wall in [46]. This optimisation method

has allowed to avoid local minimum caused by inadequate initial guesses but, unfortunately, it is not fast.

A heating arrangement with internal heaters inside the die body has been optimised in [47]-[49], where Computational Fluid Dynamics (CFD) algorithm has been applied for the pultrusion modelling of I-beam profile [47] and for C-section profile [49]. To minimise the objective function, stochastic (particle swarm optimisation) algorithm has been used in [47],[48] and compared with quadratic programming algorithm in [49]. To provide a fast simulation-optimisation, CFD algorithm has been changed with the mathematical model describing the pultrusion of cylindrical rod and solved by integration code DASSL in [48]. Optimised heating rates have been obtained correspondingly for 5 sets with 2 internal heaters in [47], for 4 heating zones of the composite surface in [48] and for 8 sets with 2 internal heaters in [49]. Everywhere the thermal efficiency of the process has been reached by improving the thermal distribution of the die body. Moreover, an efficiency of the process could be increased by an insulating the die surface in this heating arrangement. However, it is necessary to note that optimal distribution of die temperatures have been obtained with the constant pull speed.

Artificial neural networks and genetic algorithms have been applied also for the optimisation of pultrusion processes [50],[51]. So, in paper [50] the real process data from the pultrusion of rectangular profile have been used for a training of neural network. The disadvantage of this optimisation methodology relates to the considerable amount of the required training data, long training time, quality of the measured data, presence of insignificant parameters that skewed the network, as well as a little real process knowledge. Some progress in optimisation of the pultrusion process has been achieved in [51], where the relationship between processing parameters (die temperatures and pull speed) and degree of cure has been formed by artificial neural network using the simulation results instead of results of experiments.

For the first time the planning of experiments and surrogate-based methodology have been applied for optimisation of the pultrusion process with thick flat beam profile in papers [52],[53]. The optimisation problem has been solved for a single objective presenting maximisation of the average cure degree at the exit of the heating die under geometrical and process related constraints in [52] by using constrained efficient global optimisation (EGO) algorithm. Simultaneous maximisation of the pulling speed and minimisation of the total energy consumption defining as a measure of total heating area and associated temperatures have been executed in [53] applying evolutionary multi-objective optimisation (EMO) algorithm. Domination concept known as the Pareto optimality provides a way to compare solutions considering each objective separately. Unfortunately, optimisation has been executed using a steady-state thermo-chemical simulations that not allows to estimate an effectiveness of real (industrial) pultrusion processes with the temperature control executed by the heaters switch-on and -off strategy.

To investigate an effect of heating power control for 4 heaters, optimisation with heater switch-on and -off concept for the pultrusion with a constant pull speed has been performed in [54]. By this way a more accurate and realistic process simulation has been achieved. An application of embedded cylindrical heaters and corresponding duty cycles have been investigated in [55] based on an existing pultrusion die that only allowed to study a single relative position for the embedded heaters.

The restricted number of studies in the numerical optimisation of the conventional pultrusion processes could be interpreted by the complexity of the numerical problems to be solved and long time necessary for a solution of optimisation problems. Less attention in the scientific literature has been paid to the optimisation of the pultrusion processes in industrial environment. Furthermore, the effects of an industrial shop temperature and curing process allowed behind the die exit have not been examined yet. More accurate and realistic process optimisation, that has been reached in the previous studies, could be achieved by the temperature control executed by the heaters switch-on and -off strategy. For this reason, a new effective optimisation methodology should be developed, considering the parameters of industrial pultrusion processes and ambient room temperature.

1.4. Microwave assisted pultrusion processes

Nowadays, the technological process of pultrusion could be made more effective, applying new effective heating sources instead of electrical resistances with high heat losses. Among all possible heating methods, a high frequency electromagnetic energy source [56], characterised as a fast, non-contact, instantaneous, volumetric heating, suitable for materials processing [57] could be examined as the best choice for the pultrusion applications. At the time microwave heating is used successfully in various industrial curing processes [58]-[60].

Microwaves are electromagnetic waves, usually with the frequency from 300 MHz to 300 GHz and can heat up the material very fast because of contactless energy deposition inside the material, independently of the thermal conductivity of material. For an industrial application, microwaves with frequency of 915 MHz, 2.45 GHz or 5.8 GHz are used [61]. In a comparison with conventional pultrusion process, microwave assisted pultrusion could has lot of advantages [62]:

- lower energy consumption and higher efficiency;
- simultaneous heating of material through the whole volume;
- automatic control of the curing process;
- rapid heating;
- shorter processing time;
- profiles cure uniformly throughout the entire cross-section;
- improved quality and properties;
- environmentally friendly – clean and quiet process;

- the application of microwaves does not require changes in the design of working line.

Due to the complexity of coupled multi-physical problem to be solved, the pultrusion processes with microwave heating firstly have been analyzed experimentally [63]-[65]. In order to fit into microwave cavity, a transparent microwave ceramic die has been designed in [63], and the feasibility of the process has been proved by the results of heating and curing. Single frequency and variable frequency processing techniques with different microwave power have been studied in [64] for a production of graphite/epoxy composites. A short summary of the potential for a microwave assisted pultrusion in the production of fiber-reinforced composite profiles is presented in [65].

Additionally, experimental investigations have been done for different unidirectional composite profiles [66]-[68], where the experimental temperatures have been measured by inserted thermocouples into the die or composite. The degree of cure has been obtained from the differential scanning calorimetry analysis of samples cut from pultruded profiles. It is seen that an experimental measurement of temperature and degree of cure in pultruded profile is complicated and time-consuming procedure.

1.5. Numerical simulation of microwave assisted pultrusion processes

Only recently some attempts have been made to study numerically the microwave assisted pultrusion processes and first results have been published in short papers [69],[70].

The finite element model in [69] is made of two weakly coupled sub-models: electro-magnetic and thermo-chemical developed to simulate the pultrusion process producing fiberglass-epoxy cylindrical profiles with small diameter of 5 mm. The first one is for an evaluation of the electric field distribution and determination of heat generation rate for a microwave source, while the second sub-model serves an evaluation of the temperature and degree of cure distributions. In addition, couple of die external radiuses and two different sets of material die properties have been investigated to obtain an effective manufacturing process. Nevertheless, the obtained results of temperatures and degrees of cure are presented only for the centerline, where the curing starts and, therefore, it is impossible to evaluate physical justification of the developed process. A simpler electro-magnetic-thermal model has been developed, using COMSOL Multiphysics in [70], to design the microwave applicator used for a pultrusion of circular rod with the diameters of 9 mm. Due to the exothermic resin reaction, an internal heat generation is ignored in the present study, what leads to a low accuracy of the simulated temperature results at the centerline.

An influence of die length reduction, application of thermal insulation, preheating of steel die and heating of resin bath on the effectiveness of microwave assisted process has been studied in [34], where temperature and degrees of cure have been obtained for

the rod profile surface and centreline. Though, an insufficient degree of cure on the profiles surface, overheated resin and resin flow from the die exit has been obtained for the analyzed pultrusion processes. Moreover, it is necessary to note that in these studies, the electric permittivity and corresponding loss factor are used as constant values in the numerical analysis at the time, when they are depending on the temperature, degree of cure and frequency.

A very limited number of investigations [69],[70],[34] in the simulation aspects of microwave assisted pultrusion processes, slows down their development. For this reason, new reliable finite element models and algorithms should be developed.

1.6. Thesis aim and objectives

Although the pultrusion sector demonstrates a healthy growth now but a continuous increase in the cost of electricity could considerably reduce this movement or even stop it. An effectiveness and productivity of conventional pultrusion processes, preserving the quality of pultruded profiles, could be improved by the process optimization or by an application of innovative heating sources instead of electrical resistances with high heat losses. For this reason, a new effective optimisation methodology, considering all the required parameters of the industrial pultrusion processes and ambient room temperature, will be developed, based on the method of experimental design and response surface technique. More realistic and accurate process optimisation will be achieved using the temperature control executed by the heaters switch-on and -off strategy. With a non-direct optimisation methodology, the technological maps will be developed, presenting *EXCEL* tools. To develop microwave assisted pultrusion processes, as well as pultrusion tooling design and process control, new effective electro-magnetic-thermo-chemical finite element models and algorithms will be developed by using the general-purpose finite element software that results in considerable savings in development time and costs and makes available various modelling features of the finite element packages.

The main aim of the Thesis is to improve considerably the effectiveness and productivity of conventional pultrusion processes, preserving the quality of pultruded profiles. It can be done by:

- the process optimisation and interactive technological map development;
- an application of innovative heating sources instead of electrical resistances with high heat losses and development of innovative microwave assisted pultrusion processes.

1.7. Research objectives

1. Development of new electro-magnetic and coupled electro-magnetic-thermo-chemical finite element models and algorithms for a design of advanced pultrusion processes.
2. Modification of existing thermo-chemical finite element models and algorithms for a solution of coupled electro-magnetic-thermo-chemical problem and optimisation of industrial pultrusion processes.
3. Formulation and solution of optimisation problems for an improvement of effectiveness and productivity of conventional industrial pultrusion processes.
4. Development of interactive technological maps to be used in industrial shop by technologists.
5. Development of new microwave assisted pultrusion process for a production of rod profiles.
6. Estimation of the effectiveness and productivity of the developed advanced pultrusion process.

1.8. Research tools and methods

Research methods of the Thesis include:

- Finite element software ANSYS Mechanical, COMSOL Multiphysics;
- ANSYS parametric design language programming;
- Methods of response surface technique and experimental design;
- Software EDAOpt (for optimisation);
- Graphical tools of Microsoft Excel program to represent the obtained results;
- Solver tool of Microsoft Excel program for the solution of optimisation problems.

1.9. Scientific novelty of the Thesis

In Thesis, a new effective optimisation methodology, considering all the required parameters of the industrial pultrusion processes and ambient room temperature, is developed, employing the method of experimental design and response surface technique. More accurate and realistic process optimisation is achieved with the temperature control executed by the heaters switch-on and -off strategy.

A new microwave assisted pultrusion process for the production of rod profiles is developed by a solution of coupled electro-magnetic-thermo-chemical problem. It is done by using the general-purpose finite element software that results in considerable savings in development time and costs and makes available various modelling features of the finite element packages. The developed finite element models and algorithms allow to preserve a dependence of dielectric material properties on temperature as it is happened in real pultrusion processes.

1.10. Practical value of the Thesis

The results presented in Thesis are the part of the European Regional Development Fund (ERDF), project No. 1.1.1.1/18/A/053 “An effectiveness improvement of conventional pultrusion processes”. The aim of the project is an improvement of the effectiveness of conventional pultrusion processes preserving the quality of pultruded profiles and considerably reducing their cost as well as contributing to a healthier environment.

The present Thesis has direct practical value since two industrial technological processes have been considerably improved. So, the pull speed of the industrial technological process producing two rod profiles in COMPOR Ltd. has been increased by 50 - 125% and the energy consumption have been reduced by 20 – 33% per 1 meter of pultruded profile depending on the ambient room temperature by using the developed interactive technological map. Moreover, the effectiveness and productivity of industrial technological process producing rod profiles used in AIMPLAS have been increased in 3 and 5.5 times respectively applying microwave heating source instead of electrical resistances with high heat losses in the developed advanced pultrusion process.

1.11. Statements of the Thesis

The effectiveness (energy consumption) and productivity (pull speed) of conventional industrial pultrusion processes can be improved considerably by an application of the developed process optimisation methodology or by an application of innovative heating sources instead of electrical resistances and development of advanced microwave assisted pultrusion processes.

1.12. Thesis structure

Thesis consist of five chpaters:

Chapter 1 is a short summary of scientific literature, describing the pultrusion process, numerical simulations, and optimisation methodologies.

Chapter 2 presents the thermo-chemical, electro-magnetic and coupled electro-magnetic-thermo-chemical finite element models and algorithms developed for a design of microwave assisted pultrusion processes.

Chapter 3 formulates optimisation problems and solution methodology based on experimental design and response surface technique.

Chapter 4 presents the design of microwave assisted pultrusion processes and evaluation of their effectiveness and productivity.

At the end, the obtained results are discussed in the **Chapter 5** together with the recommendations for a further work.

2. MODELLING OF MULTI-PHYSICAL PROBLEMS

2.1. Electro-magnetic problem

Electro-magnetic finite element model and algorithm are necessary to determine the electric field distribution and as the result to obtain the absorbed energy field in the composite material and ceramic die which will be used later as a heating source in the subsequent thermo-chemical problem.

2.1.1Formulation of electro-magnetic problem

The electro-magnetic field is described by the well-known Maxwell's equations which in a differential form can be expressed in terms of electric $\vec{E}$ and magnetic $\vec{H}$ field intensities by the following way:

$$\nabla \times \vec{E} = -\frac{\partial \vec{B}}{\partial t},\ \nabla \times \vec{H} = \vec{J} + \frac{\partial \vec{D}}{\partial t},\ \nabla \cdot \vec{D} = \rho,\ \nabla \cdot \vec{B} = 0 \tag{2.1}$$

where $\vec{B}$ is the magnetic flux density,

$\vec{D}$ is the flux density,

$\vec{J}$ is the current density,

ρ is the charge density,

t is a time.

The corresponding constitutive relations have the following form:

$$\vec{B} = \mu\vec{H},\ \vec{D} = \varepsilon\vec{E},\ \vec{J} = \sigma\vec{E} \tag{2.2}$$

where μ is the magnetic permeability,

ε is the electric permittivity,

σ is the electric conductivity.

The magnetron harmonically oscillates the electromagnetic field at the fixed frequencies of 915 MHz or 2.45GHz recommended by the International Telecommunications Union for Industrial, Scientific and Medical use. Solving numerically these Equations (2.1)-(2.2), an intensity of electric field can be found

$$\vec{E}(x, y, z, t) = \vec{E}(x, y, z)e^{i2\pi ft} \tag{2.3}$$

where x, y, z are the components of location vector,

f is the microwave frequency.

Its values are used later for the determination of the absorbed energy field necessary for the thermo-chemical analysis.

To describe the dielectric losses, the electric permittivity is examined as a complex value:

$$\varepsilon^* = \varepsilon' - i\varepsilon'' \tag{2.4}$$

consisting of the electric permittivity itself ε' and corresponding loss factor ε''. Moreover, in pultrusion processes this is a complex function of frequency f, temperature T and degree of cure α

$$\varepsilon^*(f,T,\alpha) = \varepsilon'(f,T,\alpha) - i \cdot \varepsilon''(f,T,\alpha) \tag{2.5}$$

The electro-magnetic power per unit volume dissipated in the composite material and ceramic die due to their dielectric losses can be derived by an integration of the Poynting vector and using Maxwell's equations as in [56]:

$$Q = 2\pi f \varepsilon_0 \varepsilon'' E_{rms}^2 \tag{2.6}$$

where ε_0 is the vacuum permittivity,

E_{rms} is the root mean square of electric field.

2.1.2Finite element model and solution algorithm

Since no physical tests and literature exists which could be used for testing, the finite element model is developed additionally in *COMSOL Multiphysics* code to verify the results of simulation to be carried out in *ANSYS*. In this case the definition of absorbed energy must match in both codes. In *COMSOL* for a nonmagnetic material the absorption energy due to dielectric losses is determined automatically in the following form:

$$Q = \frac{1}{2}\mathrm{Re}(J \cdot E^*) \tag{2.7}$$

where * denotes the complex conjugate.

Considering the expression of current density (Equation (2.2)) and following dependencies:

$$\sigma = 2\pi f \varepsilon_0 \varepsilon'' \tag{2.8}$$

$$E\,E^* = E'^2 + E''^2 \tag{2.9}$$

the absorption energy field in both codes, COMSOL and ANSYS, is determined with the same expression by using an intensity of electric field

$$Q = \pi f \varepsilon_0 \varepsilon'' \left(E'^2 + E''^2 \right) \tag{2.10}$$

An effectiveness of the microwave heating is estimated later as follows

$$Q_{\%} = \frac{\sum_{i=1}^{N} Q_i V_i}{P_{MW}} \cdot 100\% \tag{2.11}$$

where Q_i is the energy absorbed in *i*-th finite element,

V_i is the volume of *i*-th finite element,

P_{MW} is the energy of microwave heating source,

N is the number of finite elements used for the modelling of ceramic die or composite.

The simulation procedures are developed in *COMSOL Multiphysics* and *ANSYS* environment. Two main requirements for the simulation: cost-effective use of a microwave source with a power output in the range of some kW and the ability to generate a homogeneous microwave field distribution for the entire products cross-section. Instead of conventional heating by electrical resistances, a magnetron, working at the fixed optional radiofrequency chosen from the ISM-frequency-bands (Industrial Scientific and Medical use), is used.

The cross-section of the products is predefined and first, the base model of a microwave set-up with an analytically known field distribution, that is most suitable for the required cross-section, is designed. The second step, an electromagnetic field intensity is computed by using universal finite element codes. Then the results are read from the finite element solution and the absorbed energy field is evaluated by the user developed program. Later an initial electromagnetic model is improved numerically towards a homogeneous field distribution and high efficiency of the provided energy. This is performed adjusting the model dimensions for specified ceramic die and cured composite materials until the target specifications are reached (Figure 2.1).

According to the Nyquist-Shannon sampling theorem [71] for the discrete sampling of a wave function, the maximum element size $x_{\max}$ of the mesh applied to the geometry has to fulfill $x_{\max} < \lambda/2$ where λ is the local wavelength. The local wavelength means that λ could be shorten by dielectric materials or afftected by conductive parts to obtain a good value for the maximum mesh element size is given by

$$x_{\max} < \frac{\lambda_0}{20\sqrt{\varepsilon_r}} \tag{2.12}$$

where λ_0 is the wavelength in free space,

$\varepsilon_r = \varepsilon' / \varepsilon_0$ is the relative permittivity.

Equations (2.1)-(2.2) are solved for the developed finite element mesh for electric field amplitudes with respect to the local material properties from Equation (2.5) by iterative or direct solvers in the frequency domain with the fixed frequency f of the magnetron. The excitation of waves and hence the power input are used by the so-called "port" boundary conditions. The heating rate Q is then calculated using Equation (2.10) and evaluated for homogeneity and efficiency.

2.1.3Simulation examples

To demonstrate features and benefits of electro-magnetic heating, the pultrusion process of rod profiles with diameter of 16 mm and made of polyester resin POLRES 305BV and glass fibres 4800 tex with fibre volume content of 55 % is studied. The scheme of the set-up for microwave heating is presented in Figure 2.2. It consists of

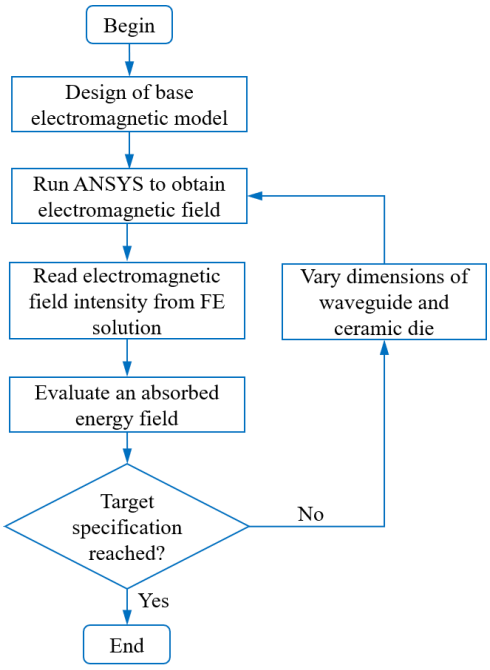

Figure 2.1. Electro-magnetic algorithm for specified ceramic die and cured composite materials.

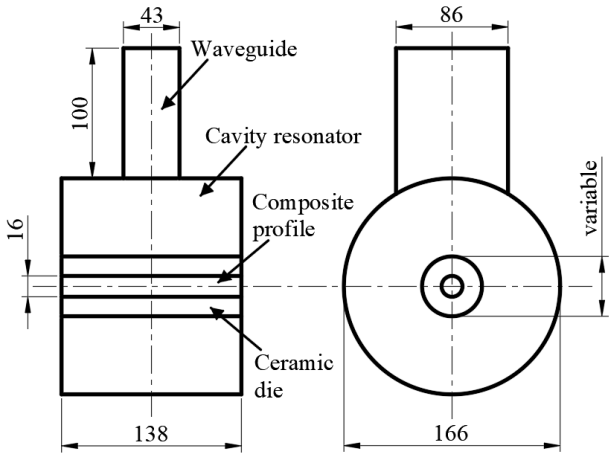

Figure 2.2. Scheme of the set up for microwave heating.

ceramic cylindrical die, cylindrical cavity resonator and waveguide transferring an electromagnetic power at industrial microwave frequency of 2.45 GHz from the magnetron to the applicator. The diameter of resonator is selected as far as possible from values, multiplied by 0.25 of wavelength in vacuum λ_0. It is taken as $1.36\lambda_0$ in our example that is between 1.25 and 1.5 of λ_0.

The general purpose of the present investigations is to provide an effective and uniformly distributed absorption energy field in the composite profile. This can be done by an application of different ceramic materials in the pultrusion die and changing its external diameter. For this reason, materials with different dielectric properties (Table 2.1.): zirconium dioxide, boron nitride and quartz glass has been chosen for a microwave transparent die. These ceramic materials are quite similar for quartz glass and boron nitride, but very differs for zirconium dioxide which has considerably larger real and imaginary parts of relative permittivity. High value of loss factor can contribute to additional (conventional) heating of composite material caused by a hot ceramic die.

Table 2.1.

Dielectric material properties

Property	Symbol (unit)	Composite	Air	Steel	Zirconium dioxide	Quartz glass	Boron nitride
Relative permeability	μ_r (-)	1	1	1	1	1	1
Relative permittivity	ε'_r (-)	5.7	1	1	29	3.5	3.0
Relative loss factor	ε''_r (-)	0.32*	0	-	0.2	0.0001	0.0001
Resistivity	R (Ω)	-	∞	0	-	-	-

*mean value of relative loss factor (Figure 2.3)

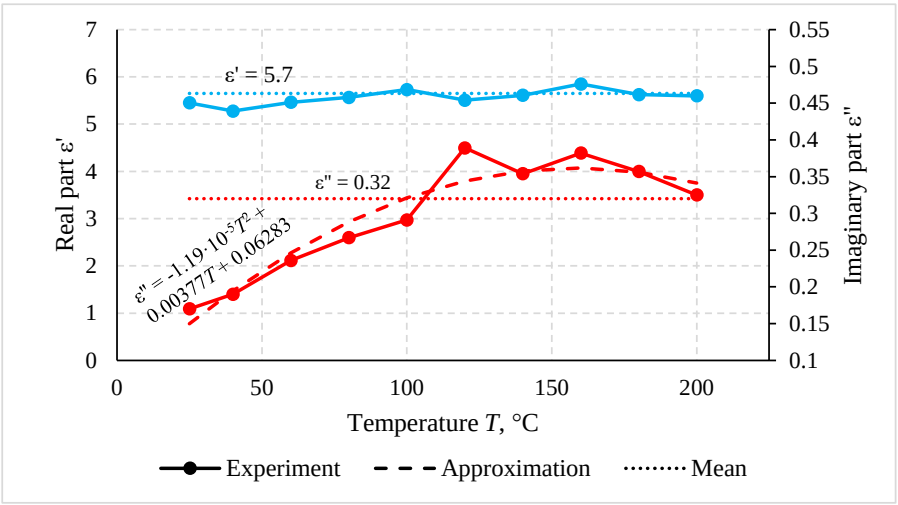

Figure 2.3. Relative permittivity and corresponding loss factor of fiber/resin composition.

The dielectric properties of polyester/glass fibre composition have been measured with the cavity perturbation method versus temperature (Figure 2.3) heating the resin from uncured till fully cured states. As it is seen, the real part of the permittivity is almost constant value and could be represented as the mean. The imaginary part is dependent on temperature and is approximated by a second-order polynomial. For the electromagnetic simulations, when the temperature distribution is unknown, the mean value of loss factor is used in calculations. The temperature-dependent imaginary part of the relative permittivity is utilized later where the coupled electro-magnetic-thermo-chemical simulations will be executed.

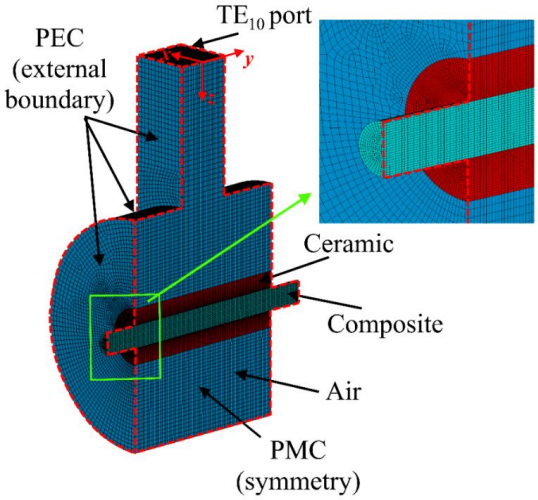

Figure 2.4. Finite element model with applied materials and boundary conditions.

The corresponding finite element model is developed in *ANSYS* (Figure 2.4) by using high frequency electromagnetic finite elements HF120. This is the first-order hexahedral element formulation with one degree of freedom - tangent component of electric field on each edge. The profile out of the cavity for a short distance of 27.6 mm to obtain the correct distribution of the electric field in a composite. Since the waveguide and cavity are made of steel, perfect electric conductor (PEC) or electric wall boundary conditions are applied to all external surfaces of the finite element model excluding the composite profile. TE_{10} mode for a rectangular port with the energy of $P_{in} = 1$ W is applied at the top of waveguide. Due to a symmetry of the problem to be solved, only one half of the domain is examined, and perfect magnetic conductor (PMC) or magnetic wall boundary conditions are applied to the symmetry plane. Assuming that an influence of the pull speed of the composite material on electric field distribution is negligible, the transport phenomena is neglected in the present electromagnetic analysis.

A convergence study is executed for the set-up of microwave heating with the ceramic die made of zirconium dioxide. For this purpose, three finite element models with different meshes: coarse, normal and fine are analyzed.

Table 2.2.

Parameters of finite element models and convergence study results

Parameter	Domain	Mesh		
		Fine	Normal	Coarse
Maximal recommended FE size (Equation (2.12), mm	Zirconia dioxide		1.1	
	Composite		2.6	
	Air		6.1	
Maximal FE size in cross-section, mm	Zirconia dioxide	1.1	3.4	4.6
	Composite	1.0	2.1	2.7
	Air	3.6	6.1	8.1
FE size in pull direction, mm		0.99	6.8	15.8
FE number	Zirconia dioxide	262080	3120	576
	Composite	42336	1176	208
	Air	276380	15564	3105
Total FE number		580796	19860	3889
Total DOF number		2383946	86535	18198
Solution time*, min		110	32.7	29.4
Absorbed energy, %	Zirconia dioxide: $Q_{cd}^{\%}$	35.7	32.7	29.4
	Composite: $Q_{comp}^{\%}$	40.0	37.5	30.6

*8 core Intel® i9-9900 CPU @ 3.10GHz PC with 32 GB RAM

The finite element sizes of the electro-magnetic problems with different finite element meshes are presented in Table 2.2. together with the absorbed energies in the ceramic die and composite profile. It is seen that only a little difference (6 – 8%) is observed for the absorbed energies obtained with the normal and fine meshes. To simplify simulations by using same finite element mesh in the electro-magnetic and thermo-chemical analysis, and to considerably reduce the dimension of the finite element problem and corresponding solution time, the finite element model with normal mesh is chosen for the subsequent parametric study and design of advanced pultrusion process.

The parametric study is carried out for the ceramic dies made of different materials in wide diameters diapason (24-64 mm) with a simulation step of 8 mm reducing the dimension of this step to 1 and 0.1 mm near the point with a maximal absorbed energy.

Ceramic die made of zirconium dioxide

The parametric study has been carried out with the purpose to define an effective and uniformly distributed absorption energy field in the rod composite profile in dependence on the diameter of ceramic die made of zirconium dioxide. The results presented in Appendix 1 demonstrate that the maximum of absorbed energy is obtained for a die with the diameter close to 40 mm.

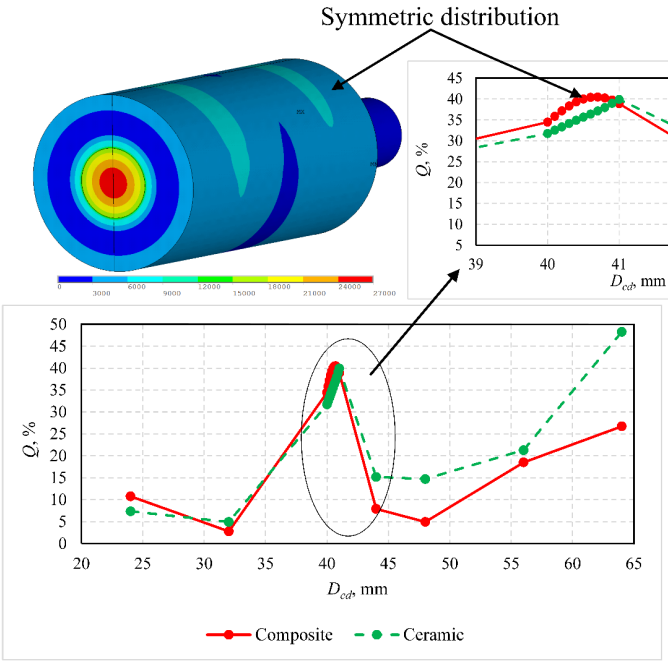

Figure 2.5. Dependence of absorbed energy on diameter of ceramic die made of zirconium dioxide.

Then the parametric study has been continued for more narrow diameter range (40 – 44 mm) with a smaller step of 1 mm. Simulation results (Figure 2.5) demonstrate that symmetrically distributed absorption energy field in the cross-section of composite does not coincide with a maximal absorbed energy. Since the present electro-magnetic analysis requires simultaneous fulfilment of two requirements on effective and uniformly distributed absorption energy fields, ceramic die with a symmetric distribution and the external diameter of 40.5 mm has been chosen for a subsequent analysis. Corresponding distribution of the absorbed energy field along profile centerline and middle resonator cross-section is presented in Figure 2.6. This figure demonstrates that even slight changes (tenths of a millimeter) in the die diameter led to considerable changes in the absorption field distribution. Here with changes in absorption energy field are observed both in the field intensities Figure 2.6 (a) and their symmetry lost (Figure 2.6 (b)). For this reason, more accurate processing of ceramic dies should be preferred.

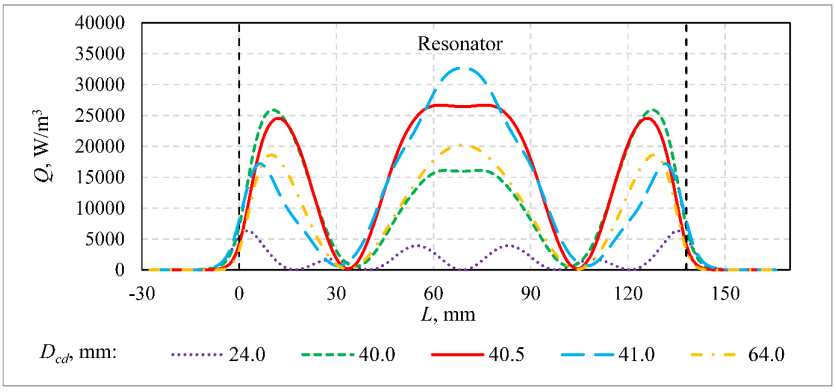

a

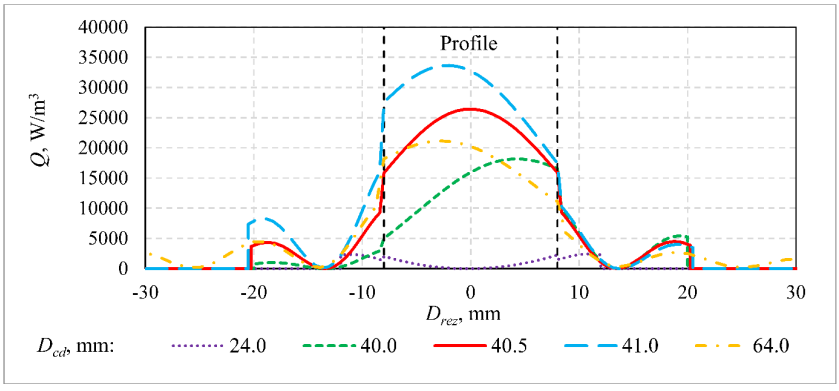

b

Figure 2.6. Distribution of absorbed energy for ceramic die made of zirconium dioxide along profile centerline (a) and middle cross-section (b).

Ceramic die made of quartz glass

For this parametric study the initial die diameter has been taken as an optimal solution obtained in the previous investigations for the ceramic die made of zirconium dioxide: 40.9 mm. Unfortunately, this diameter has not provided an effective and symmetric absorption energy field (Appendix 2). However, decreasing the die diameter till 33.8 mm, the desired solution has been obtained.

Ceramic die made of boron nitride

Again, as an initial die diameter the optimal solution obtained for the ceramic die made of zirconium dioxide (40.9 mm) has been taken. Executed calculations show that this diameter does not provide an effective and symmetric absorption energy field (Appendix 3). Therefore, the parametric study has been carried out in two directions, decreasing and increasing the die diameter. For both symmetrical solutions obtained, one of them with the die diameter of 60.8 mm has larger effectiveness. For this reason, it has been taken as a desirable.

Table 2.3.

Field intensities and corresponding parameters of set-ups for a microwave heating

D_{cd}, mm	E, V/m	Q, W/m^3	$Q^{\%}_{comp}$,%	$Q^{\%}_{cd}$,%
Ceramic die: zirconium dioxide				
40.5	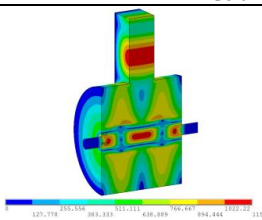	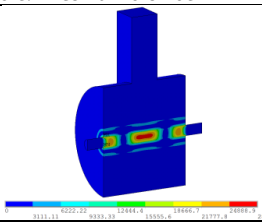	40.0 40.0*	35.7 35.9*
Ceramic die: quartz glass				
33.8	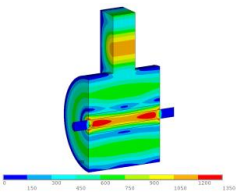	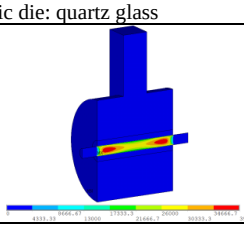	73.3 73.0*	0.03 0.03*
Ceramic die: boron nitride				
60.8	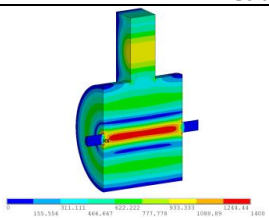	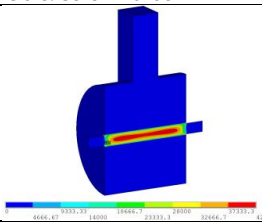	84.4 86.8*	0.04 0.05*

*COMSOL solution

Conclusions on parametric study

Intensities of electric and absorption energy fields together with an energy absorbed in the composite material and pultrusion die have been obtained by using fine finite element mesh, and they are given in Table 2.3 for different ceramic materials. It is seen that more effective pultrusion set-up can be obtained with ceramic die made of boron nitride and conduction heating effect from the hot pultrusion die cannot be ignored in the numerical analysis for the ceramic die made of zirconium dioxide since microwave absorption losses have approximately the same values for the die and composite. Moreover, for the ceramic materials having close permittivity parameters (Table 2.1), completely different diameters of pultrusion die (Table 2.3) have been obtained that requires more accurate measurements of dielectric properties of ceramic materials.

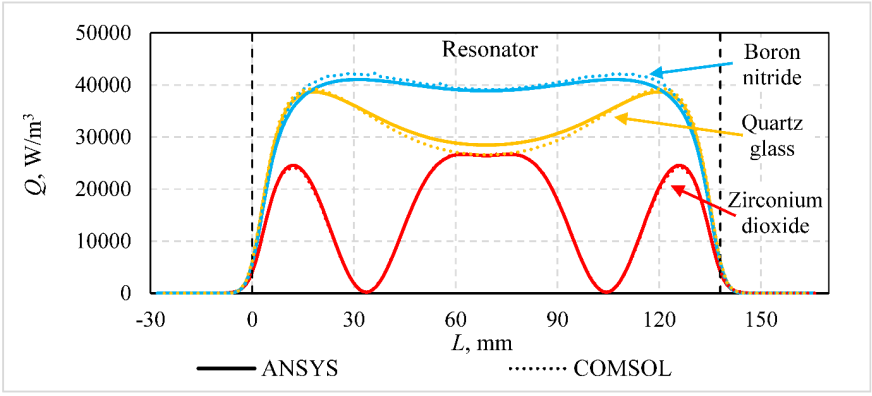

a

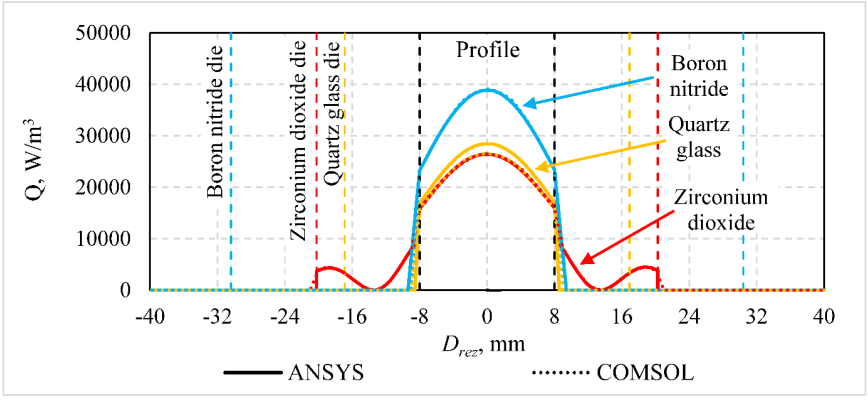

b

Figure 2.7. Distribution of absorbed energy for ceramic die made of different materials along profile centerline (a) and along profile middle cross-section (b).

Distribution of the absorbed energy along profile centerline and middle resonators cross-section is presented in Figure 2.7. where is clearly seen that highest process effectiveness can be reached with an application of the ceramic die made of boron nitride and an absorbed energy field in the composite profile decay very quickly outside the resonator (Figure 2.7. (a)) for all the examined set-ups. For this reason, in the finite element models the profile is out of the cavity only on a short distance of 27.6 mm from both sides. Figure 2.7. (b) demonstrates also that the absorbed energy field penetrates ceramic die on a short distance for boron nitride and quartz glass materials and far enough for zirconium dioxide having high electric permittivity.

To verify the finite element models and algorithm developed for the electro-magnetic analysis in *ANSYS*, the same problems have been solved in *COMSOL Multiphysics* [72]. The results of *COMSOL* after rigorous convergence study are presented in Table 2.3. and Figure 2.7. together with *ANSYS* results, where very good agreement between both results is observed which indicates their high accuracy and reliability. So, the difference between significant microwave energies calculated by *ANSYS* and *COMSOL* and absorbed in the composite materials lies in the boards of 0 – 0.2% for different set-ups, but in the ceramic die – 0.6%.

The parametric study shows that for the same microwave set-up but using different ceramic materials for the pultrusion die, different heat transfer processes should be examined in the consequent thermo-chemical analysis. So, if for the ceramics with low relative loss factor, heat transfer is executed only by the energy absorbed in composite material and starts inside the profile, for ceramic with high internal losses – an ignore of conventional heating (conduction) from the hot ceramic die is impossible since microwave absorption losses are approximatively the same values for the die and composite. Moreover, for the ceramic materials with close permittivity parameters, it was impossible to obtain close diameters of pultrusion dies for an effective and homogeneous absorption field.

2.2. Thermo-chemical problem

Thermo-chemical finite element model and algorithm are necessary to determine the temperature and degree of cure field distribution and as the result to evaluate the quality of pultruded profiles.

2.2.1 Formulation of thermo-chemical problem

The thermo-chemical problem describing the conventional pultrusion processes consists of three governing equations: the energy equation for the tool, the energy equation for the composite moving in the pull direction and the species equation (transport equation) for the resin:

$$\begin{cases} \rho c_p \dfrac{\partial T}{\partial t} - \dfrac{\partial}{\partial x}\left(k_x \dfrac{\partial T}{\partial x}\right) - \dfrac{\partial}{\partial y}\left(k_y \dfrac{\partial T}{\partial y}\right) - \dfrac{\partial}{\partial z}\left(k_z \dfrac{\partial T}{\partial z}\right) = 0 \\ \bar{\rho}\,\bar{c}_p \left(\dfrac{\partial T}{\partial t} + u\dfrac{\partial T}{\partial x}\right) - \dfrac{\partial}{\partial x}\left(\bar{k}_x \dfrac{\partial T}{\partial x}\right) - \dfrac{\partial}{\partial y}\left(\bar{k}_y \dfrac{\partial T}{\partial y}\right) - \dfrac{\partial}{\partial z}\left(\bar{k}_z \dfrac{\partial T}{\partial z}\right) - q = 0 \\ \left(\dfrac{\partial \alpha}{\partial t} + u\dfrac{\partial \alpha}{\partial x}\right) = R_r \end{cases} \quad (2.13)$$

where T is the temperature,

ρ and C_p are the density and specific heat of the tooling materials,

k_x, k_y, k_z are the thermal conductivities of the tooling materials in x, y, z directions,

u is the pull speed,

$\bar{\rho}$ and $\bar{C}_p$ are the lumped density and specific heat for the composite material,

$\bar{k}_x$, $\bar{k}_y$, $\bar{k}_z$ are the lumped thermal conductivities of the composite material in x, y, z directions,

q is the generative term related to the internal heat generation due to the exothermic resin reaction,

$\alpha = H(t)/H_{tr}$ is the degree of cure,

$H(t)$ is the amount of heat evolved during the curing up to time t.

Heat transfer in the composite occurs because of conduction and from the exothermic chemical reaction initiated by the die temperature. Due to the exothermic resin reaction, the generative term associated with the internal heat generation is written as:

$$q = V_r \rho_r H_{tr} R_r \quad (2.14)$$

where V_r is the resin volume fraction,

ρ_r is the resin density,

R_r is the rate of resin reaction determined as:

$$R_r(\alpha, T) = \frac{\partial \alpha}{\partial t} = \frac{1}{H_{tr}} \frac{dH(t)}{dt} = K(T) \cdot f(\alpha) \quad (2.15)$$

where $f(\alpha)$ depends on the resin properties and varies with the applied resin reaction

model,

$K(T)$ is defined by the Arrhenius relationship:

$$K(T) = K_0 \exp\left(-\frac{E}{RT}\right) \tag{2.16}$$

where $R = 8{,}314$ J/mol·K is the universal gas constant.

It is important to note that coefficients of the Arrhenius relationship: the activation energy E and the frequency factor K_0 are physical values and they could be determined using the Kissinger method or ASTM E 698 standard methodology from DSC tests [73]. Coefficients of the selected function $f(\alpha)$ are obtained in a simple way by a fitting of the experimental heat flow curves using the least squares method [74].

The reinforcement is saturated with the resin before entering the heated die in pultrusion process. Therefore, it is reasonable to assume that the resin does not flow. In most cases the continuous model with lumped material properties evaluated by the rule of mixture is used for a simulation of the pultrusion processes:

$$\begin{aligned} \bar{\rho} &= (1-V_r)\rho_f + V_r\rho_r \\ \bar{c}_p &= \frac{(1-V_r)\rho_f c_{pf} + V_r\rho_r c_{pr}}{\bar{\rho}} \\ \bar{k} &= \frac{k_f k_r \bar{\rho}}{(1-V_r)\rho_f k_r + V_r\rho_r k_f} \end{aligned} \tag{2.17}$$

where indexes f and r relates to the fibres and resin, respectively.

The Equation system (2.13) can be solved by using initial and boundary conditions. It is assumed that at time $t = 0$, the curing composite has the temperature is $T = T^0$ and the degree of cure is $\alpha = \alpha^0$, where index "0" denotes the initial values. The temperature of the composite at the die entrance and everywhere in the composite at the first step of numerical algorithm is prescribed as the pre-heat resin temperature. The value of the cure rate at the die entrance and throughout the composite in the first step of numerical algorithm is assumed to be zero or a very small value depending on the resin curing kinetic model. In some pultrusion processes this value could be much higher relative to the ambient room temperature which is used also as a boundary condition of the die to describe the convection effect, showing the transfer of thermal energy between a pultrusion die and the air surrounding it as a result of a temperature difference. In this case the rate of energy exchange at the boundary q_b should be

accounted as additional boundary condition. It is important to note that the power flow at the composite entrance and exit in the die is specified to be zero. Isolated boundary conditions can also be used to reduce unnecessary heat losses and save energy in pultrusion processes.

In the case of pultrusion processes with a temperature control, the thermal energy introduced into the die by electrical heaters is controlled by the thermocouples located in such die points where the measured temperature should be lower than admissible. When the operating temperature on the thermocouple reaches an admissible, delivery of electrical energy to the heaters is interrupted and the measured temperature drops. The temperature dropping is till the previously defined value when the electrical heaters are turned on again. It is necessary to note that the controlled temperatures could be the same or differs in dependence on the chosen heating algorithm, and, due to inertia effect, the measured temperatures could be a little bit higher or lower than corresponding admissible temperatures in time of turning off or on the electrical heaters.

2.2.2Finite element model and solution algorithm

The present algorithm is developed in *ANSYS Mechanical* environment and is based on the mixed time integration scheme and nodal control volumes method to solve simultaneously the coupled energy and transport Equations (2.13),(2.18). by using an iteration technique. A uniform finite element discretization of the pultruded composite profile is applied in the pull direction. The nodal control volumes are constructed based on the finite element mesh as presented in Figure 2.8. Centres of the control volumes coincide with the nodal points of the finite element. In the control volume the distribution of a field variable is assumed constant and its value is defined by the field variable calculated at the representative finite element node.

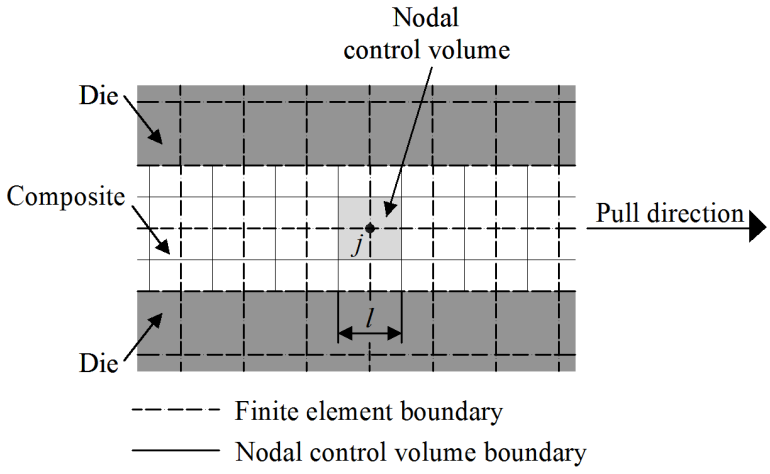

Figure 2.8. Finite element and nodal control volume meshes.

At the beginning it is assumed that the degree of cure has the same value α^0 in every nodal control volume of the composite, mostly it equals zero. After that, the transient thermal finite element analysis is used to obtain an initial state of temperatures for each element. From the temperature field, the rate of cure for the nodal control volume j at any time step i is calculated by the user developed program:

$$\frac{\partial \alpha_j^i}{\partial t} = \left[\frac{\Delta \alpha_j^i}{\Delta t} \right] = K_0 \exp\left(-\frac{E}{RT_j^i} \right) f(\alpha_j^{i-1}) \tag{2.18}$$

For $t > 0$, the degree of cure can be obtained continuously by the following equation:

$$\alpha_j^i = \alpha_j^{i-1} + \left[\frac{\Delta \alpha_j^i}{\Delta t} \right] \Delta t \tag{2.19}$$

where Δt is the time step:

$$\Delta t = \frac{1}{p} \cdot \frac{l}{u} \tag{2.20}$$

where l is the length of nodal control volume in the pulling direction,

u is the pulling speed

p is the number of sub-steps.

If the procedure of sub-stepping is not applied, $p = 1$. The exothermic effects of cure reaction are evaluated as the equivalent nodal heat power for a nodal control volume or node j by the following relation:

$$q = V_r \rho_r H_{tr} R_r = V_r \rho_r H_{tr} \left[\frac{\Delta \alpha_j^i}{\Delta t} \right] \tag{2.21}$$

These values will be applied to obtain the temperature field for a new step of iteration. Hence, a movement of the composite saturated with resin is simulated by shifting the temperature and degree of cure fields after each calculation step. It is important to note that at the entrance of the die, the degree of cure remains unchanged and is equal to α^0 at any step of iterations. The algorithm is presented in Figure 2.9.

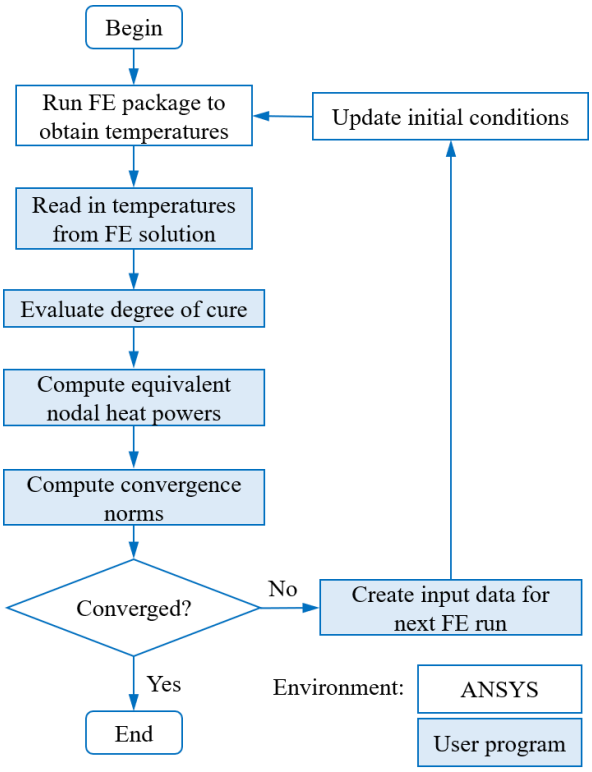

Figure 2.9. Thermo-chemical algorithm for conventional pultrusion processes.

In the case of simulation of conventional pultrusion processes with a temperature control, the temperatures obtained from the transient thermal finite element analysis are used as well for the control of work of electrical heaters. In real conditions this control is executed by thermocouples located in the corresponding points of the die. The modified thermo-chemical algorithm is presented in Figure 2.10.

2.2.3Algorithms' validation

The thermo-chemical algorithm [30] based on the mixed time integration scheme and nodal control volumes method has been successfully validated by the analysis of pultrusion process for different profiles.

In [75] the validation is realized for a cylindrical rod profile with diameter of 16 mm controlled in-line by new cure sensors, measuring the temperature and electrical resistivity of the resin on the profile surface. In this case, heating of the pultrusion die was realised by 12 electrical heaters. A greater difference in results has been observed in the first sensor, where the resin was in the gelation stage. Whereas, a very good agreement has been obtained in the areas where the resin was almost fully cured.

Similarly, the validation has also been done for an I-beam profile analysing pultrusion process for the real time with a complex temperature control in [76]. The

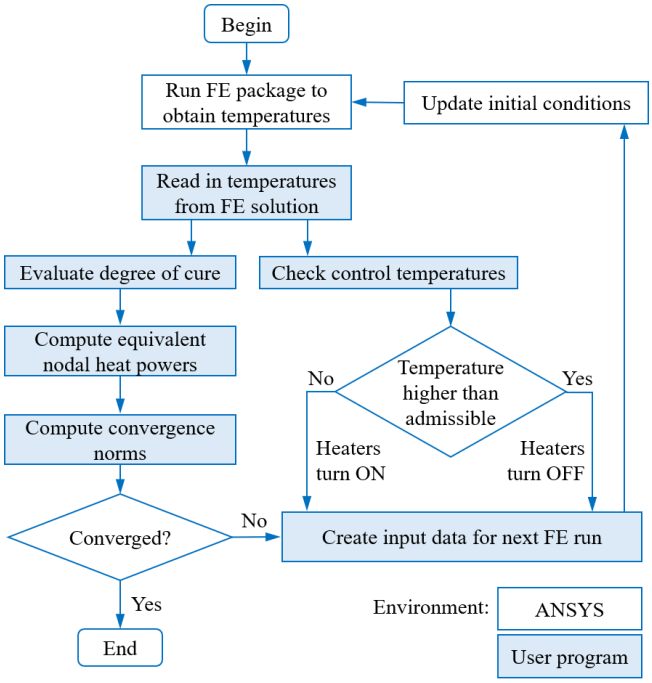

Figure 2.10. Thermo-chemical algorithm for conventional pultrusion process with a temperature control.

additional length of the beam was arranged at the die exit to extend the thermo-chemical analysis to the post-die region. In this case, the difference between the experimental and simulated results had practically disappeared after the transient period, where the resin was also fully cured.

2.3. Electro-magnetic-thermo-chemical problem

2.3.1 Formulation of electro-magnetic-thermo-chemical problem

For the microwave assisted pultrusion processes the system of Equations (2.13) describing the thermo-chemical problem should be a little bit modified:

$$\begin{cases} \rho c_p \dfrac{\partial T}{\partial t} - \dfrac{\partial}{\partial x}\left(k_x \dfrac{\partial T}{\partial x}\right) - \dfrac{\partial}{\partial y}\left(k_y \dfrac{\partial T}{\partial y}\right) - \dfrac{\partial}{\partial z}\left(k_z \dfrac{\partial T}{\partial z}\right) - Q_{cd} = 0 \\ \bar{\rho}\,\bar{c}_p \left(\dfrac{\partial T}{\partial t} + u\dfrac{\partial T}{\partial x}\right) - \dfrac{\partial}{\partial x}\left(\bar{k}_x \dfrac{\partial T}{\partial x}\right) - \dfrac{\partial}{\partial y}\left(\bar{k}_y \dfrac{\partial T}{\partial y}\right) - \dfrac{\partial}{\partial z}\left(\bar{k}_z \dfrac{\partial T}{\partial z}\right) - q - Q_{comp} = 0 \\ \left(\dfrac{\partial \alpha}{\partial t} + u\dfrac{\partial \alpha}{\partial x}\right) = R_r \end{cases} \quad (2.22)$$

The second equation is completed with the term $Q_{comp}(f,T,\alpha)$ presenting the absorbed energy field Q_{comp} in composite material and the first equation – with the term $Q_{cd}(f,T)$ presenting the absorbed energy field in ceramic die taking into account only for the materials with high dielectric losses where f is the microwave frequency. The first equation is modified only in the case when the dielectric losses of ceramic material are high and they cannot be excluded from the thermo-chemical analysis. The energy and transport equations are coupled since an exothermic heat release term appears in the energy equation of the moving composite, but the electro-magnetic and thermo-chemical problems are coupled due to the relative electric permittivity, which is used for a computation of both absorption energy fields and in general case presents complex value dependent on the microwave frequency, temperature, and degree of cure (Equation (2.5).

2.3.2Finite element model and solution algorithm

To solve the system of coupled governing Equation (2.22), an iterative finite element algorithm, preserving an electric permittivity dependence on the microwave frequency, temperature, and degree of cure, has been developed (Figure 2.11.). In the first stage of this algorithm, an experimental set-up for a microwave heating is designed to satisfy of two requirements: an application of cost-effective microwave source with an output power in the range of some kW and generation of homogeneous absorption field distribution in the profile cross-section to keep away from non-uniform heating. In the present study the cross-section of the profile is known a priory. For this reason, the first step of an electro-magnetic analysis develops a base model of the microwave set-up with an analytically known field distribution most suitable for the requested cross-section.

In the second step, an electro-magnetic field intensity is computed in ANSYS by using the sparse solver in harmonic analysis with the fixed magnetron frequency. Then the results are read from the finite element solution and the absorbed energy field is evaluated by the user developed program. To reach homogeneous field distribution and high efficiency of the delivered energy, the initial electro-magnetic model is improved by changing the dimensions of waveguide and ceramic die until the target requirements are satisfied.

In the second stage, when a microwave set-up is predefined, the absorption energy fields determined for composite and die are transferred by the user developed program into the thermo-chemical algorithm, when they are used as energy sources in corresponding thermo-chemical analysis. In the case, when electric permittivity is examined as a complex value dependent on the microwave frequency, temperature and degree of cure, intensities of the absorption energy fields are updated in relation to the temperature fields obtained in the thermo-

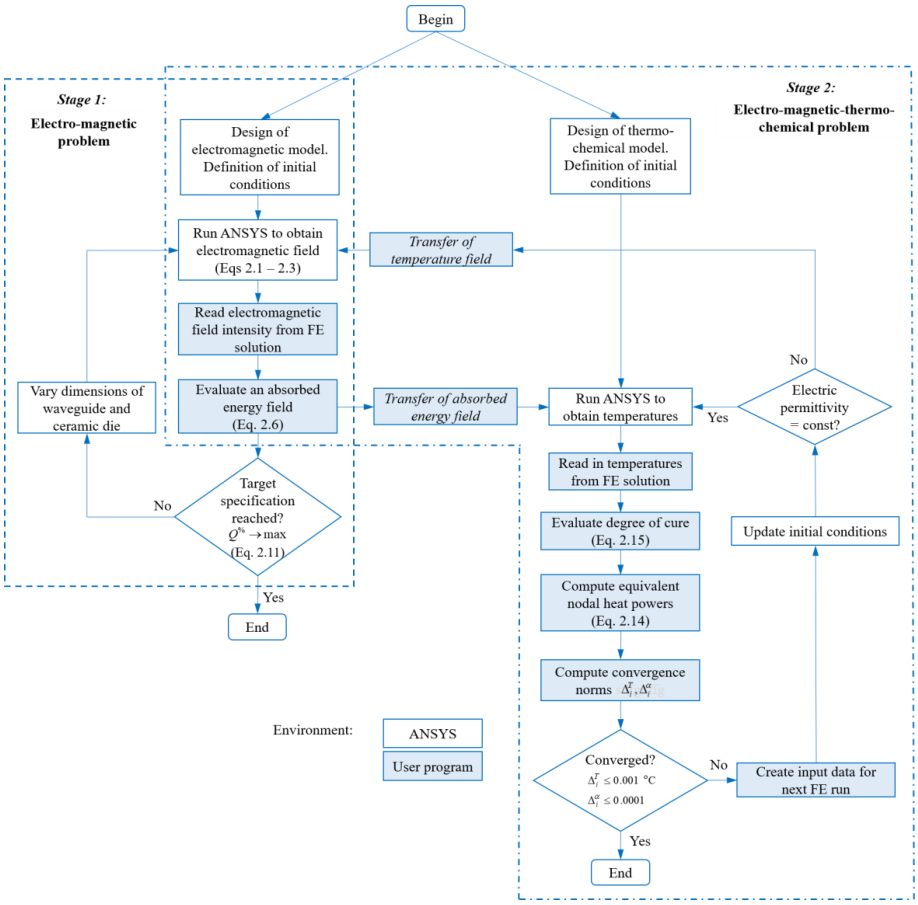

Figure 2.11. Coupled electro-magnetic-thermo-chemical algorithm for a simulation of microwave assisted pultrusion process.

chemical analysis and the coupled electro-magnetic-thermo-chemical problem is solved without dimensions` corrections for the waveguide and ceramic die. The system of Equations (2.22) is solved with a certain set of initial and boundary conditions. It is assumed that in the first step of numerical algorithm the temperature throughout the composite is taken as the resin preheating temperature, while the degree of curing is equal to zero or very small value depending on the resin curing kinetic model. The convection effect between pultrusion die, composite outside die and surrounding air is accounted in the model with the rate of energy exchange q_b at the boundary, but the power flux for the composite at the first and last modelled cross-sections is specified as zero. The microwave field is reflected at the surfaces of waveguide and cavity resonator and does not penetrate the metallic regions. For this reason, their walls are not physically presented in the electro-magnetic finite element model. These surfaces are treated as a perfect electric conductor (PEC) and introduced into the finite element

model as electric wall boundary conditions. The wave excitations or the power input from magnetron is simulated by using "port" boundary conditions. To reduce a dimension of the finite element models to be developed, a symmetry boundary conditions are applied in both problems: symmetry in electro-magnetic problem is described as a perfect magnetic conductor (PMC) or magnetic wall boundary conditions and no heat flow through the symmetry plain is allowed in thermo-chemical problem.

2.3.3Simulation examples

To simulate thermo-chemical behavior of composite material in microwave assisted pultrusion set-up (Figure 2.2), thermal material properties of steel and ceramic dies, composite and its constituents as well as surrounding air are prerequisite (Appendix 4). The rate of resin reaction is described by using the Kamal-Sourour curing kinetic model:

$$\frac{\partial \alpha}{\partial t} = \left(K_1 \exp\left(-\frac{E_1}{RT} \right) + K_2 \exp\left(-\frac{E_2}{RT} \right) \cdot \alpha^m \right) \cdot (1-\alpha)^n \qquad (2.23)$$

with the parameters presented in

Table *2.4.*

For the simulation of MW assisted pultrusion process the resin from the class of polyesters has been chosen since its degradation temperature is quite high – 270 °C, like demonstrate experiments carried out in *COMPOR* Ltd [12]. To guarantee no material destruction, this temperature has been a little bit reduced till 250 °C here and in the subsequent analyses. To avoid the resin flow from the die exit, the degree of cure on the profile surface leaving the die should be higher than 0.7 including the safety coefficient of 1.1. The desired degree of cure field intensity in the profile cross-section at the end of process simulation is estimated as 0.95 … 1. In this case it is possible to speak about its homogeneity and good quality of pultruded profile.

The finite element model for a simulation of thermo-chemical behaviour of rod profile (Figure 2.12) has been created in *ANSYS Mechanical* by using 3-D thermal solid

Table 2.4.

Thermal material properties

Parameter	Symbol (unit)	Polres 305BV
Heat reaction	$H_{tr,}$ (J/kg)	323074
Frequency factor	K_1 (s^{-1})	14289310986
Frequency factor	K_2 (s^{-1})	285.870
Activation energy	E_1 (J/mol)	85573
Activation energy	E_2 (J/mol)	33141
Order of the reaction	n	2.342

Order of the rection	*m*	0.519

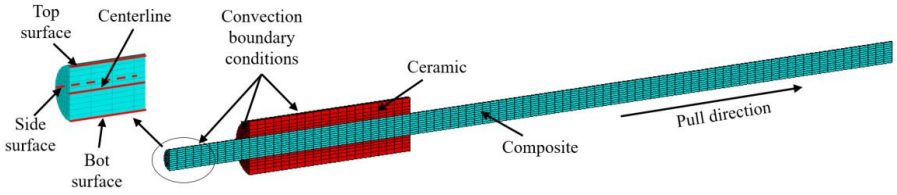

Figure 2.12. Thermo-chemical finite element model for a simulation of pultrusion process.

finite elements Solid 70. The element has eight nodes with a single degree of freedom - temperature at each node and the orthotropic material properties. Taking into account symmetry of the problem under consideration, only a half of the die and profile is modelled. Air in cavity resonator has been excluded from the thermo-chemical finite element model. Its influence has been taken into account with convection boundary conditions for a simulation of heat exchange between external surface of ceramic die and air inside resonator. The same convection boundary conditions with heat transfer coefficient of 10 W/(m^2 C) have been applied to external surface of the profile outside the resonator.

To investigate the thermo-chemical behaviour of pultruded profile in post-die region (behind the microwave resonator), its length has been considerably increased till 414 mm (3 lengths of cavity resonator). The profile prolongation has not changed a distribution of electric and absorbed energy fields in ceramic die and composite profile since the electric field actually does not propagate along the profile outside the resonator. To illustrate this assumption, new electro-magnetic finite element model has been developed (Figure 2.13). Distribution of the absorbed energy along profile centreline for the die with external diameter of 40.9 mm and made of zirconium dioxide is presented for both cases in Figure 2.14.

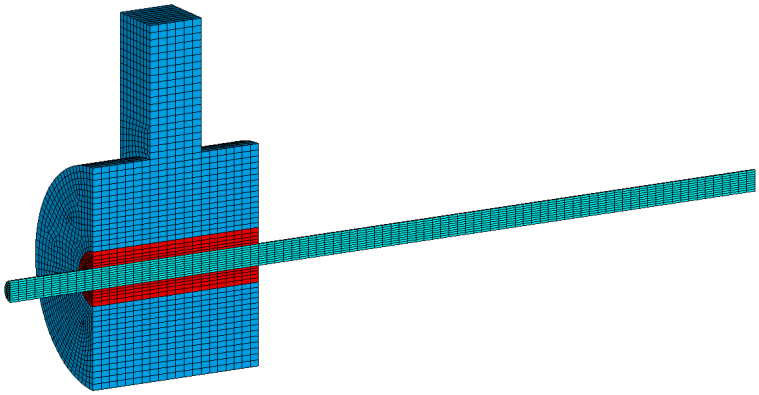

Figure 2.13. Electro-magnetic finite element model for a simulation of pultrusion process.

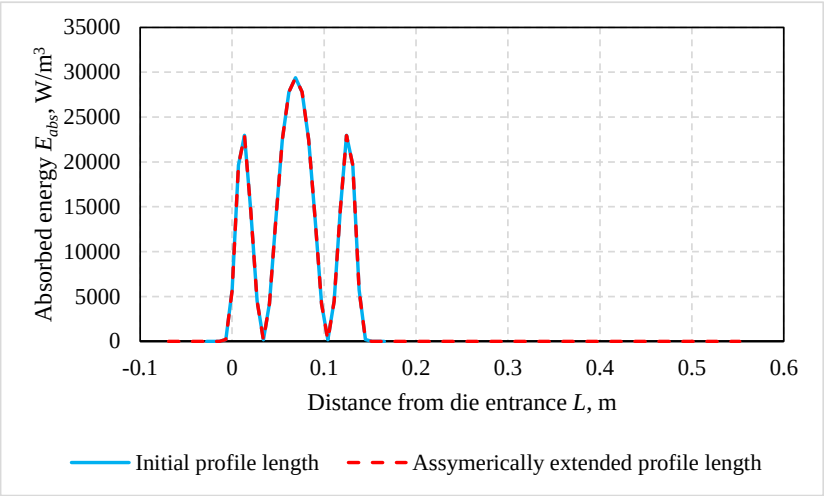

Figure 2.14. Distribution of the absorbed energy along profile centreline.

Electro-magnetic-thermo-chemical analysis with constant permittivity

The results of physically justified microwave assisted pultrusion process operating with the applied microwave energy of 0.6 kW and pull speed of 50 cm/min are presented in Figure 2.15. for the set-up with ceramic die made of boron nitride, which is more effective from the examined solutions to the largest microwave energy absorbed in composite material (Table 2.3). Figure 2.15 demonstrates that all the constraints on the allowable and desired degree of cure on profile surface at die exit and in final product are executed now.

The problem of resin flow from the die exit and improvement of the process productivity (pull speed increase) can be solved also by an increase of the die length outside the resonator cavity. In our case the die part outside the resonator cavity has the same dimensions as ceramic die (Figure 2.2), but it is made of steel material. Since steel presents perfect electric conductor (Table 2.1), no changes in intensities of electric and absorbed energy fields obtained earlier for the set-up with a simple die made of boron nitride (Table 2.3) have been observed. The corresponding results of thermo-chemical analysis for the modified pultrusion set-up are given in Figure 2.16. demonstrating that all constraints taken for the development of microwave assisted pultrusion processes are executed now.

It is necessary to that the productivity of modified process has been improved in twice by increasing the pull speed till 100 cm/min, but this requires considerably higher microwave energy applied (1.1 kW) that has been used in the previous pultrusion process. Of course, effectiveness and productivity of the analyzed pultrusion process can be improved by their optimization.

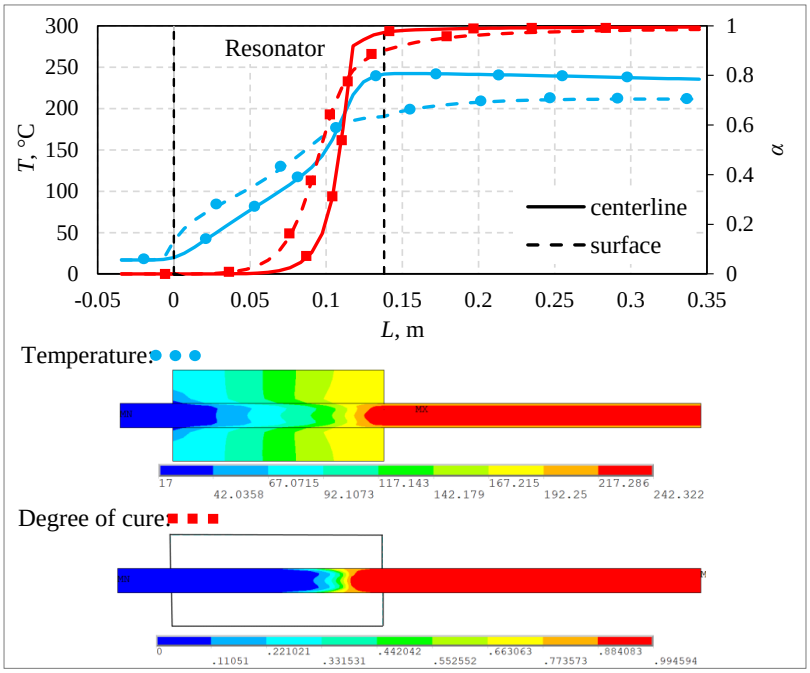

Figure 2.15. Distribution of temperature and degree of cure along pultruded profile for ceramic die made of boron nitride.

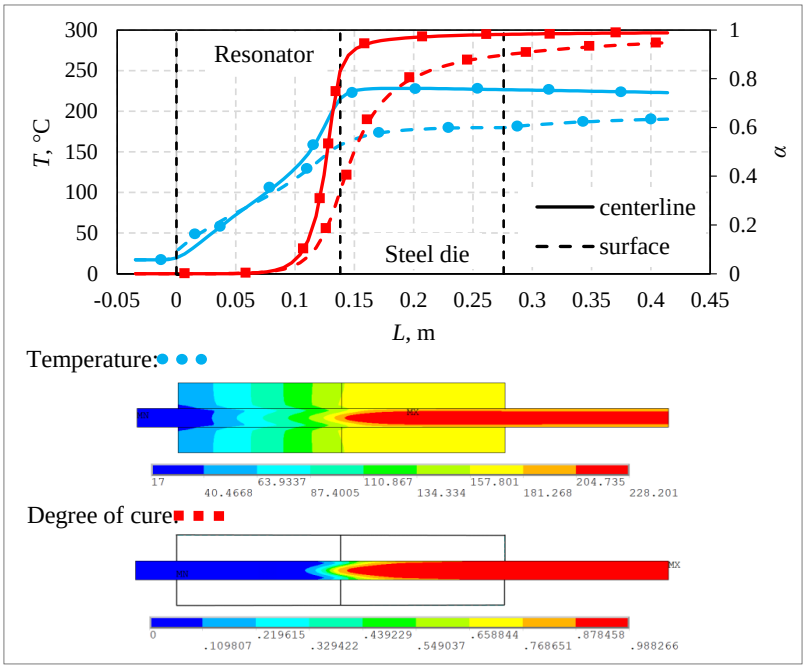

Figure 2.16. Distribution of temperature and degree of cure along pultruded profile for modified pultrusion die.

Electro-magnetic-thermo-chemical analysis with variable permittivity

For the real pultrusion process a dependence of dielectric material properties on temperature, which relates in turn to the resin curing (exothermic chemical reaction), cannot be ignored. The experimental dielectric losses of polyester/glass fiber composition have been approximated by a second-order polynomial function (Figure 2.3) for a subsequent utilization in the numerical analysis. In this case coupled electro-magnetic-thermo-chemical problem (Equation (2.22)) is solved with an application of the developed algorithm (Figure 2.11) where the electric and absorbed energy fields are updated in each time step due to the changes in dielectric properties of pultruded profile (stage 2). The finite element model of current pultrusion set-up with the ceramic die made of boron nitride and operating with the pull speed of 98.18 cm/min, applied energy of 0.92 kW and under ambient room temperature of 17°C is presented in Figure 2.17.

The diameter of ceramic die has been determined in stage 1 (Table 2.3) to provide an effective and uniformly distributed absorption energy field in the cross-section of composite profile. The results present the temperature, degree of cure, electric and absorption energy fields in some time steps in Appendix 5.

Temperature-dependent dielectric properties cause thermal runaway effect because the loss factor of relative electric permittivity ε'' increases with a temperature rise. As a result, the hottest zone absorbs more energy and heats up even more. Changes over time for the absorbed energy are presented in Figure 2.18, where it is seen that the absorbed energy in composite and maximal absorbed energy becomes a stable in 8 and 11 s after the process start. Further, only their slight (5%) increase and decrease respectively for total and maximal absorbed energy is observed. Corresponding distributions of the absorbed energy fields along profile centerline and in corresponding profile cross-section are given in Figure 2.18. for initial and steady-state process.

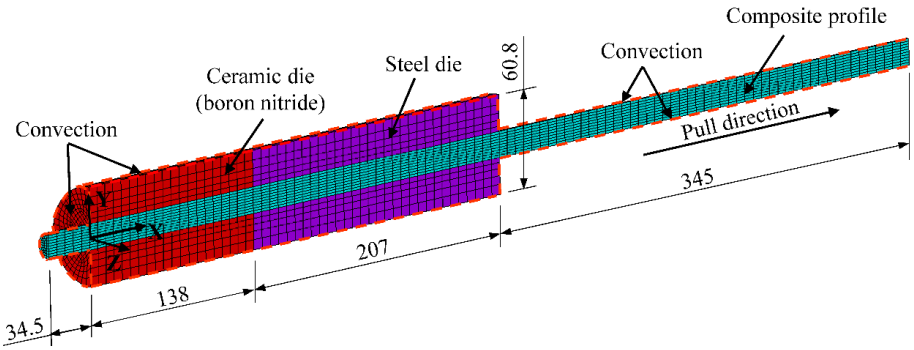

Figure 2.17. Finite element model for thermo-chemical analysis.

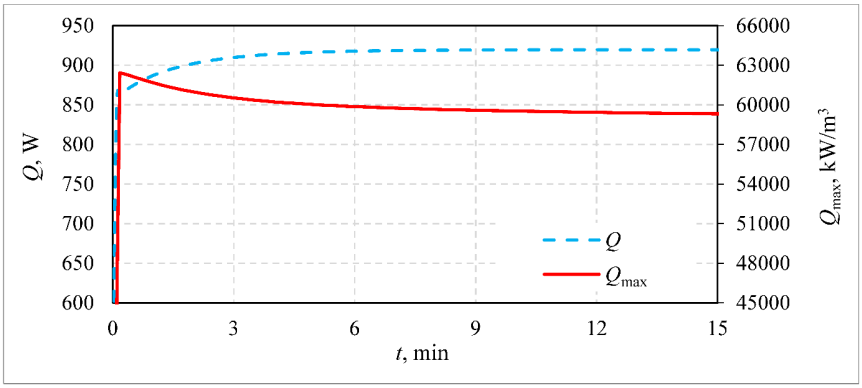

Figure 2.18. Dependence of absorbed energy on time.

An influence of thermal runaway effect is seen in Figure 2.19 (a), where in the case of temperature-dependent dielectric properties distribution of the absorption energy along resonator is changed from symmetric to concentrated at the resonator exit. However, Figure 2.19 (b) clearly demonstrates a performance of the uniformly distributed absorption energy field in the cross-section of composite profile during curing process. In this case no hot spots appear in the pultruded profile and quality product can be obtained. It is necessary to note that changes in composite material dielectric losses practically do not influence an electric field which is almost constant (permittivity of composite material is taken as a constant value).

The temperature and degree of cure on profile centerline, where the curing starts, reach their steady state also very quickly (Figure 2.20). Small horizontal lines at the process start show the time necessary for the profile cross-section movement from a heating zone to the last analyzed cross-section. After time (40 s) composite is fully cured in centerline. To reach desirable degree of cure on the profile surface, more time is required (Figure 2.20). However, this time could be considerably reduced also by a preheating of the steel die to its operating temperatures by electric heaters.

To study an influence of different models used for a description of dielectric material properties, the same analysis has been carried out with a constant loss factor of electric permittivity presented by the mean values obtained for the full management range ($\varepsilon'' = 0.32$) or for the process operating temperature 100…200°C ($\varepsilon'' = 0.35$). Distribution of the absorbed energy fields along profile centerline and in the corresponding cross-sections is presented in Figure 2.19, but temperature and degree cure along profile centerline and surface after 28 min from the pultrusion process start are given in Figure *2.21*. It is seen that using the temperature dependent dielectric material properties, the process is operating with higher temperatures (Figure 2.21 (a)) and curing in the profile is faster (Figure 2.21 (b)) than has been obtained with the mean values. This is clear since in real microwave assisted pultrusion process the heating zone becomes stable very quickly and it operates at high temperatures corresponding to high dielectric losses (Figure 2.3). It is necessary to note that in the analyzed case

pulltrusion process with temperature dependent dielectric properties satisfies to all the process constraints examined earlier while the process simulated with mean values does not correspond to requirements on resin flow from the die exit and quality of final product.

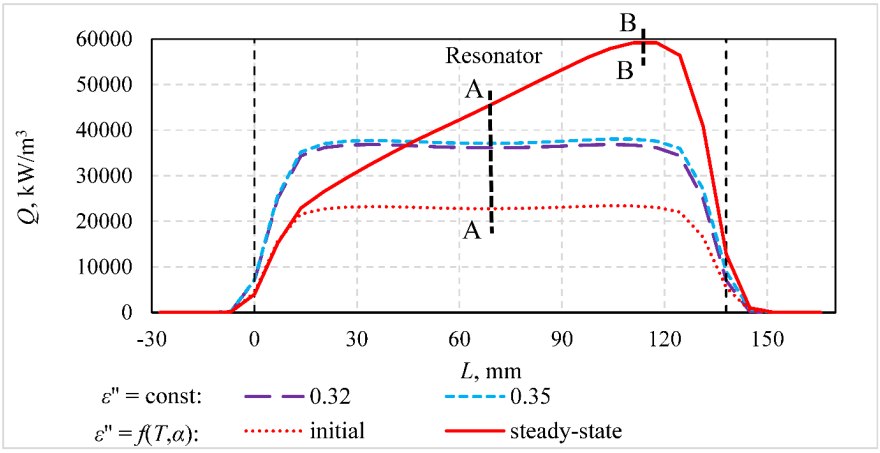

a

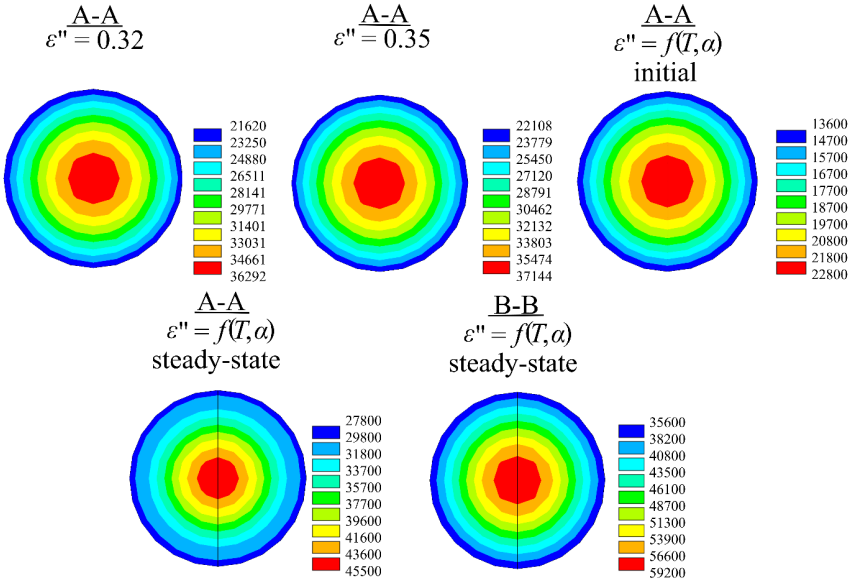

b

Figure 2.19. Distribution of absorbed energy for ceramic die made of boron nitride along profile centerline (a) and corresponding cross-section (b).

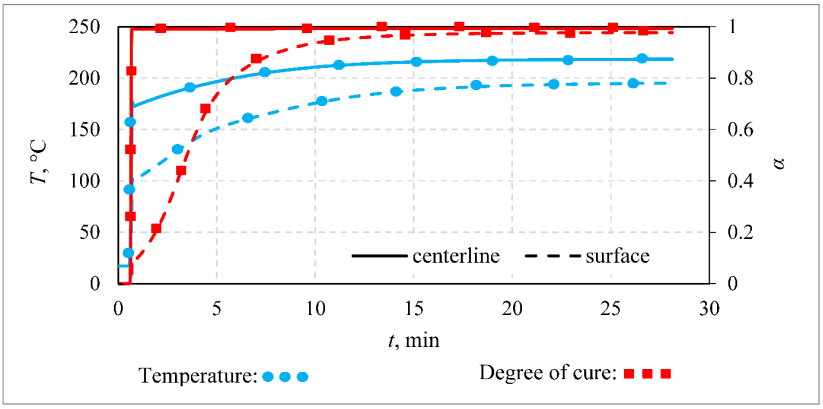

Figure 2.20. Dependence of temperature and degree of cure on time for the last simulated profile cross-section.

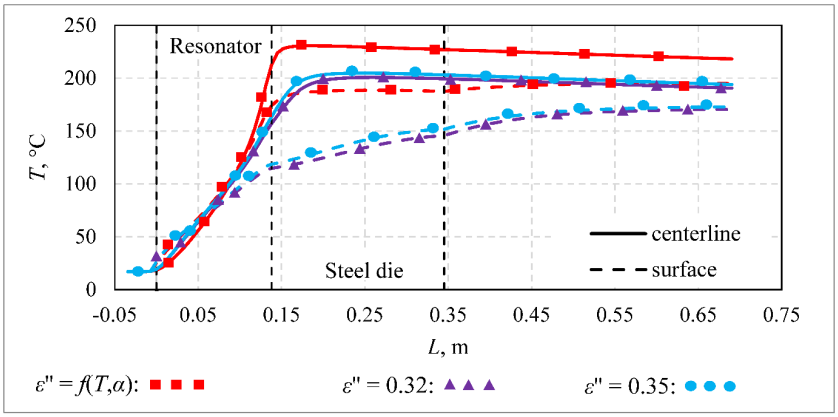

a

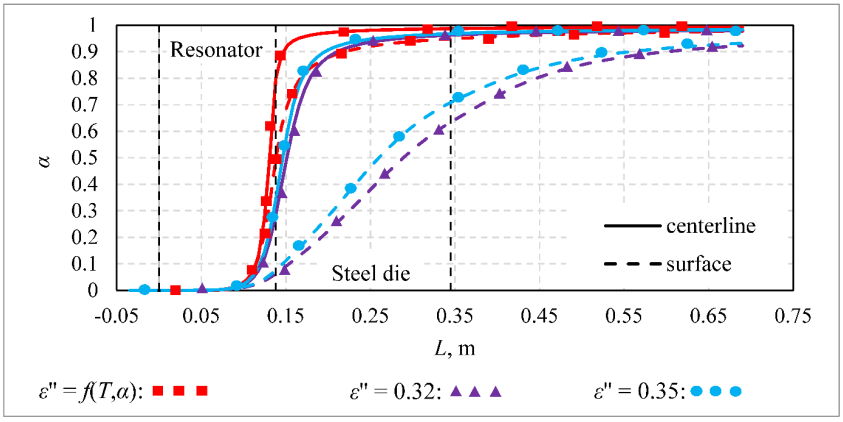

b

Figure 2.21. Distribution of temperature (a) and degree of cure (b) along pultruded profile for ceramic die made of boron nitride with temperature dependent and mean dielectric properties.

3. OPTIMISATION OF CONVENTIONAL PULTRUSION PROCESSES

New effective optimisation methodology, taking into account all the required parameters of the industrial pultrusion processes and ambient room temperature, is developed, employing the method of experimental design and response surface technique. More accurate and realistic process optimisation, that have been reached in the previous studies, is achieved with the temperature control executed by the heaters switch-on and -off strategy. Using non-direct optimisation methodology, technological maps, presenting *EXCEL* tools, are developed additionally for the technologists' convenience.

3.1. Optimisation methodology

Considering the high dimensionality of numerical problems to be solved, a non-direct optimisation methodology is developed using the method of experimental design [77] and response surface technique [78]. It is a set of mathematical and statistical techniques and is suitable for the analysis of such problems where several variables are affected the response of interest and the main objective of procedure is to optimise this response. Optimisation methods based on experimental design, compared to other approaches, are effective for optimal design and processes with computationally expensive analyses, combining modelling and optimisation steps and requiring less intervening the analyst. Moreover, this approach is very general and allows to optimise any processes or systems under arbitrary conditions respecting any objective function, such as, durability, costs, reliability, performance, taking into account all requirements [79]-[80]. The optimisation methodology based on experimental design and response surface technique developed for the optimisation of conventional pultrusion processes is presented in Figure 3.1. It should be noted that at each of these stages, the problem can be solved using different methods.

3.1.1 Experimental design

Different methods can be used for the plan of experiments: Factorial, Latin Hypercube, Box-Behnken, D-optimal, Uniform Design, Orthogonal Array, Central composite, Orthognal Latin Hypercube, etc [77]. Since in our case a distribution of the design variables in the design space is unknown, the plan of experiments with regular as possible distribution of the points of experiments in the domain of factors is chosen. To create this plan, the following criterion is used:

$$\Phi = \sum_{i=1}^{n} \sum_{j=i+1}^{n} \frac{1}{l_{ij}^2} \Rightarrow \min \tag{3.1}$$

where n is the number of experiments,

l_{ij} is the distance between the experimental points numbered *i* and *j* ($i \neq j$).

Physically, it is equal to the minimum of the potential energy of the repulsive forces for the points with unit mass if the magnitude of these repulsive forces is inversely proportional to the distance between the points.

The plan of experiments is described by the matrix of plan B_{ij}. The domain of factors is defined as $x_j \in [x_j^{\min}, x_j^{\max}]$ and the points of experiments are calculated using the following expression:

$$x_j^{(i)} = x_j^{\min} + \frac{1}{n-1}\left(x_j^{\max} - x_j^{\min}\right)\left(B_{ij} - 1\right), \quad i = 1,2,...,n, \quad j = 1,2,...,k \tag{3.2}$$

The minimal number of experimental points during the optimisation problem is determined as $N = 2L$, where $L = (k+1)(k+2)/2$ and *k* is the number of design parameters.

3.1.2FEM simulations

Finite element analysis is performed at each point of the plan of experiments. In this case, a coupled thermo-chemical problem described above in Thesis chapter 2.2.2. is solved.

3.1.3Response surfaces

Different approximation technique can be used to build the response surfaces using the numerical results obtained at the points of the developed plan of experiments. There are Polynomial (Global), Neural Networks, Radial Basis Functions, Kriging, Splines, Rational Functions, etc. [78]. In our case, the approximations are obtained using a conventional un-weighted least square estimation, excluding some points. Various polynomial functions with the first, second and third orders are suitable for describing the response surfaces in the present study:

$$\hat{y} = a_0 + \sum_{i=1}^{k} a_i x_i + \sum_{i=1}^{k} a_{ii} x_i^2 + \sum_{i=1}^{k}\sum_{j=i}^{k} a_{ij} x_i x_j + \sum_{i=1}^{k} a_{iii} x_i^3 + \sum_{i=1}^{k}\sum_{j=i}^{k}\sum_{l=1}^{k} a_{ijl} x_i x_j x_l + ... \tag{3.3}$$

where $a_0, a_i, a_{ii}, a_{ij}, a_{iii}, a_{ijl}, ...$ are unknown coefficients,

k is the number of design parameters.

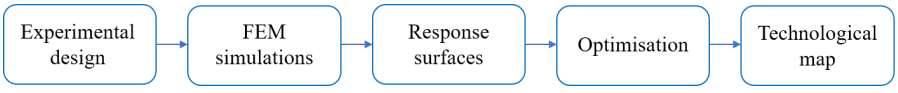

Fig. 3.1. Optimisation methodology.

Various error can be used to assess the accuracy of the designed response surfaces. One of them is the maximum relative error at the bad point:

$$\Delta_{\max} = \frac{|y_i - \hat{y}_i|}{|y_i|} \times 100\% \tag{3.4}$$

where y_i and $\hat{y}_i$ are the values of original and approximating functions in the sample point x_i of experimental design.

The root mean squared error is estimated as

$$\sigma = \sqrt{\frac{\sum_{i=1}^{n} (y_i - \hat{y}_i)^2}{n}} \tag{3.5}$$

and its relative value is determined with respect to the range of the approximating function in the domain of interest:

$$\sigma_r = \frac{\sigma}{A_F} \times 100\% \tag{3.6}$$

where $A_F = \max(y_i) - \min(y_i)$,

$i = 1,...,n$.

To assess the adequacy of approximations, the relative cross-validation error can be used:

$$\sigma_{cross} = \frac{\sqrt{\frac{\sum_{i=1}^{n} (y_i - \hat{y}_{i(i-1)})^2}{n}}}{\sigma_0} \times 100\,\% \tag{3.7}$$

where $\hat{y}_{i(i-1)}$ is the predicted value for x_i, if *i*-th experimental point is not used for an approximation building and $\sigma_0 = \sqrt{\frac{\sum_{i=1}^{n} (y_i - \bar{y})^2}{n-1}}$ is the standard deviation of response from the mean value $\bar{y} = \frac{\sum_{i=1}^{n} y_i}{n}$ in experimental points.

If the relative cross-validation error is close to 100% or even larger, the obtained model is useless.

Some information about the goodness of model's fit could be obtained using a statistical measure called as the coefficient of determination:

$$R^2 = 1 - \frac{\sum_{i=1}^{n} (y_i - \hat{y}_i)^2}{\sum_{i=1}^{n} (y_i - \bar{y})^2} \tag{3.8}$$

Its value close to 1 indicates that the regression line perfectly fits the experimental data perfectly, but a good coefficient of determination is not a guarantee of a good approximation. In the case, when the number of fitting coefficients p is only slightly less than number of experimental runs n, the quality of approximations could also be measured by the adjusted coefficient:

$$R_{adj}^2 = 1 - \frac{n-1}{n-p-1} \times \frac{\sum_{i=1}^{n} (y_i - \hat{y}_i)^2}{\sum_{i=1}^{n} (y_i - \bar{y})^2} \tag{3.9}$$

Its value larger than 0.9 is typically required for an adequate approximation.

3.1.4Optimisation

The constrained non-linear optimisation problem is formulated in the following form:

$$\begin{aligned} &\min F(x); H_i(x) \geq 0; G_j(x) = 0 \\ &i = 1,2,...,I;\ j = 1,2,...,J \end{aligned} \tag{3.10}$$

where I and J are the numbers of inequality H and equality G constraints. This problem is replaced with an unconstrained minimisation problem, where constraints are considered with the penalty functions. New version of the random search method [30] or the generalised reduced gradient algorithm are used to solve the formulated optimisation problems. The analysis of the significance of the design parameters presented in the approximation functions is also carried out in the following chapters.

3.1.5Technological map

The technological map of pultrusion process is developed for a designer convenience and presents an *EXCEL* tool based on the results of optimisation. This technological map allows to find an optimum solution for any combination of the parameters of pultrusion process and ambient room temperature as well as to carry out the parametric study for any design variable.

3.2. Optimisation of rod profile

The pultrusion tool for a production of two rod profiles simultaneously is presented in Figure 3.2. The dimensions of the die: 500 x 150 x 110 mm, and the distance between two profile channels is 40 mm. The die is heated by two electrical heater platens located at the top and bottom edges and near the die exit. Dimensions of the heaters are 300 x 150 x 15 mm and its electrical power is 2750 W. The operation of heaters is controlled by a thermocouple located between them as shown in Figure 3.3. Pultrusion die is made of steel with thermal properties presented in Table 3.1. and thermal properties of electrical heaters are given in Table 3.2.

Cross-section and dimensions of the pultruded composite profile are given in mm in Table 3.8. The materials used for a production of the rod profile are glass fibre tex4800 with the fibre mass fraction of 78% and polyester resin C-L ISO 112G. Their thermal properties are described in Table 3.3. The rate of resin reaction is described by using the Kamal-Sourour curing kinetic model, with the parameters presented in Table 3.4.:

$$\frac{\partial \alpha}{\partial t} = \left(K_1 \exp\left(-\frac{E_1}{RT} \right) + K_2 \exp\left(-\frac{E_2}{RT} \right) \cdot \alpha^m \right) \cdot (1-\alpha)^n \qquad (3.11)$$

3.2.1FE model and solution convergence

The finite element model for a simulation of two rods pultrusion has been created in *ANSYS Mechanical* by using 3-D thermal solid finite elements Solid 70. The element has eight nodes with one degree of freedom - temperature at each node and the orthotropic material properties. Given the symmetry of the problem under consideration, only a quarter of the die is modelled. An additional length of 300 mm of the rod is arranged at the die exit to extend the thermo-chemical analysis to the post-die region. Scheme of the considered pultrusion process, used to develop the finite element model, is presented in Figure 3.4.

Fig. 3.2. Pultrusion tool.

Fig. 3.3. Location of thermocouple.

Table 3.1.

Thermal properties of die material.

Property	Symbol (unit)	Steel
Density	ρ (kg/m^3)	7720
Specific heat	C (J/(kg·K))	470
Thermal conductivity	K_x (W/(m·K))	43

Table 3.2.

Thermal properties of heater material

Property	Symbol (unit)	Heater
Density	ρ (kg/m^3)	2700
Specific heat	C (J/(kg·K))	896
Thermal conductivity	K_x (W/(m·K))	180

Table 3.3.

Thermal properties of composite material

Property	Symbol (unit)	Tex 4800	C-L ISO 112 G	Lumped
Density	ρ (kg/m^3)	2500	1100	1953
Specific heat	C (J/(kg·K))	1235	1360	1263
Thermal conductivity	K_x (W/(m·K))	11	0.209	0.890
Thermal conductivity	K_y (W/(m·K))	1	0.209	0.546

Table 3.4.

Kinetic parameters of resin

Parameter	Symbol (unit)	C-L ISO 112G
Heat reaction	H_{tr}, (J/kg)	223385
Frequency factor	K_1 (s^{-1})	$2.6 \cdot 10^{13}$
Frequency factor	K_2 (s^{-1})	$1.2 \cdot 10^{12}$
Activation energy	E_1 (J/mol)	116769
Activation energy	E_2 (J/mol)	200000
Order of the reaction	n	1.27
Order of the reaction	n	0.0011

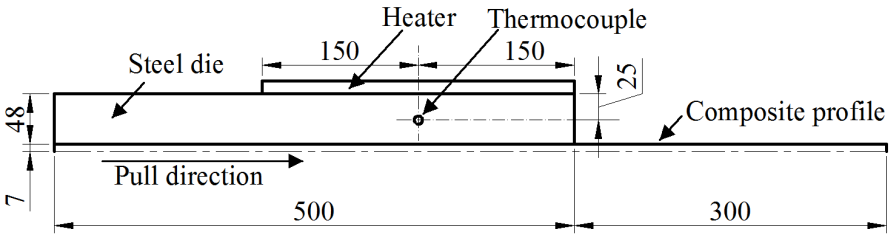

Fig. 3.4. Scheme of pultrusion process.

Rigorous convergence study has been executed before utilisation of the finite element model in in optimisation process. For this aim, three different finite element (FE) models with varied meshes have been build (Figure 3.5.-3.7.). The number of finite elements used for each model and the length of finite elements in pull direction are given in Table 3.5. The parameters and initial conditions that have been used for the convergence study:

- pull speed 30 cm/min,
- control temperature at thermocouple 140°C,
- room and resin temperature at die entrance 20°C,
- at time $t = 0$ all nodal points of die and heaters have the room temperature,
- die preheating time without composite 20 min,
- pultrusion simulation time after preheating 5 min,
- according to Equation (2.20), time step of the solution is 4 s for the FE model with coarse mesh, 2 s for the FE model with normal mesh and 1 s for the FE model with fine mesh. This signifies that not just the convergence study in dependence on FE number has been executed, but also the convergence study in dependence on solution time step has been examined at the same time.

Distribution of temperature and degree of cure along profile centreline and surface for the finite element models with different meshes are presented in Figure 3.8. and Figure 3.9. It is seen that only a slight difference is observed for the degree of cure along profile centreline obtained with normal and fine meshes and no difference is observed for the degree of cure along profile surface using the same meshes. It is necessary to note that for the temperature distribution along profile centreline and surface, all the finite element models with different meshes give practically the same results. Due to this and to significantly reduce the size of the finite element model and corresponding solution time, the finite element model with normal mesh is chosen for the further parametric investigation and optimisation.

Table 3.5.

Parameters of finite element models

	Course mesh	Normal mesh	Fine mesh
FE length in pull direction, mm	20	10	5
FE number in the cross-section of composite profile	56	183	850
FE number in the cross-section of die	110	562	2185
Total number of elements	5320	45500	375800

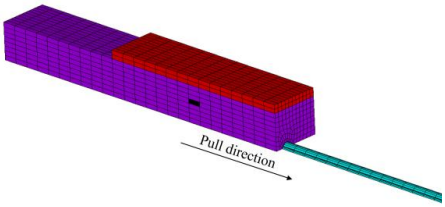

Fig. 3.5. Finite element model with course mesh.

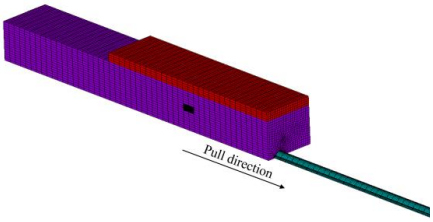

Fig. 3.6. Finite element model with normal mesh.

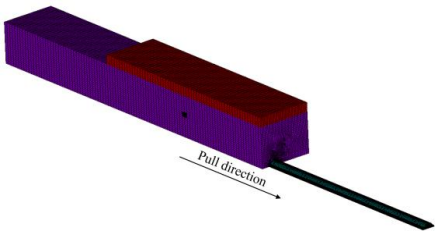

Fig. 3.7. Finite element model with fine mesh.

3.2.2Parametric study

The parametric study has been conducted to investigate the possible effects of design factors on the temperature and degree of cure in composite profile, as well as on the working time of heaters to define the precise constraints for tested variables.

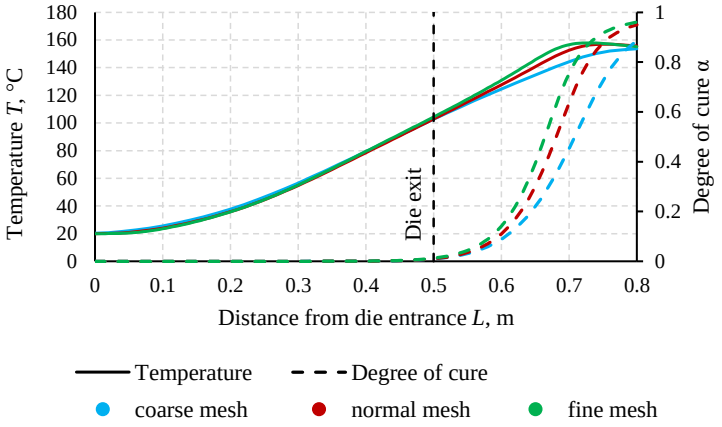

Fig. 3.8. Temperature and degree of cure distribution along profile centreline.

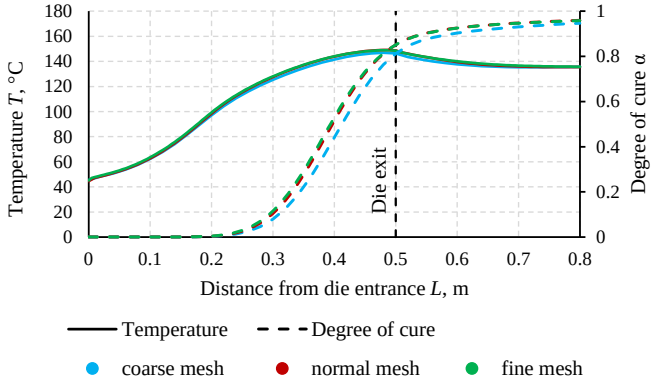

Fig. 3.9. Temperature and degree of cure distribution along profile surface.

The final optimisation problem is formulated by the results of this study. The parameters and initial conditions used in the parametric study are the same as in the convergence study, except that the pultrusion simulation time after preheating is increased to 30 min. This is done to guarantee the steady-state conditions for the pultrusion process under study, as presented in Figure 3.10. for the pultrusion set-up given in Figure 3.11. The process energy consumption is estimated in the parametric study using a relative time of the heaters work in the manufacturing process:

$$k_t = \frac{t_{work}}{t_{sim}} \tag{3.12}$$

where t_{work} is the time of heaters work,

t_{sim} is a simulation time of the pultrusion process without the preheating time.

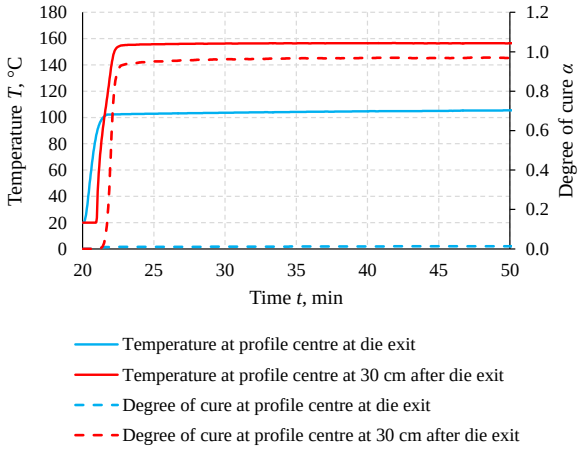

Fig. 3.10. Dependences of temperature and degree of cure on time.

Effect of heater position

Three different locations of heaters are investigated in the present study like presented in Figures 3.11.- 3.13. The temperature and degree of cure distribution along profile centreline and surface are given in Figure 3.14. and Figure 3.15. correspondingly. The simulation results show that location of heaters at the die enter does not allow to receive high value of the degree of cure. To obtain its desirable value, heaters should be located between centre and exit position on the die. Since we plan to compare the optimal results with the parameters written into technological map for the real pultrusion process, the location of heaters at the die exit will be examined in the subsequent optimisation problem.

It is necessary to note that the energy consumption of the process evaluated by the relative time of heaters work (Equation (3.12) is the same $k_t = 0.18$ for all three positions of heaters. This is due to the fact that the same location of the thermocouple under centre of heaters and the same control temperature are used as well as no changes in the parameters describing the pultrusion process and ambient room temperature are examined.

Effect of room temperature

An effect of ambient room and correspondingly resin temperature on the results of optimisation has never been investigated but it could have a considerable influence. For this reason, the pultrusion process has been simulated for four different room and resin temperatures (10, 20, 30 and 40°C) often presenting an ambient temperature in industrial shops. Results of this parametric study are given in Figure 3.16. and Figure 3.17. It is seen from these figures that ambient room temperature has no influence on the degree of cure distribution along profile surface (Figure 3.17.) but demonstrates considerable effect in relation to the temperature and degree of cure distribution along profile centreline (Figure 3.18.). This phenomenon could have considerable energy consumption effect. For this reason, an ambient room and correspondingly resin

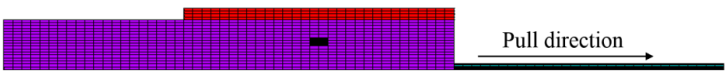

Fig. 3.11. Position of heaters at die exit.

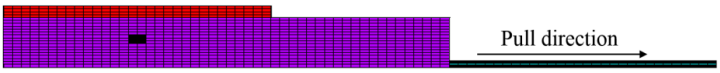

Fig. 3.12. Position of heaters at die enter.

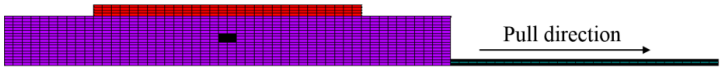

Fig. 3.13. Position of heaters at die centre.

temperature will be examined like the design parameter in the subsequent optimisation problem.

The energy consumption of the process evaluated by the relative time of heaters work (Equation (3.12)) and presented in Table 3.6 confirms this assumption. It is clearly seen in Table 3.6 that the pultrusion process is more effective by 26% if the ambient temperature in the industrial shop is 40°C instead of 20°C.

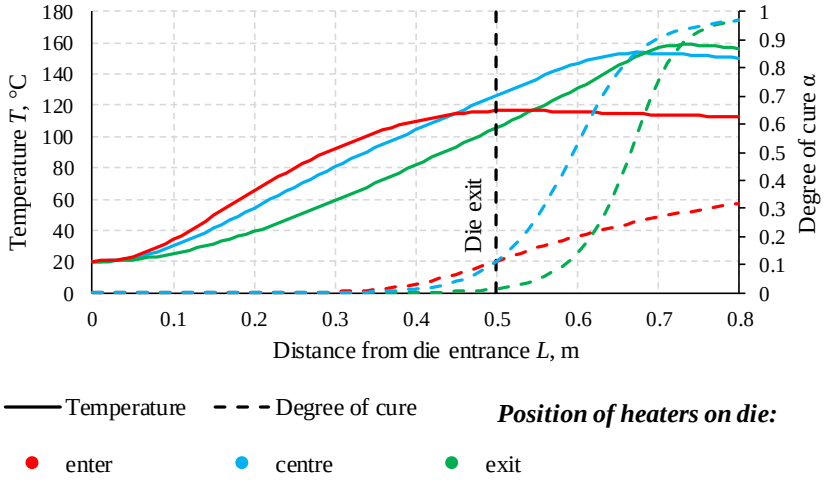

Fig. 3.14. Temperature and degree of cure distribution along profile centrline.

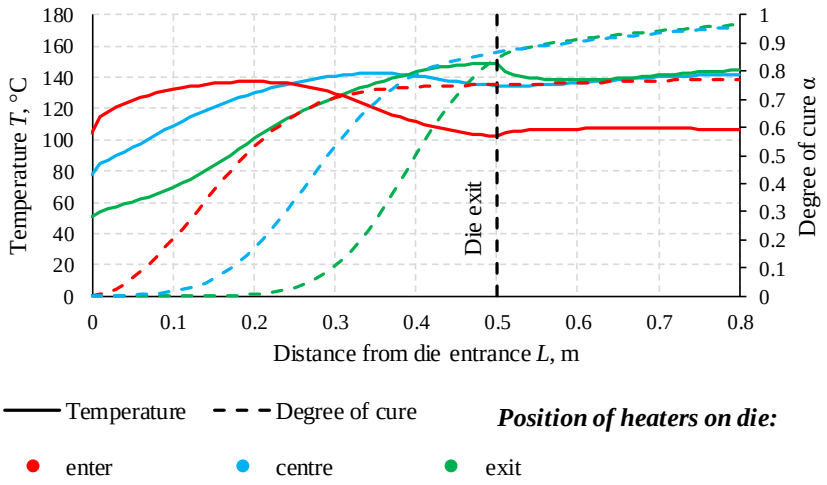

Fig. 3.15. Temperature and degree of cure distribution along profile surface.

Table 3.6.

Energy consumption of the process with different room temperatures

Room temperature, °C	10	20	30	40
Relative time of heaters work k_t	0.19	0.18	0.16	0.14

Table 3.7.

Energy consumption of the process with different die lengths

Die length, mm	500	300
Relative time of heaters work k_t	0.18	0.14

Effect of die length

To save an expensive steel material used for the production of pultrusion die and to reduce high costs of its treatment, possible reduction of the die length is investigated in the present study. In this case the die length is reduced from 500 mm (initial die) till 300 mm (shortened die) where the die length is the same with the length of applied heater. It is expected that in the case of shortened die, resin curing could happen a little bit later. For this reason, a simulation length of the pultruded profile is increased in twice from 300 mm till 600 mm.

Results of this parametric study, temperature and degree of cure distribution along profile centreline and surface, are presented in Figure 3.18. and Figure 3.19. It is seen that the die with a reduced length can provide enough heat for the resin curing. However, in this case it is necessary to be very careful, since a danger of very high curing in the die entrance exists that can lead to a premature resin gelation at the entrance and to the pultrusion process stop.

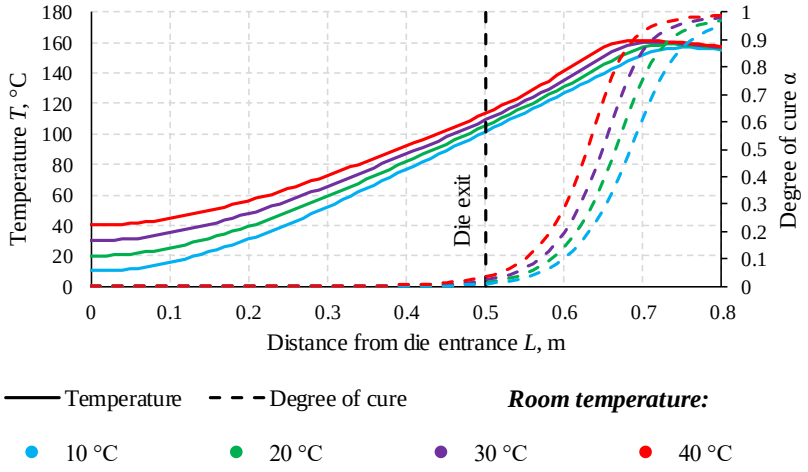

Fig. 3.16. Temperature and degree of cure distribution along profile centreline.

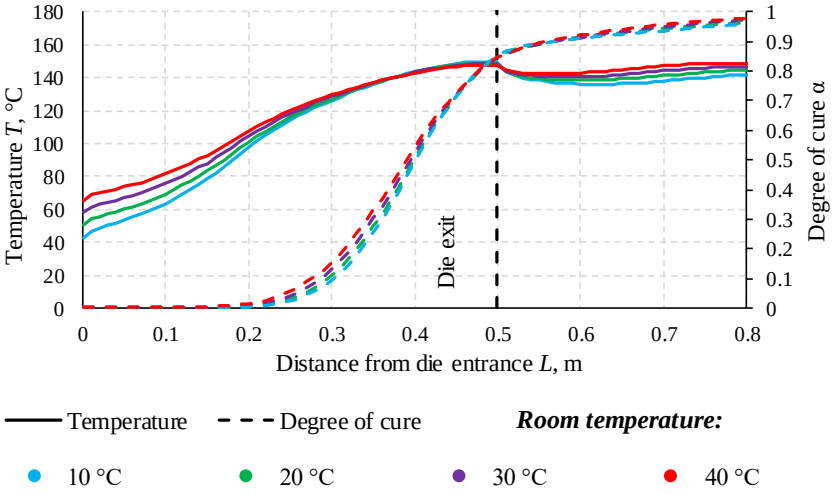

Fig. 3.17. Temperature and degree of cure distribution along profile surface.

With the shortened die more effective pultrusion process could be obtained that is demonstrated by the values of relative time of heaters work presented in Table 3.7. In general, an examined die could be shortened but this parameter is not taken into consideration formulating an optimisation problem, since we plan to optimise an industrial pultrusion process with an existing die.

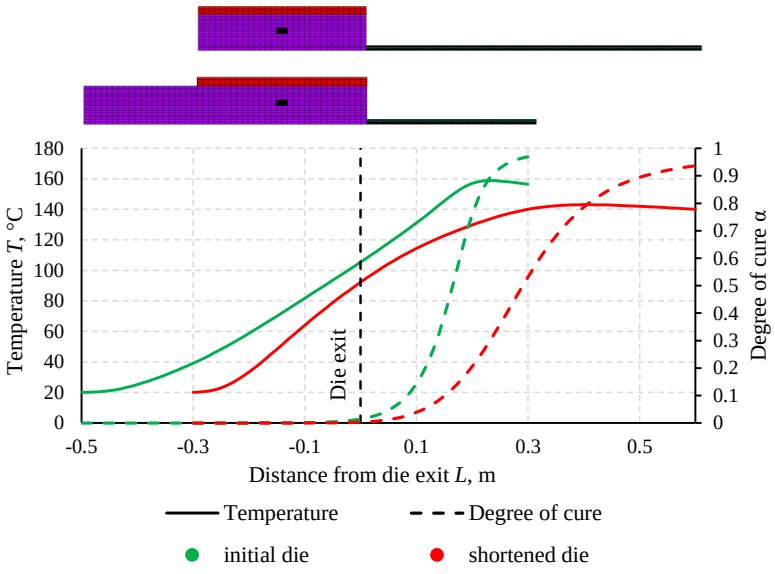

Fig. 3.18. Temperature and degree of cure distribution along profile centreline.

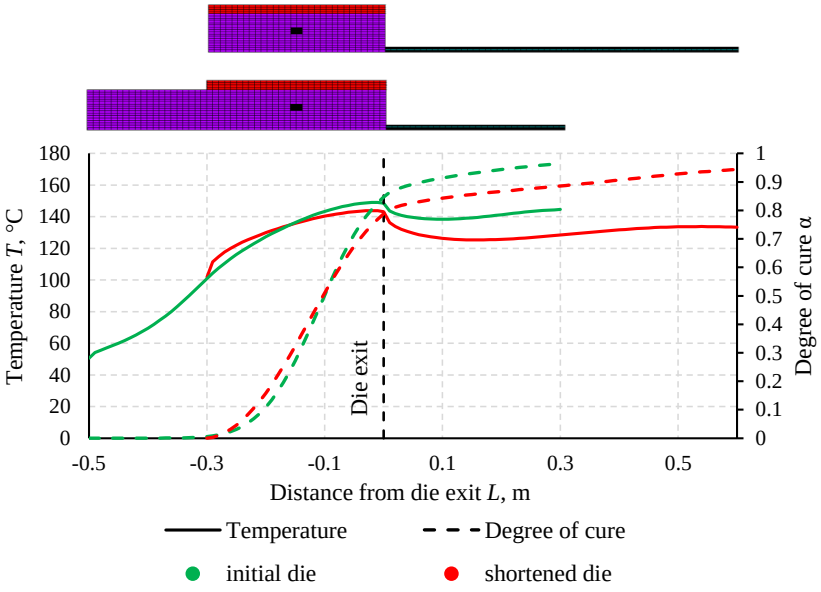

Fig. 3.19. Temperature and degree of cure distribution along profile surface.

3.2.3 Formulation of optimisation problem

Based on the results of parametric study, an optimisation problem for the pultrusion of two rod profiles have been formulated and described in Table 3.8.

The heaters platens are located at the die exit, as in the real technological process. Since resin curing is expected in the post-die region, the modelling of the profile length after the die exit is extended till 1 m.

The optimisation problem is formulated for two objective functions. The first describes an effectiveness of pultrusion process and minimises an electrical energy (kWh) necessary for a production of pultruded profile with the length of 1 m:

$$\frac{n \cdot W_{heater} \cdot k_t}{m \cdot V_{pull}} \rightarrow \min \tag{3.13}$$

where n is the number of heaters,

m is the number of simultaneously produced profiles and in our case $m = 2$,

W_{heater} is the power of electrical heater in kW, V_{pull} is the pull speed in m/h,

k_t is the relative time of heaters work determined by Equation (3.12).

The second objective function is connected with a productivity of pultrusion process and maximises the pull speed:

$$V_{pull} \rightarrow \max \tag{3.14}$$

Table 3.8.

Optimisation problems for conventional pultrusion process of rod profile

Profile cross-section	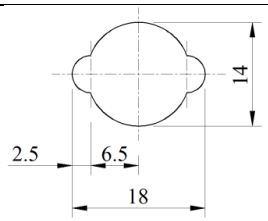	
Finite element model	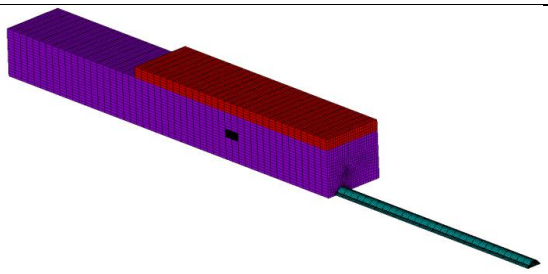	
Resin	C-L ISO 112G (polyester resin)	
Quantity of resin	22%	
Objective function	Minimisation of energy (kWh) per meter of pultruded profile: $\frac{n \cdot W_{heater} \cdot k_t}{m \cdot V_{pull}} \rightarrow \min$ Maximisation of pull speed: $V_{pull} \rightarrow \max$	
Parameters		
	Constant	
Power electrical heater, W	2750	2750
Number of electrical heaters	2	8
Variable		
	Min value	*Max value*
Pull speed, cm/min	20	45
Room and resin temperature, °C	10	40
Control temperature on 1 group of electrical heaters, °C	115	150
	Constraints	
Temperature in profile, °C	-	150
Degree of cure in profile	0.95 at 1.0 m from die exit	-
Degree of cure in profile at die exit	0.70 on the profile surface	-

Several parameters of the pultrusion process (power and number of electrical heaters) are taken into consideration as constant values in optimisation problem, another (pull speed and control temperature on heaters), and room and resin temperature are examined as design variables with the boarders describing the design space. Constrains are introduced into optimisation procedure with the aim to provide a qualitative profile production when the resin is fully cured and no overheated during the pultrusion process. The minimal value of the degree of cure is determined in the cross-section of profile, which is located 1 m from the die exit. Moreover, for the rod pultrusion is not necessary to check all the profile points for overheating and enough only to control points with the maximal temperature on the profile surface and centreline. Since in some points of experimental design the finite element simulations demonstrate a situation presented in Figure 3.20., when an exothermic chemical reaction is complete or very close to the finish on the surface of composite material leaving the die and at the same time resin is in the gel stage in the middle of the profile, an additional constraint requiring a minimum degree of cure on the profile surface at the die exit $\alpha_{surf}^{exit} \geq 0.7$ must be applied. This constraint guarantees that resin on the surface is in a solid state.

3.2.4Solution of optimisation problem

The plan of experiments with as regular a distribution of the points of experiments in the factor domain as possible is developed for 3 design parameters and 30 experiments. Then the finite element analysis is performed at each point of the plan of experiments. The sampling points and results of simulations are given in Table 3.9. Figure 3.21.-3.23. demonstrate the points of the design space affected by the constraints taken in the optimisation problem. It is seen that the optimal solution could be found for all ambient room and resin temperatures but in narrow pull speed and control temperatures range. This information could be useful also for an accuracy improvement of the response surfaces to be developed by reducing the number of design points not important for the examined technological process.

The response surfaces are developed in the next step by the conventional un-weighted least square estimation, excluding some points in the case of

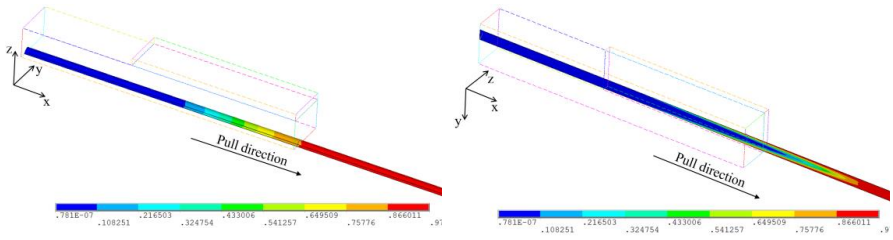

Fig. 3.20. Distribution of degree of cure after 50 min (view from different angles).

Table 3.9.

Sampling points and simulation results

Exp.Nr.	Plan				Results				
	V_{pull}, cm/min	$T_{control}$, °C	T_{room}, °C	T_{surf}, °C	α_{surf}	T_{cent}, °C	α_{cent}	α_{surf}^{exit}	k_t
1	45.00	136.72	30.69	144.0	0.812	128.8	0.662	0.590	0.17
2	28.62	116.21	18.28	122.9	0.444	109.1	0.346	0.242	0.13
3	30.34	143.97	36.90	152.6	0.997	165.1	1.000	0.910	0.14
4	26.03	131.90	40.00	144.7	0.986	154.7	0.998	0.694	0.12
5	43.28	130.69	20.34	138.1	0.595	110.9	0.273	0.438	0.18
6	20.86	142.76	34.83	152.9	0.998	165.7	1.000	0.958	0.12
7	24.31	135.52	14.14	145.0	0.988	158.8	0.999	0.821	0.15
8	32.93	133.10	32.76	140.8	0.952	146.4	0.986	0.636	0.14
9	42.41	145.17	23.45	154.2	0.972	147.0	0.975	0.836	0.19
10	22.59	137.93	24.48	149.0	0.995	162.8	1.000	0.886	0.14
11	40.69	134.31	38.97	141.3	0.889	138.4	0.912	0.575	0.14
12	41.55	141.55	13.10	150.8	0.916	134.2	0.842	0.762	0.20
13	34.66	115.00	28.62	120.9	0.321	102.9	0.183	0.177	0.13
14	26.90	148.79	27.59	158.5	0.999	169.7	1.000	0.973	0.15
15	23.45	118.62	26.55	125.1	0.770	127.7	0.885	0.353	0.12
16	27.76	119.83	35.86	125.6	0.724	126.2	0.814	0.328	0.11
17	37.24	125.86	25.52	132.6	0.609	115.3	0.435	0.372	0.15
18	29.48	129.48	21.38	137.4	0.912	140.4	0.970	0.573	0.14
19	32.07	140.34	11.03	150.1	0.980	153.6	0.995	0.833	0.18
20	44.14	121.03	29.66	126.9	0.328	100.9	0.121	0.215	0.15
21	38.97	117.41	17.24	123.7	0.284	98.0	0.101	0.186	0.15
22	21.72	123.45	15.17	132.4	0.917	140.9	0.982	0.520	0.13
23	31.21	124.66	10.00	132.6	0.658	117.8	0.551	0.409	0.16
24	36.38	122.24	37.93	128.2	0.570	116.3	0.457	0.299	0.12
25	35.52	139.14	22.41	147.8	0.968	148.9	0.988	0.765	0.17
26	33.79	150.00	19.31	159.9	0.997	165.5	0.999	0.957	0.18
27	39.83	127.07	12.07	134.6	0.516	106.9	0.214	0.375	0.18
28	20.00	128.28	31.72	143.0	0.984	152.9	0.998	0.692	0.11
29	25.17	147.59	16.21	157.8	0.998	169.6	1.000	0.973	0.16
30	38.10	146.38	33.79	155.2	0.993	160.2	0.998	0.892	0.16

necessity. They are built for the following behaviour functions: the maximal temperatures on profile surface (T_{surf}) and centreline (T_{cent}), the minimal degree of cure on profile surface (α_{surf}) and centreline (α_{cent}) in cross-section located at distance of 1 m form die exit, the minimal degree of cure on profile surface at die exit (α_{surf}^{exit}) and the relative time of heaters work (k_t). It is necessary to note that only one regression function k_t directly enters into the objective function (Equation (3.13)). Any other presents a constraint in the optimisation problem.

To develop a suitable approximation of simulation results, various order polynomial functions are evaluated. The coefficients of first-, second- and third-order regression

polynomials are given in Table 3.10-Table 3.12. The relative errors are calculated between simulation and approximated results and smaller errors are obtained for the regression functions approximating the maximal temperatures on the profile surface and centreline, degree of cure on the profile surface at the die exit and relative time of heaters work. In relation to an accuracy of the degree of cure approximations, the relative errors are higher especially for the points with lower degree of cure ($\alpha < 0.5$). Since these points are out of interest, designing the pultrusion process, their large relative errors are not significant for an optimisation procedure and could be not involved into approximation process. Other approximation errors, which characterize their accuracy and reliability are summarised in Table 3.13. Analysing these errors, the second order polynomials could be recommended for use in the subsequent optimisation problem, as they present lower-order regression functions with the desired accuracy and reliability.

However, it is interesting to investigate their behaviour, as well as behaviour of first- and third-order polynomials, reducing the number of experimental points utilised in the building of the response surfaces to be developed for the description of the degree of cure on the profile surface and centreline.

Table 3.10.

Coefficients of first-order polynomial

Coef.	$T_{surf,}$ ℃	α_{surf}	$T_{cent,}$ ℃	α_{cent}	α_{surf}^{exit}	k_t
Const	-0.656749	-1.15855	-57.567	-1.38623	-2.190104	-0.035223
V_{pull}	-0.144326	-0.013080	-1.53345	-0.022158	-0.010450	0.002006
T_{cont}	1.10501	0.017512	1.78677	0.020606	0.023647	0.0011944
T_{room}	-0.004542	0.0026274	0.340417	0.0052889	0.000178	-0.001568

Table 3.11.

Coefficients of second-order polynomial.

Coef.	T_{surf}, °C	α_{surf}	T_{cent}, °C	α_{cent}	α_{surf}^{exit}	k_t
Const	-51.44295	-9.204234	-280.209	-7.425009	-4.560321	-0.033301
V_{pull}	-0.798867	-0.136409	-4.26529	-0.216959	-0.033399	0.0003284
T_{cont}	1.974302	0.166964	5.81882	0.154499	0.065081	0.001266
T_{room}	0.291701	0.020888	0.57647	0.039125	0.001399	0.000120
V_{pull}^2	0.009118	-0.000227	-0.02275	-0.000614	0.000076	-0.000010
$V_{pull} \times T_{cont}$	0.001975	0.000992	0.02542	0.001653	0.000136	0.000021
$V_{pull} \times T_{room}$	-0.007867	0.000233	0.03198	0.000574	-0.000007	-0.000018
T_{cont}^2	-0.003412	-0.000667	-0.01750	-0.000671	-0.000173	-0.000002
$T_{cont} \times T_{room}$	-0.001266	-0.000184	-0.00828	-0.000371	-0.000002	-0.000009
T_{room}^2	0.002388	-0.000028	-0.00324	-0.000055	-0.000017	0.0000014

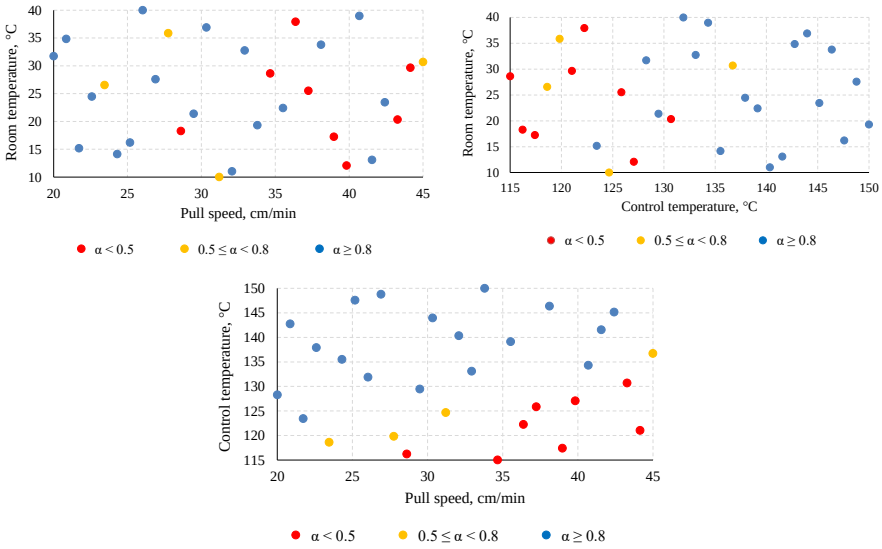

Fig. 3.21. 2D views of the plan of experiments with highlighted points corresponding to low degree of cure.

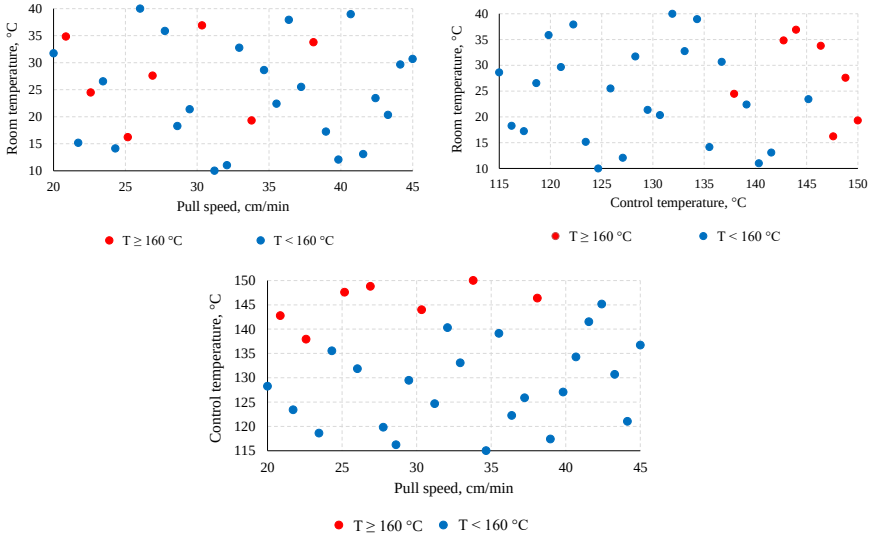

Fig. 3.22. 2D views of the plan of experiments with highlighted points corresponding to overheated resin.

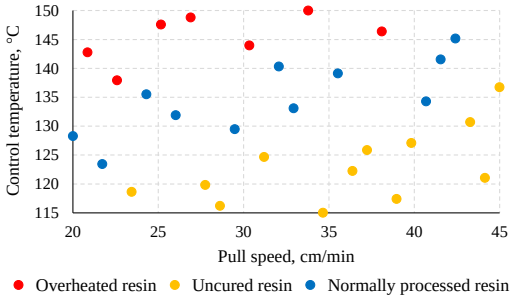

Fig. 3.23. 2D view of the plan of experiments with highlighted points corresponding to low degree of cure and overheated resin.

It is logical to exclude from the design space the points with the largest relative error. There are points with the low value of degree of cure ($\alpha < 0.5$). So, four experimental points (2, 13, 20 and 21) are excluded from the process of approximation for the degree of cure on profile surface and six experimental points (2, 5, 13, 20, 21 and 27) – from the process of approximation for the degree of cure on profile centreline.

Table 3.12.

Coefficients of third-order polynomial

Coef.	T_{surf}, °C	α_{surf}	T_{cent}, °C	α_{cent}	α_{surf}^{exit}	k_t
Const	-48.608	6.359272	2830.02	39.24108	34.486234	1.032543
V_{pull}	11.2343	-0.17794	18.7261	0.047855	0.3584979	-0.020623
T_{cont}	0.9365	-0.13188	-68.6766	-0.90763	-0.916195	-0.018441
T_{room}	-10.75	-0.23923	-12.2406	-0.34647	-0.040380	0.0026299
V_{pull}^2	0.1010	0.002105	0.4247	0.001772	0.0023382	0.0001172
$V_{pull} \times T_{cont}$	-0.2156	0.000280	-0.5231	-0.00354	-0.00694	0.0003043
$V_{pull} \times T_{room}$	-0.0593	0.001267	-0.0849	0.000381	0.0000830	-0.000164
T_{cont}^2	0.0157	0.001365	0.5965	0.007498	0.0080871	0.0001165
$T_{cont} \times T_{room}$	0.1665	0.003372	0.1913	0.005473	0.0005116	-0.000049
T_{room}^2	0.0348	0.000387	0.0570	0.000137	0.0002516	0.0000972
V_{pull}^3	-0.0003	0.000006	0.0009	0.000035	0.0000009	-0.000001
$V_{pull}^2 \times T_{cont}$	-0.0005	-0.00002	-0.0040	-0.00005	-0.000017	-0.000001
$V_{pull}^2 \times T_{room}$	0.0003	-0.00001	-0.0004	0.000010	-0.000003	0.0000011
$V_{pull} \times T_{cont}^2$	0.0009	0.000008	0.0029	0.000032	0.0000308	-0.000001
$V_{pull} \times T_{cont} \times T_{room}$	0.0003	-0.000005	0.0011	-0.00002	0.0000004	0.0000007
$V_{pull} \times T_{room}^2$	-0.0002	0.000004	-0.0001	0.000029	0.0000016	-0.000001
T_{cont}^3	-0.0001	-0.000005	-0.0017	-0.00002	-0.000023	-0.000001
$T_{cont}^2 \times T_{room}$	-0.0006	-0.000013	-0.0008	-0.00002	-0.000002	0.0000003
$T_{cont} \times T_{room}^2$	-0.0002	-0.000001	-0.0005	-0.000005	-0.000002	-0.000001
T_{room}^3	-0.0001	-0.000006	0.0001	-0.000007	-0.000001	0.0000008

The coefficients of new regression polynomials are given in

Table 3.14. Another errors of approximations describing their accuracy and reliability are summarised in Table 3.15. It is seen from Table 3.15. that no improvement of the quality of approximations has been reached eliminating some points with the low value of degree of cure for the first- and second-order polynomials. However, it is necessary to note that, eliminating some points, the accuracy and reliability of third-order regression equations have been increased. In addition to the selected second-order polynomials, an analysis of the significance of the design parameters presented in the approximation functions has been performed. Results of this analysis are given in diagrams presented in Figures 3.24.-3.29. These diagrams demonstrate that of the considered design parameters, the control temperature has the highest relative influence on the process conditions, the room temperature has the least, but the pull speed is in between.

Table 3.13.

Accuracy and reliability of approximations

Symbol, unit	σ_{cross}, %	R^2_{adj}	σ	σ, %	Δ_{max}, % (Point Nr.)
1st -order approximation					
$T_{surf,}$ °C	13.4	0.98	1.50	12.3	3.5 (28)
α_{surf}	49.7	0.79	0.11	45.8	41.7 (21)
$T_{cent,}$ °C	21.5	0.96	4.50	19.8	6.8 (6)
α_{cent}	56.5	0.73	0.17	52.4	88.1 (21)
α_{surf}^{exit}	14.6	0.98	0.04	13.5	9.3 (16)
k_t	11.5	0.99	0.003	10.6	5.0 (16)
2nd -order approximation					
$T_{surf,}$ °C	14.3	0.99	1.30	11.0	2.2 (28)
α_{surf}	17.9	0.98	0.03	14.6	26.6 (21)
$T_{cent,}$ °C	18.1	0.98	3.30	14.4	7.4 (21)
α_{cent}	33.4	0.93	0.09	27.3	200.0 (21)
α_{surf}^{exit}	14.5	0.99	0.03	12.0	31.3 (13)
k_t	8.8	0.99	0.002	7.3	2.2 (7)
3rd -order approximation					
$T_{surf,}$ °C	21.4	0.99	1.20	10.4	1.1 (13)
α_{surf}	34.9	0.99	0.04	18.9	19.5 (21)
$T_{cent,}$ °C	15.4	0.96	1.90	8.1	1.7 (21)
α_{cent}	66.5	0.88	0.11	35.2	200.0 (21)
α_{surf}^{exit}	3.1	0.99	0.004	1.7	1.6 (2)
k_t	14.4	0.99	0.002	8.4	2.2 (10)

Table 3.14.

Coefficients of polynomials after elimination of some points

Coef.	1st-order polynomials		2nd-order polynomials		3rd-order polynomials	
	α_{surf}	α_{cent}	α_{surf}	α_{cent}	α_{surf}	α_{cent}
Const	-0.58443	-0.37542	-9.66892	-9.428822	-43.3088	-65.5360
V_{pull}	-0.01046	-0.01332	-0.15739	-0.255681	-1.08128	-1.87115
T_{cont}	0.012884	0.012163	0.178614	0.1929395	1.112321	1.745203
T_{room}	0.0021294	0.001425	0.021313	0.0424421	0.135233	0.328566
V_{pull}^2	-	-	-0.00036	-0.000884	-0.00352	-0.02022
$V_{pull} \times T_{cont}$	-	-	0.001199	0.0020761	0.016052	0.033526
$V_{pull} \times T_{room}$	-	-	0.000258	0.0005038	0.002067	0.007039
T_{cont}^2	-	-	-0.00073	-0.000861	-0.00912	-0.01537
$T_{cont} \times T_{room}$	-	-	-0.00019	-0.000372	-0.00214	-0.00501
T_{room}^2	-	-	-0.00003	-0.000081	-0.00048	-0.00285
V_{pull}^3	-	-	-	-	-0.00002	-0.00005
$V_{pull}^2 \times T_{cont}$	-	-	-	-	0.000038	0.000164
$V_{pull}^2 \times T_{room}$	-	-	-	-	-0.000001	0.000042
$V_{pull} \times T_{cont}^2$	-	-	-	-	-0.000062	-0.00015
$V_{pull} \times T_{cont} \times T_{room}$	-	-	-	-	-0.000015	-0.00007
$V_{pull} \times T_{room}^2$	-	-	-	-	0.000004	0.000012
T_{cont}^3	-	-	-	-	0.000025	0.000045
$T_{cont}^2 \times T_{room}$	-	-	-	-	0.000009	0.000023
$T_{cont} \times T_{room}^2$	-	-	-	-	-0.000001	0.000011
T_{room}^3	-	-	-	-	0.000007	0.000012

Table 3.15.

Accuracy and reliability of approximations after eliminations of some points

Symbol, unit	σ_{cross}, %	R_{adj}^2	σ	σ, %	Δ_{max}, % (Point Nr.)
		1st-order approximation			
α_{surf}	59.8	0.70	0.09	54.4	24.7 (27)
α_{cent}	79.1	0.49	0.13	71.2	46.1 (17)
		2nd-order approximation			
α_{surf}	20.7	0.97	0.03	16.3	3.6 (11)
α_{cent}	52.3	0.86	0.07	37.9	15.6 (17)
		3rd-order approximation			
α_{surf}	22.4	0.99	0.02	9.6	3.2 (27)
α_{cent}	24.8	0.99	0.01	8.1	1.4 (3)

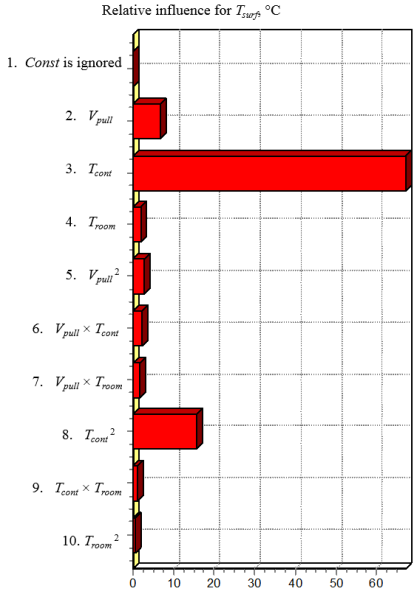

Fig. 3.24. Significance analysis for the maximal temperature on profile surface.

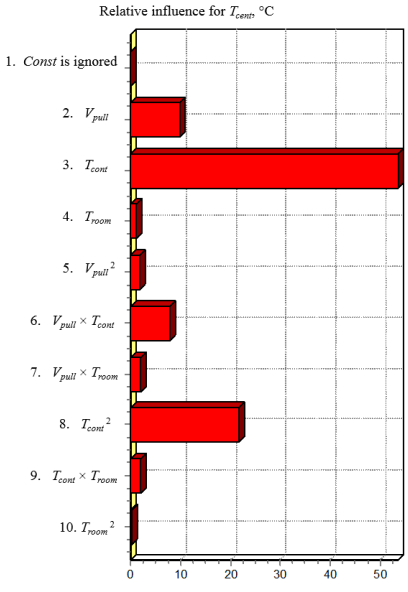

Fig. 3.25. Significance analysis for the maximal temperature on profile centreline.

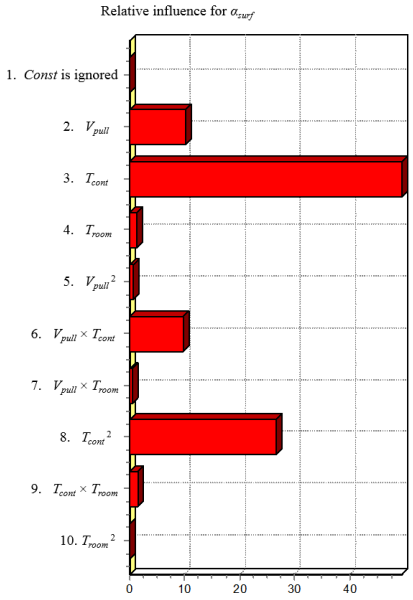

Fig. 3.26. Significance analysis for the degree of cure on profile surface.

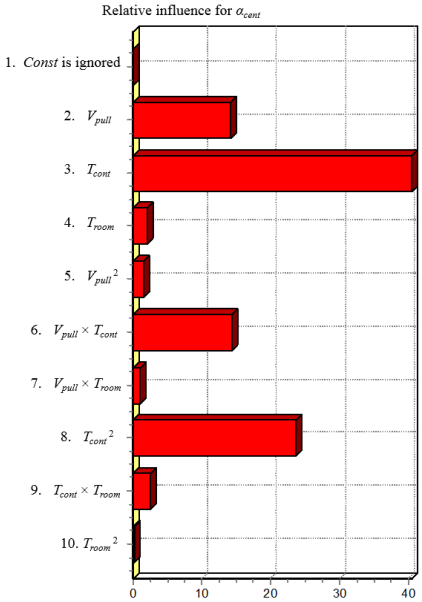

Fig. 3.27. Significance analysis for the degree of cure on profile centreline.

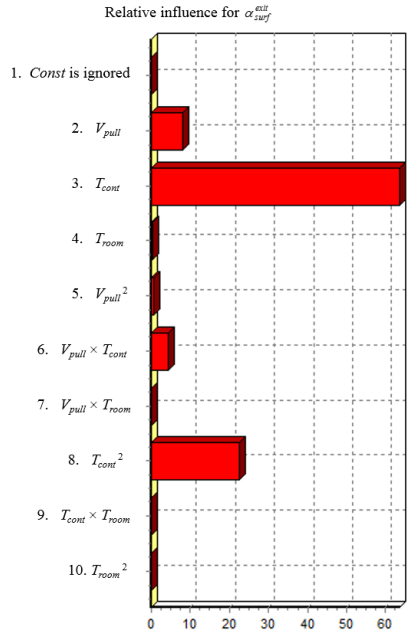

Fig. 3.28. Significance analysis for the degree of cure on profile surface at die exit.

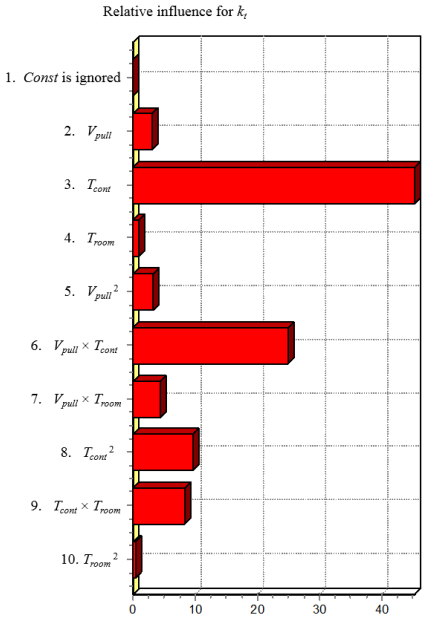

Fig. 3.29. Significance analysis for the relative time on heaters work.

Eventually, an optimisation problem with second-order polynomials for two objective functions (Equations (3.13)-(3.14)) is solved using the generalised reduced gradient nonlinear algorithm embedded in *Microsoft Excel © Solver*. The optimal parameters of the designed pultrusion process have been obtained for both objective functions. They are presented in Table 3.16. Process is more efficient at higher ambient temperatures.

The optimal results are validated by the finite element solution at optimal point (Table 3.17). Very good agreement is observed between the optimal and finite element solutions. The temperature and degree of cure distribution in the composite profile for the optimal point is presented in Figures 3.30. and 3.31. respectively.

Table 3.16.

Optimal design parameters

	Min value	Max value	Optimal
Pull speed, cm/min	20	45	45
Room and resin temperature, °C	10	40	40
Control temperature on electrical heaters, °C	115	150	142

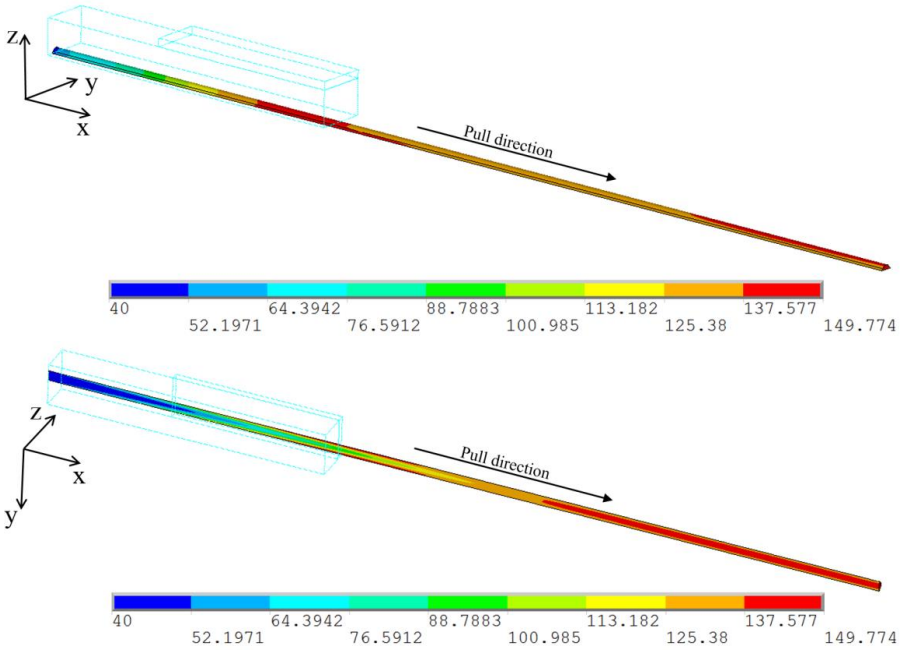

Fig. 3.30. Temperature distribution for optimal solution (view from different angles).

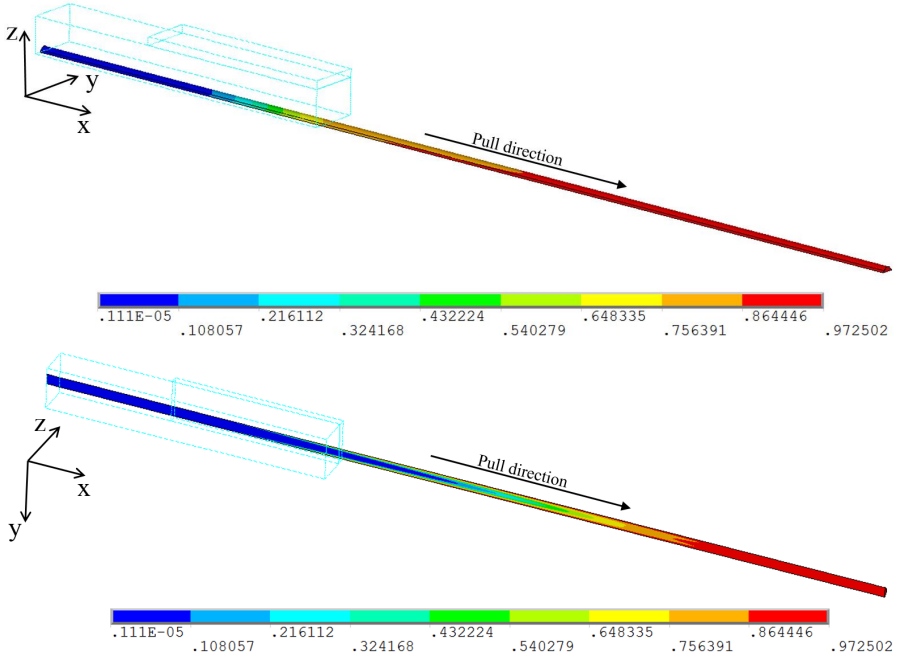

Fig. 3.31. Degree of cure distribution for optimal solution (view from different angles).

Table 3.17.

Validation of optimal results

	Optimisation	FE analysis	Difference, %
Maximal temperature on profile surface, °C	149.5	149.8	0.2
Minimal degree of cure on profile surface	0.96	0.96	0
Maximal temperature on profile centreline, °C	146.2	147.0	0.5
Minimal degree of cure on profile centreline	0.95	0.97	2.0
Minimal degree of cure on profile surface at die exit	0.73	0.74	1.4
Energy consumption, W/m	16.2	16.2	0

3.2.5Technological map

The technological map based on regression polynomials has been developed in *EXCEL* environment for an effective design of two rods pultrusion process. An interface of this *EXCEL* tool is presented in Figure 3.32. and it consists of two major sections:

- calculation of process conditions (temperatures and degrees of cure in the composite profile, and process energy consumption) for the defined process parameters, and ambient room and resin temperature (fixed pull speed, heaters control temperature and room temperature),
- optimisation of process parameters by minimisation of energy consumption (Equation (3.13)) or maximisation of pull speed (Equation (3.14)) taking into account previously defined constrains of the process conditions (Table 3.8). It is necessary to note that some parameters in the optimisation process could be examined as constant values.

Availability of COMPOR technological map for the examined pultrusion process (Figure 3.33.), has allowed to estimate an effectiveness of the optimised process. It is necessary to note that parameters of the pultrusion process are the constant values for different room and resin temperatures in the COMPOR technological map.

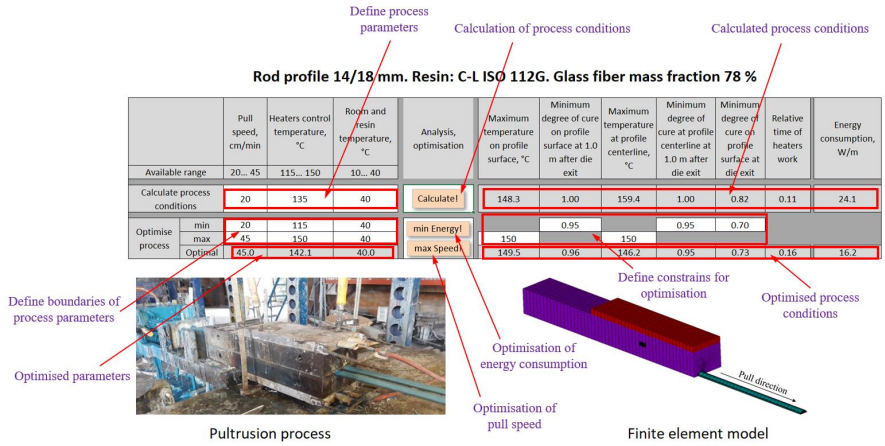

Fig. 3.32. Interface of the developed technological map.

To follow industrial shop conditions, the optimisation problem has been solved repeatedly for different ambient room temperatures. The process optimised parameters are presented in Table 3.18. together with the results obtained by the regression equations using an information from COMPOR technological map. It is clearly seen that using COMPOR technological map the profile resin is fully cured, but overheated in the centre of cross-section for all examined room temperatures. Applying the developed optimisation methodology, it is possible to avoid an overheating of the resin preserving the profile quality in the same time. Moreover, it is possible to increase the pull speed of the technological process by 50 - 125% and to reduce the energy consumption by 20 – 33% per 1 meter of pultruded profile depending on the ambient room temperature. By this way, an application of the developed optimisation methodology has allowed to increase considerably the productivity and effectiveness of the examined pultrusion process.

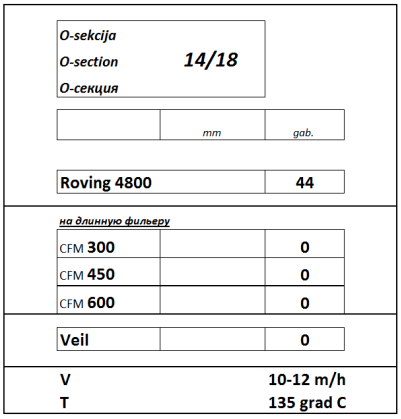

Fig. 3.33. COMPOR technological map.

Table 3.18.

Comparison of process parameters obtained by COMPOR and optimised technological maps for different room temperatures

	COMPOR technological map				**Optimised technological process**			
Pull speed, cm/min	20				29.9	35.4	39.9	45.0
Control temperature of electrical heaters, °C	135				138	141	142	142
Room and resin temperature, °C	**10**	**20**	**30**	**40**	**10**	**20**	**30**	**40**
Maximal temperature on profile surface, °C	146	146	147	148	147	150	150	150
Minimal degree of cure on profile surface	1.00	1.00	1.00	1.00	0.97	0.97	0.97	0.96
Maximal temperature on profile centreline, °C	161	161	161	159	150	150	148	146
Minimal degree of cure on profile centreline	1.00	1.00	1.00	1.00	0.95	0.95	0.95	0.95
Minimal degree of cure on profile surface at die exit	0.82	0.82	0.82	0.82	0.77	0.79	0.77	0.73
Energy consumption, W/m	**33.4**	**30.3**	**27.2**	**24.1**	**26.7**	**22.6**	**19.3**	**16.2**

4. DEVELOPMENT OF ADVANCED PULTRUSION PROCESSES

4.1. Simulation of microwave assisted pultrusion

An application of the developed finite element models and algorithms is demonstrated by a development of real microwave assisted pultrusion process producing rod profile with the diameter of 16 mm (Figure 4.1.). The scheme of this innovative process is presented in Figure 4.2. and it consists of steel die with the length of 950 mm and cross-section dimensions of 54 x 60 mm, and microwave block attached to the die and consisting of the ceramic inlet (zirconium dioxide) and waveguide. Dielectric and thermal material properties of steel and ceramic dies, composite and its constituents as well as surrounding air are presented in Table 2.1. and Appendix 6 respectively. The rate of resin reaction is described by using the Kamal-Sourour curing kinetic model (Equation (2.23) with the parameters given in Table 4.1. For a generation of microwaves, the magnetron with frequencies of 915 MHz and 2.45 GHz is used.

The electromagnetic finite element model is built in *ANSYS* by using high frequency electromagnetic finite elements HF120. This is a first-order hexahedral element formulation with one degree of freedom – tangent component of electric field (AX) on each edge. A rectangular port with the applied energy of 1 W at the top of waveguide and TE_{10} mode is used.

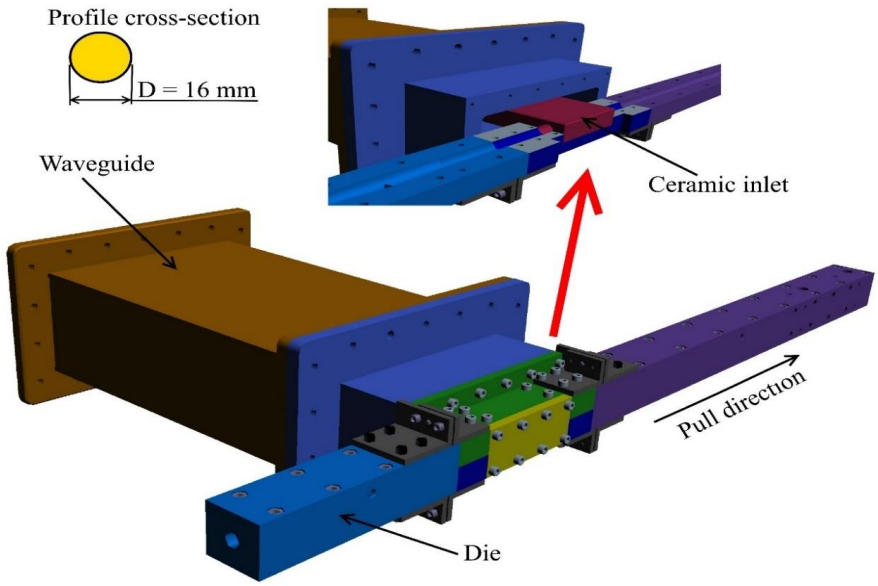

Fig. 4.1. Microwave assisted pultrusion process.

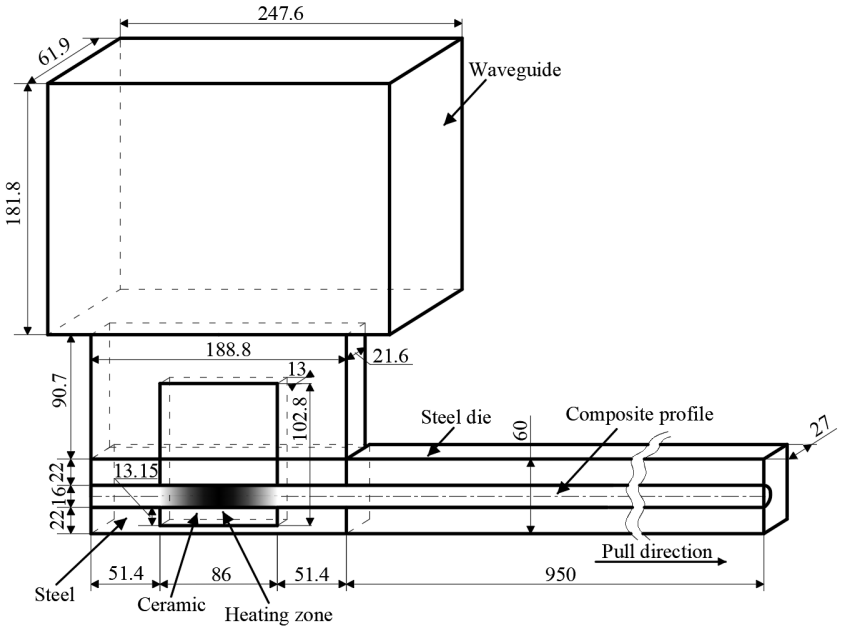

Fig. 4.2. Scheme of microwave assisted pultrusion process (symmetry used).

Perfect electric conductor (PEC) or electric wall boundary conditions (AX = 0) are applied to all surfaces of waveguide since it is made of steel. Steel die is separated from another parts (air, ceramic, composite) by PEC boundary conditions since electric field does not propagate in the steel. It means that steel die does not participate in the electromagnetic analysis in fact, but it is modelled to keep the finite element model with the same node and element numbering in the thermo-chemical analysis. Due to a symmetry of the examined problem, only one half of the pultrusion set-up is modelled and PEC boundary conditions are applied to a symmetry plane. The corresponding electromagnetic finite element model is presented in Figure 4.3.

Convergence study is carried out by using the finite element model presented in Figure 4.3. with 5 different meshes. The models 1 – 4 from Table 4.1. are created as

Table 4.1.

Kinetic parameters of resin Polres 3056BV

Parameter	Symbol (unit)	Polres 305BV
Heat reaction	H_{tr}, (J/kg)	323074
Frequency factor	K_1 (s^{-1})	$1.43 \cdot 10^{10}$
Frequency factor	K_2 (s^{-1})	285.870
Activation energy	E_1 (J/mol)	85573
Activation energy	E_2 (J/mol)	33141
Order of the reaction	n	2.342
Order of the reaction	m	0.519

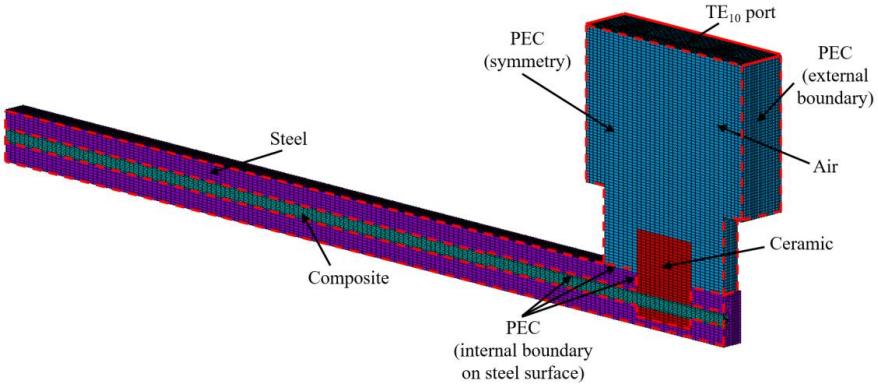

Fig. 4.3. Electromagnetic finite element model with applied materials and boundary conditions.

usable for a pultrusion analysis, but model 5 with a fine mesh – just to estimate the results of convergence study.

The parameters of finite element models are given in Table 4.2. together with the energy absorbed in composite material and ceramic die, results of electromagnetic analysis for different finite element meshes are presented in Table 4.3., but distributions of electric and absorbed energy fields along profile centreline are demonstrated in Figure 4.4. and Figure 4.5. It is seen that model 1 built using less number of finite elements can be used for a subsequent electromagnetic analyses since the difference in comparison with the model 5 having a finer mesh is lower than 4% in absorbed energy obtained for the composite profile and ceramic.

To verify the results of electromagnetic analysis obtained in *ANSYS*, the finite element model for the same microwave assisted pultrusion process has been developed and analysed in *COMSOL Multiphysics*.

Table 4.2.

Convergence study

Model	FE length in pull direction, mm	Max dimension of FE in cross-section, mm			Number of FE in pull direction	Number of FE in half of comp. cross-section	Total number of FE	Energy absorbed in comp. profile, %	Energy absorbed in ceramic, %
1	7.25	2.2	4.0	3.3	157	48	99501	7.4	7.7
2	7.25	1.4	3.8	3.3	157	70	104525	7.4	7.8
3	4.63	2.2	4.0	3.3	246	48	141357	7.4	7.6
4	4.63	1.4	3.8	3.3	246	70	149229	7.4	7.8
5	4.63	1.1	2.1	1.7	246	122	524567	7.6	8.0

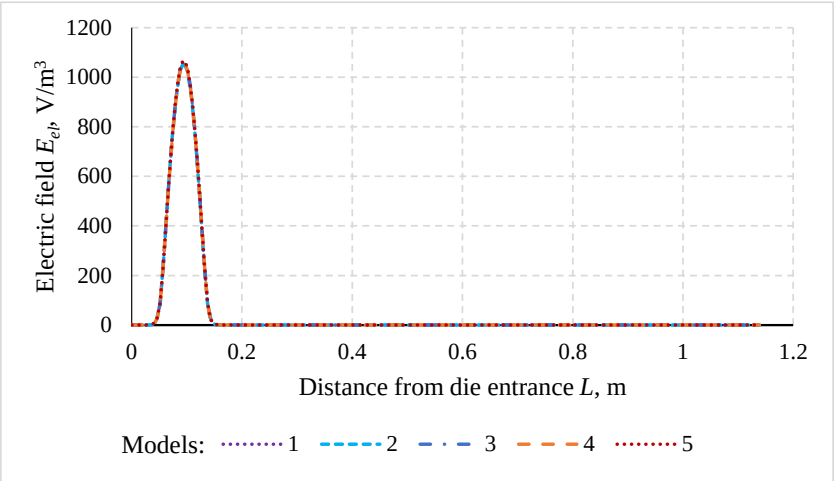

Fig. 4.4. Distribution of electric field along profile centreline for different finite element meshes.

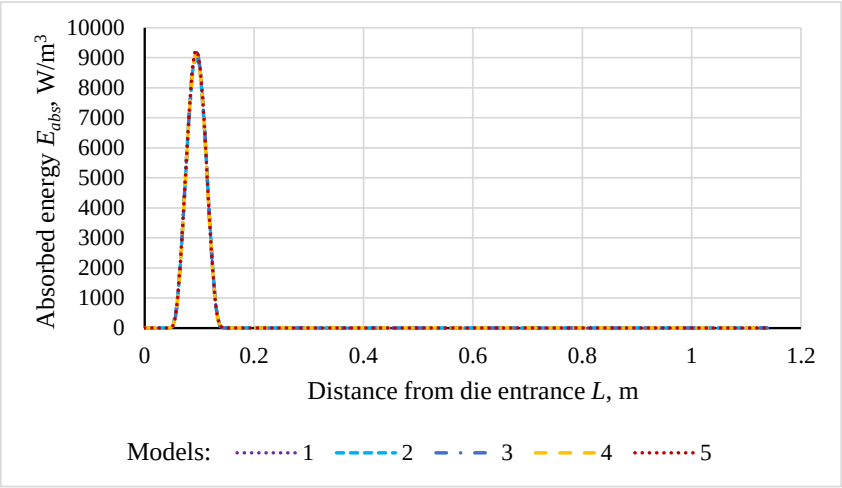

Fig. 4.5. Distribution absorbed energy field along profile centreline for different finite element meshes.

The finite element models and results of electromagnetic analysis are given in Table 4.5., but distribution of the electric and absorbed energy fields along profile centreline is presented in Figure 4.6. and Figure 4.7. It is seen that no difference is observed between results obtained by different finite element software: *ANSYS* and *COMSOL Multiphysics*. This talks about high reliability of the developed electromagnetic finite element model and algorithm.

Unfortunately, a building of the thermo-chemical finite element model by a simple replacement of the developed electromagnetic finite element model and using 3-D

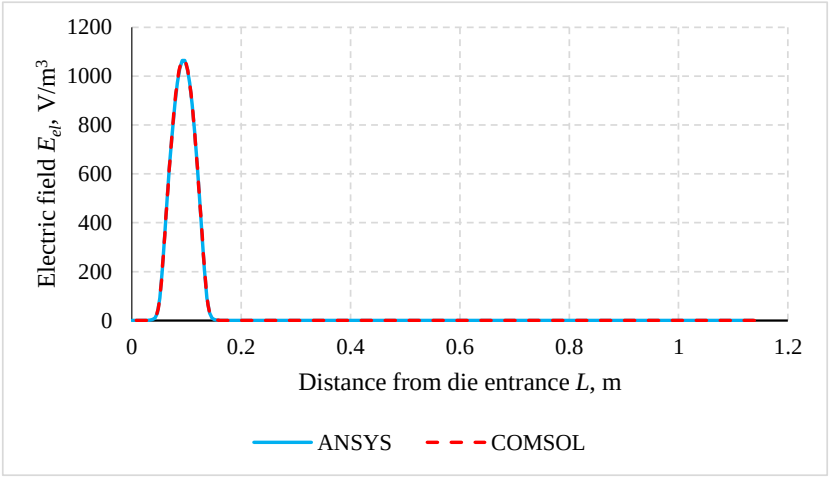

Fig. 4.6. Distribution of electric field along profile centreline calculated by *ANSYS* and *COMSOL*.

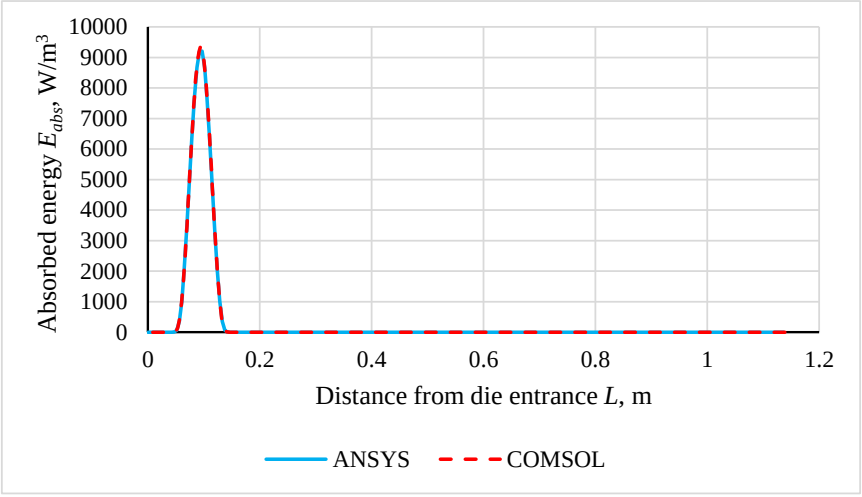

Fig. 4.7. Distribution of absorbed energy field along profile centreline calculated by *ANSYS* and *COMSOL*.

thermal solid finite elements Solid 70 is difficult due to impossibility to model a convective mass transfer of air in *ANSYS APDL*. For this reason, the waveguide air is excluded from the thermo-chemical model and convection boundary conditions with the heat transfer coefficient of 10 W/(m2 °C) are applied to contact surfaces of waveguide air and ceramic/steel parts of pultrusion set-up to simulate a heat exchange between pultrusion tool and air inside the waveguide. The modified finite element model is presented in Figure 4.8., but the results of the thermo-chemical analysis are

given in Appendix 7. It is seen that the resin is not overheated. However, no guarantee exists for the resin no flow from the die exit since the degree of cure a little bit lower than desirable. Moreover, a little bit non-homogeneous curing field with the values lower than desirable is observed for the profile cross-section leaving the die. It is necessary to note also that due to the high temperature of the ceramic inlet, the conduction heating from the ceramic die prevails over the heating caused by dielectric losses in composite material.

Results of thermo-chemical analysis presented in Appendix 7 show that the die length can be shortened without any losses for the pultrusion process. This will contribute to a reduction of costs necessary for the pultrusion die production (less material) and high precision treatment of working surfaces. The length of steel die is decreased in 5 times (from 950 to 190 mm) that leads to the total length reduction of pultrusion set-up in 3 times (from 1138.8 to 378.8 mm). To investigate the curing process in profile leaving the die, its length is not changed. Results of this analysis are presented in the first column of Appendix 8. It is seen that the die length reduction does not change a distribution of the temperature and degree of cure in pultruded profile. Moreover, it is seen in Figure 4.9. that curing process in the shorter steel die is faster due to an absence of additional thermal losses in a massive die.

The results of Appendix 8 show that the resin is not overheated, could flow from the die exit and the final degree of cure distribution is homogeneous but with the values which are less than desirable. To overcome these problems, the parametric study has been executed and one of the possible solutions satisfying all the taken constraints on the process is presented in the second column of Appendix 8.

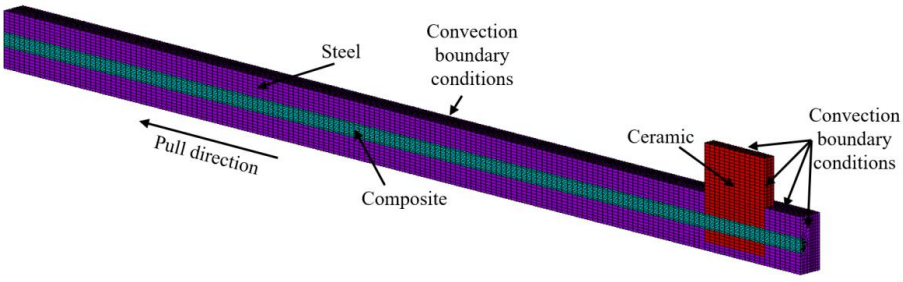

Fig, 4.8. Thermo-chemical FE model with applied materials and boundary conditions.

Table 4.3.

Results of electromagnetic analysis for different finite element meshes

	Model	Electric field, E_{el}, V/m	Absorbed energy field, E_{abs}, W/m^3
1	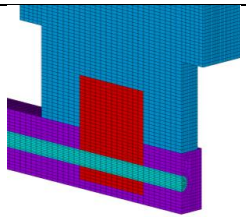	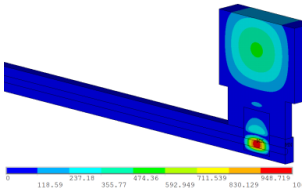	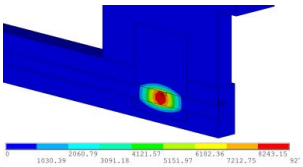
2	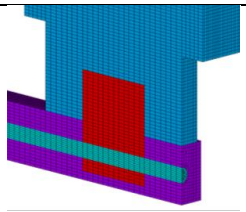	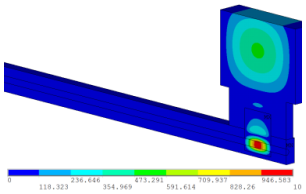	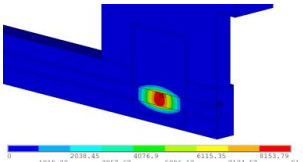
3	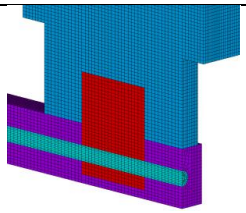	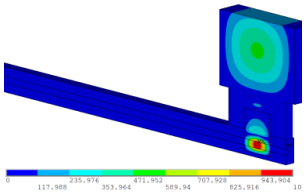	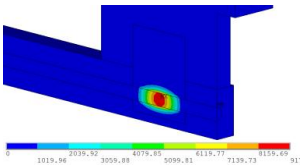
4	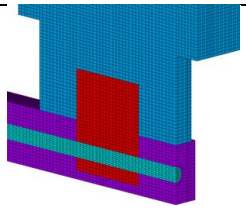	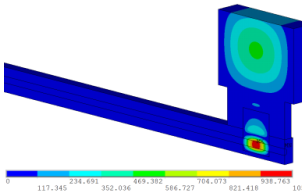	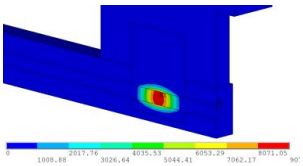
5	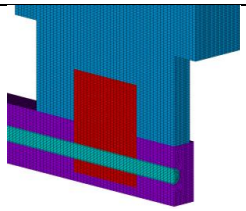	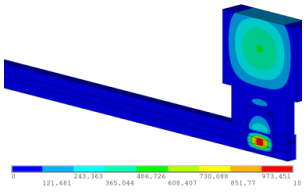	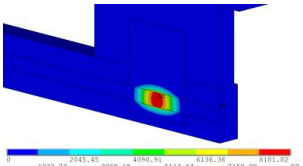

Table 4.4.

Comparison of *ANSYS* and *COMSOL* results.

ANSYS	*COMSOL Multiphysics*
Finite element models (only half has been analysed in ANSYS)	
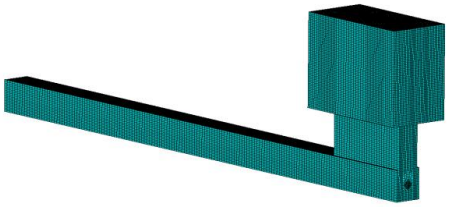	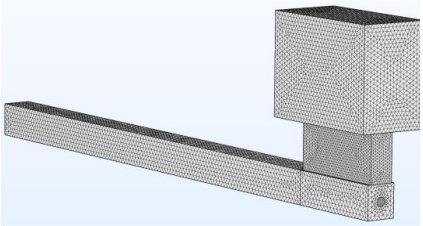
Electric field, E_{el}, V/m	
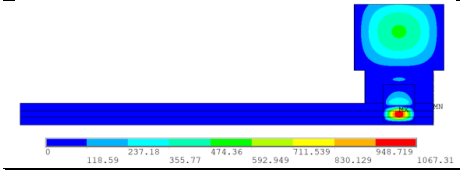	
Absorbed energy field, E_{abs}, W/m^3	
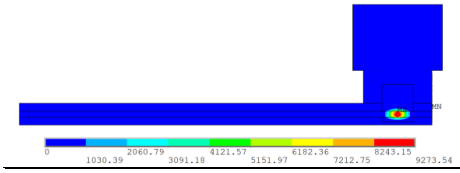	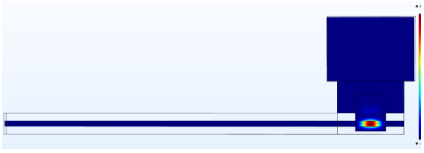
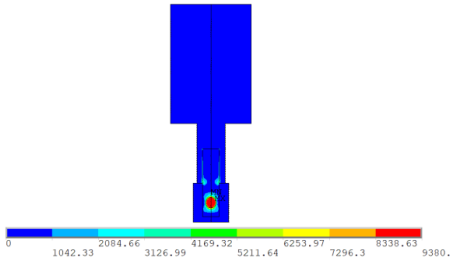	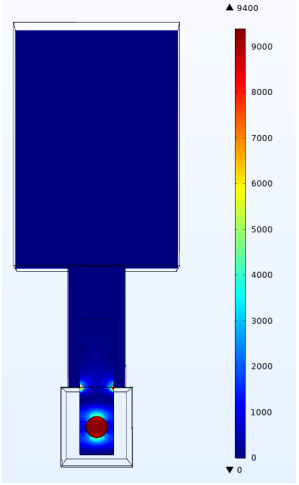

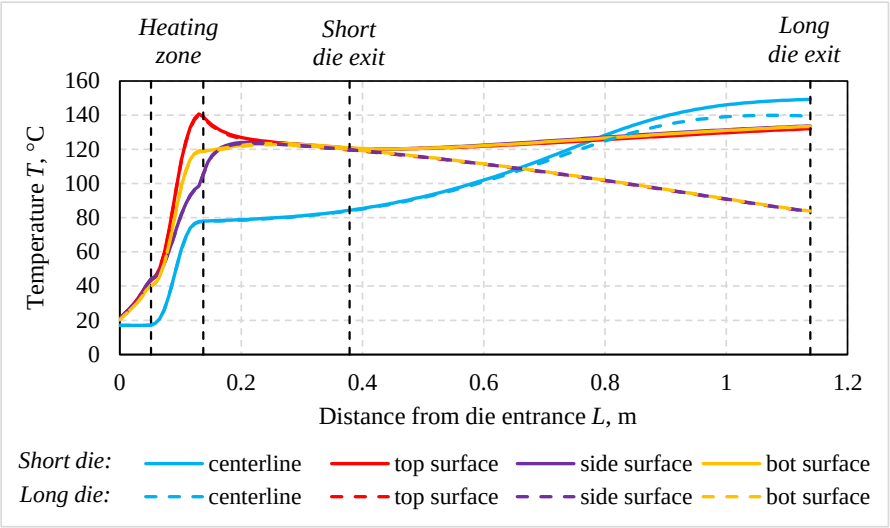

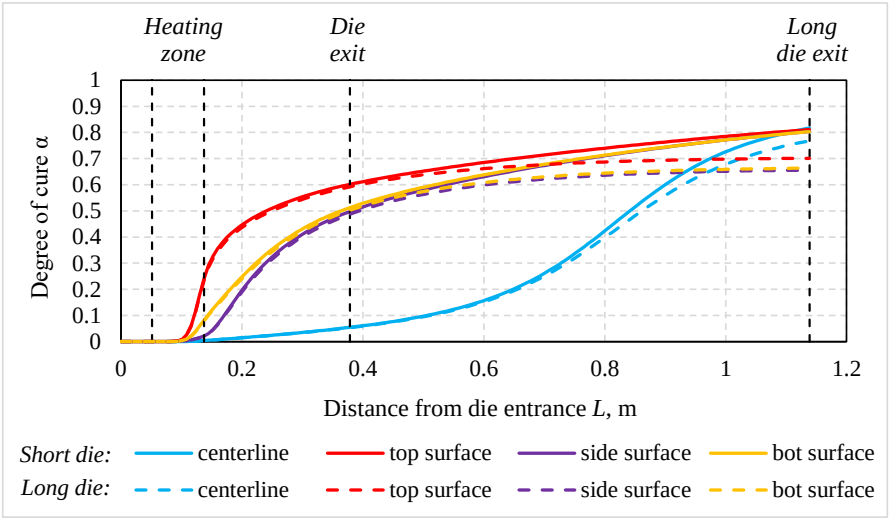

Fig. 4.9. Distribution of temperature and degree of cure along profile for the steel dies with different length.

To increase an effectiveness of the microwave assisted pultrusion process examined above, a magnetron with the higher frequency can be applied. This leads to a proportional increase of the absorbed energy in composite material (Equation (2.10)). Then electromagnetic analyses for the ceramic dies made of different materials have been executed by using simplified (without examination of steel die) electromagnetic finite element model (Figure 4.10.).

Their results are presented in Table 4.4. It is seen that the microwave block initially designed for a zirconium ceramic and operating frequency of 915 MHz is not directly suitable for other materials and frequendcies. Since the ceramic block made of boron nitride at frequency of 2.45 GHz demonstrates highest effectiveness and good homogeneity, it is chosen for a subsequent electromagnetic analysis. An amount of absorbed energy in composite material can be increased in this case by a slight modification of microwave block dimensions.

Scheme of the modified ceramic block is presented in Figure 4.11. The parametric study has been carried out with two design parameters: location of the hole for pultruded profile H_1 and high of the ceramic block H. Results of electromagnetic analysis with the modified ceramic block dimensions are presented in Table 4.6. So, varying location of the hole for a pultruded profile (reduction of H_1), more symmetrical absorption energy field in the composite material has been obtained. An increase of the high of ceramic block H has contributed to a considerable growth of absorbed energy field in the composite material without collapse of symmetry. The final distribution of the absorbed energy field is presented in Figure 4.12. for the case when H = 110 mm and H_1 = 9 mm.

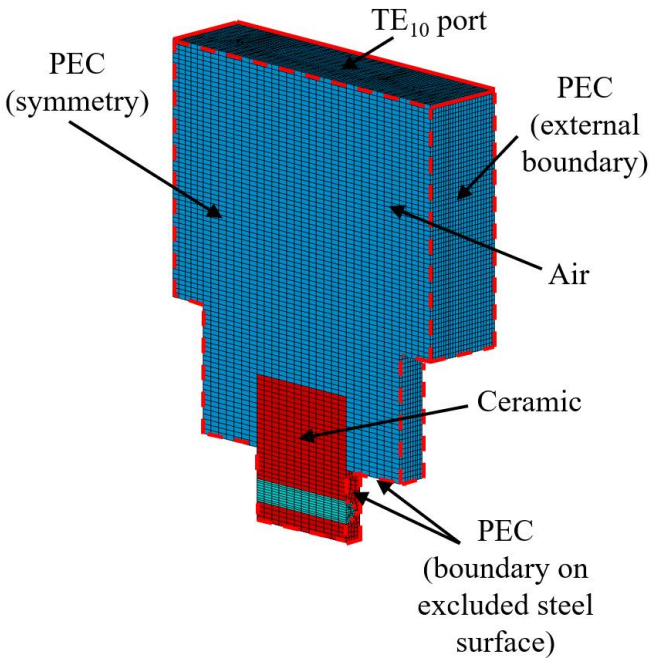

Fig. 4.10. Simplified electromagnetic finite element model with applied materials and boundary conditions.

Table 4.5.

Results of electromagnetic analysis for the ceramic dies made of different materials

Frequency, GHz	Ceramic material	Electric field E_{el}, V/m	Absorbed energy field, E_{abs}, W/m^3	Energy absorbed in comp., %	Energy absorbed in die, %
0.915	Zirconium dioxide	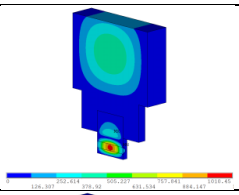	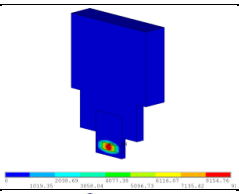	7.4	7.7
	Quartz glass	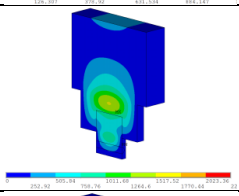	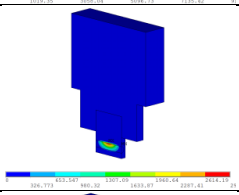	1.6	0.02
	Boron nitride	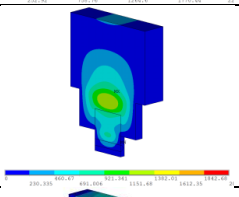	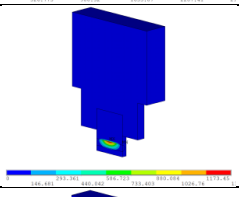	0.7	0.02
2.45	Zirconium dioxide	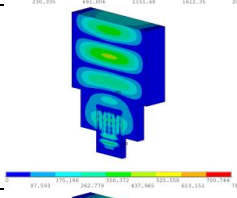	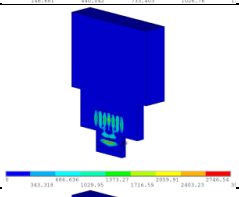	0.8	8.0
	Quartz glass	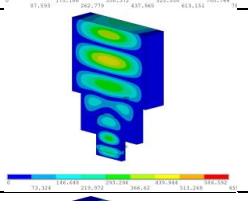	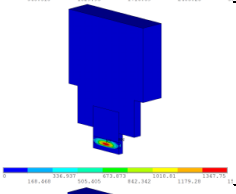	1.1	0.01
	Boron nitride	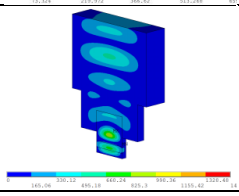	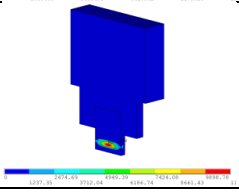	8.6	0.02

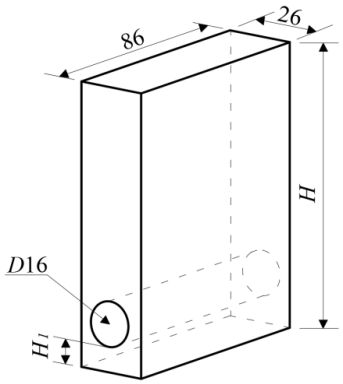

Fig. 4.11. Modified ceramic block.

Table 4.6.

Results of electromagnetic analysis with the modified ceramic block

H, mm	*H1*, mm	Electric field E_{el}, V/m	Absorbed energy field, E_{abs}, W/m^3	Energy absorbed in comp., %
102.8	11.0	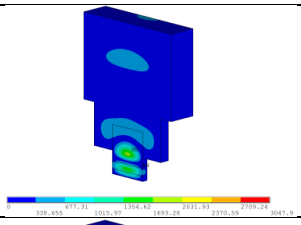	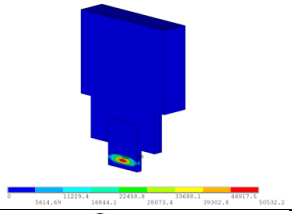	41.0
102.8	9.0	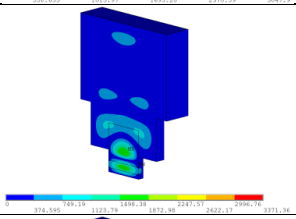	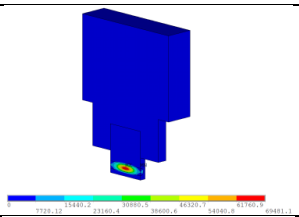	57.0
110.0	9.0	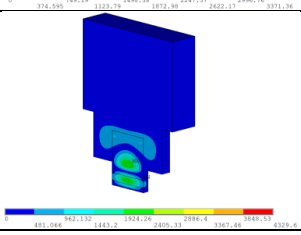	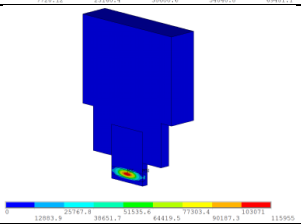	95.5

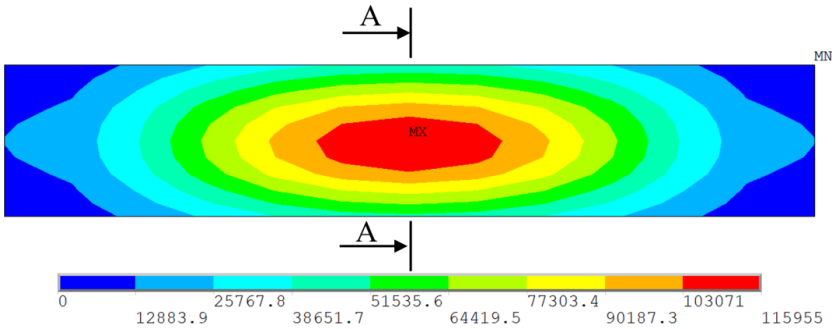

a

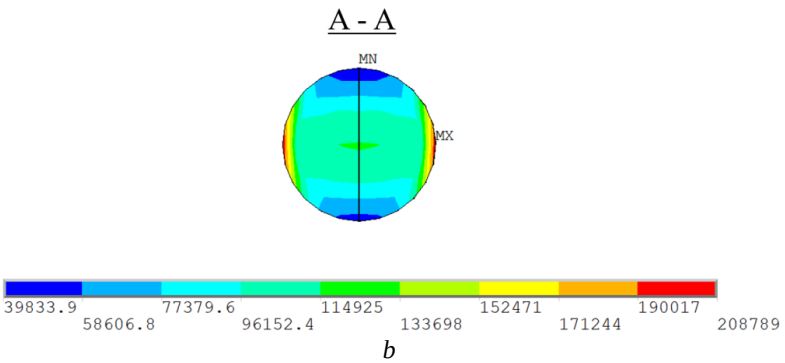

b

Fig. 4.12. Distribution of the absorbed energy: *a* – profile longitudinal-section, *b* – profile cross-section.

The results of thermo-chemical analysis for the modified pultrusion set-up are presented in the first column of Appendix 9. It is seen that resin is not overheated and profile is already fully cured at die exit. However, an effectiveness of the developed microwave assisted pultrusion process can be improved by a reduction of the applied microwave energy (850 W), preserving the quality of pultruded profile and satisfying to all the constraints taken for the pultrusion process. Additional results are presented in the second column of Appendix 9. It is necessary to note that homogeneous curing fields (first case: 0.98 … 0.99, second case: 096 … 0.98) have been finally obtained despite on the inhomogeneous but symmetrical absorbed energy field (Figure 4.12.) used in the analyses.

Finally, more effective microwave assisted pultrusion process has been analysed additionally using temperature-dependent dielectric properties of the composite material (Figure 2.3.). For a simulation the coupled electro-magnetic-thermo-chemical algorithm presented in Figure 2.11. has been used. Results are presented in Appendix 10. It is seen that resin is a little bit overheated (275 °C) now. To avoid overheating, an applied microwave energy has been reduced to 550 W preserving the quality of pultruded profile (homogeneous degree of cure field: 0.96 … 0.98).

4.2. An effectiveness evaluation

An effectiveness of the developed microwave assisted pultrusion processes has been estimated in comparison with the real conventional pultrusion process [76] which has been successfully verified experimentally under the ambient room temperature of 17°C. The results demonstrating productivity (dependent on pull speed) and effectiveness (dependent on energy consumption) are presented in Table 4.7. for both technological processes. It is necessary to note that the productivity and effectiveness of the real conventional process has been taken as 100 %. Results in Table 4.6. show that by using magnetron with the high frequency of 2.45 GHz it is possible to increase a productivity of the pultrusion process more than in 5.5 times but an effectiveness - almost until 3 times. An application of magnetron with the lower frequency of 915 MHz has allowed only to improve a productivity more than in 3 times but the energy consumption has been considerably increased. By this way to develop an effective microwave assisted pultrusion process with a high productivity, the magnetrons with high frequency of 2.45 GHz should be recommended.

It is necessary to note that high effectiveness and productivity of microwave assisted pultrusion processes have been obtained without their optimisation. An application of optimisation could improve these values additionally.

Table 4.7.

An effectiveness of microwave assisted pultrusion process

Product Pultrusion	Rod with diameter of 16 mm made of polyester resin POLRES 305BV (v_f = 45%) and glass fibres 4800 tex (v_f = 55%)					
	Conventional [82]	Microwave assisted				
Schemes or finite element models	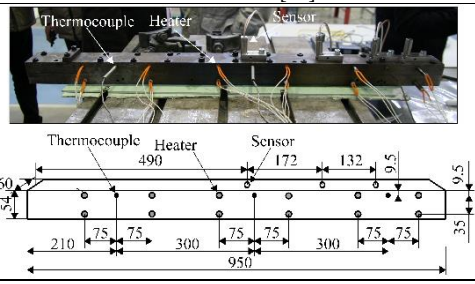	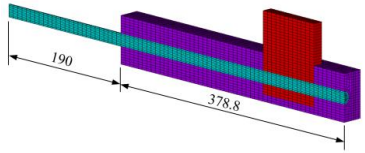		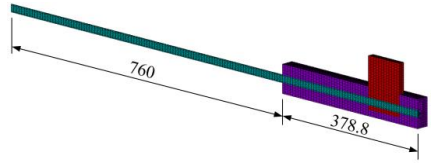		
Dielectric properties of resin taken in simulation	Constant	Constant		Constant		Temperature dependent
Heating system	12 electrical heaters, 315 W each	Magnetron: 915 MHz, 5290 W Ceramic block: zirconium dioxide		Magnetron 2.45 GHz Ceramic block: boron nitride		
				1000 W	850 W	850 W	550 W
Heating system operating mode	Controlled by proportional-integral-derivative controller (automatically switches ON and OFF)	Continuous (always ON)				
Pull speed, cm/min	18	59		100		
Energy consumption of steady-state process, W/m	24.8	149.4		16.7	14.2	14.2	9.2
Productivity, %	100	327.8		555.6		
Effectiveness, %	100	602.4		67.3	57.3	57.3	37.1

5. CONCLUSIONS

The investigations presented in Thesis have been carried out in order to improve an effectiveness and productivity of conventional pultrusion processes preserving the quality of pultruded profiles and to reduce their cost. An application of the developed non-direct optimisation methodology based on the planning of experiments and response surface technique and holistic simulation tools developed for the design of innovative microwave assisted pultrusion processes has allowed to increase considerably effectiveness and productivity of existing conventional pultrusion processes operating in industrial and laboratory shops. The main conclusions from the obtained results of the Thesis:

1. The analysis of scientific literature review has shown that less studies are conducted on advanced microwave pultrusion processes and their simulations compared to the conventional pultrusion processes. Systematic optimisation procedures are used to provide a better quality of pultruded profiles, but still the impact of an industrial shop temperature and curing process allowed behind the die have not been examined yet.
2. New electro-magnetic-thermo-chemical finite element models and algorithms have been developed for a holistic simulation of microwave assisted pultrusion processes, as well as for the pultrusion tooling design and process control. For this purpose, the general-purpose finite element software *ANSYS* has been used that results in considerable saving in development time and costs, and also makes available various modelling features of the finite element packages. This has allowed to solve coupled electromagnetic-thermo-chemical problem with temperature dependent dielectric material properties. The parametric study confirms that microwave assisted pultrusion processes operate with high speed (fast curing) and their working temperatures are higher than occur in the conventional pultrusion processes. For this reason, resins with high dielectric losses and high destruction temperatures are the best choice for this application. Moreover, they should be tested by DSC machines in higher speeds than used previously for conventional pultrusion processes. It is important to note that all the finite element models and algorithms developed in the present study have been successfully validated by the results obtained by authors in some specialized software (*COMSOL Multiphysics*), experimentally or using open literature.
3. New optimisation problems have been formulated based on results of parametric study taking into account all the required parameters of the industrial pultrusion processes. Non-direct optimisation methodology based on the planning of experiments and response surface techniques has been successfully developed for the design of conventional pultrusion processes. This approach has allowed to evaluate the effectiveness and productivity of industrial

pultrusion processes with the temperature control by the heaters switch-on and-off strategy. In this way, more realistic values of electrical energy spent on heating the die have been obtained. Allowing the resin to cure outside the pultrusion die has allowed to developed more effective pultrusion process. However, in this case an exothermic chemical reaction is transferred to the die exit and additional constraint must be introduced into formulated optimisation problem. This is minimal degree of cure of the composite material at die exit. This limitation guarantees that resin at the die exit does not flow and it is in a solid state.

4. The present optimal solutions have been obtained for the existing pultrusion dies used now in the industrial shop. In this study no possibility has existed to change the dies' design. However, highest effectiveness of the technological process could be obtained for a joint optimal design of the die and process itself, and for the resin chosen in initial stage. In this case it is possible to save additionally an expensive steel material used for the production of pultrusion die and to reduce high costs of its treatment.
5. New interactive technological map using non-direct optimisation methodology has been developed for the examined technological process. It not only allows to define the process conditions (temperature and degree of cure in composite profile) for the fixed process parameters and ambient room temperature, but also to minimise the energy consumption or to maximise the pull speed for an actual ambient temperature in industrial shops. An application of the developed technological map has demonstrated a considerable improvement of the process effectiveness and productivity in comparison with an existing technological map used now in the industrial shop. To increase an operating speed of the developed technological map, the generalised reduced gradient nonlinear algorithm has been applied for the solution of formulated optimisation problems. This is done with the purpose to use these technological tools in all possible computers even with slow CPU speed. However, it is necessary to remember that in this case the optimal solutions in some problems could be highly dependent on the initial conditions and the obtained solution may not be optimised globally.
6. Evaluation of the developed microwave assisted pultrusion process in comparison with the real conventional pultrusion process verified experimentally has demonstrated its considerable productivity (more than 5.5 times) and effectiveness (almost until 3 times) preserving high quality of pultruded profiles.

The results presented in Thesis are the part of the European Regional Development Fund (ERDF), project No. 1.1.1.1/18/A/053 "An effectiveness improvement of conventional pultrusion processes". The aim of the project is an improvement of the effectiveness of conventional pultrusion processes preserving the quality of pultruded

profiles and considerably reducing their cost as well as contributing to a healthier environment.

For the future investigations, in order to preserve the quality of pultruded profiles and evaluate the structural behaviour and geometrical precision, the thermo-mechanical finite element model and algorithm should be developed to calculate the process stresses and deformations.

APPENDICIES

Appendix 1

Electric and absorbed energy fields for zirconium dioxide die

Diameters of ceramic die *D*cer, mm	Electric field *E*, V/m	Absorbed energy field *Q*, W/m^3	Energy absorbed in composite %	Energy absorbed in die %
24	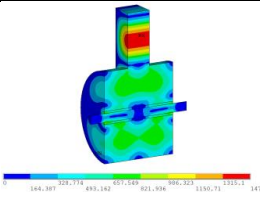	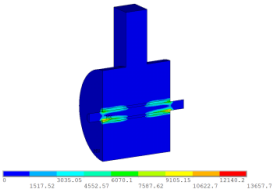	5.43	5.65
32	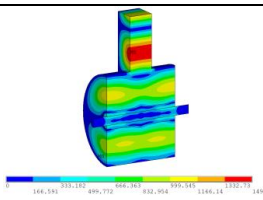	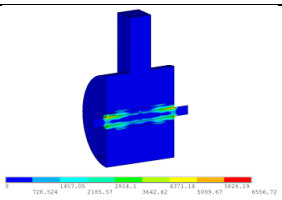	3.17	4.43
40	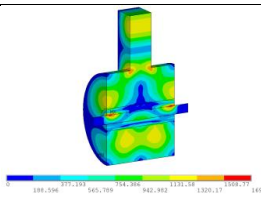	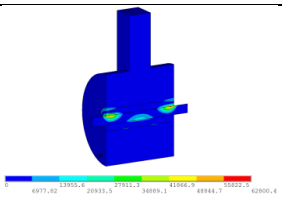	28.1	27.8
40.6	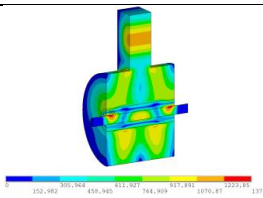	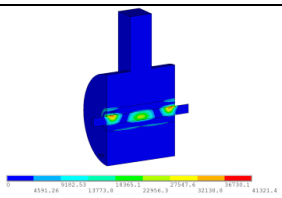	37.1	32.3
40.8	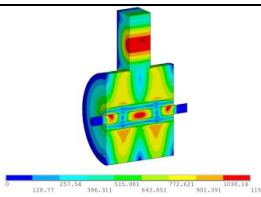	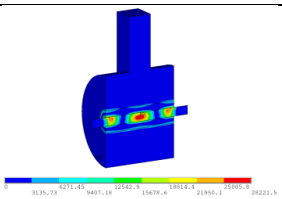	37.8	32.7

40.9	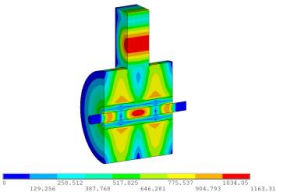	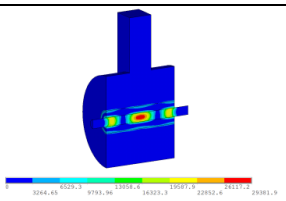	37.5	32.7
41.0	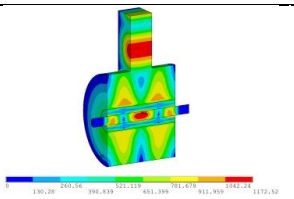	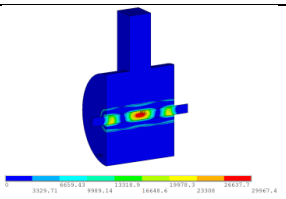	37.0	32.6
44.0	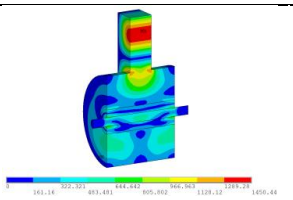	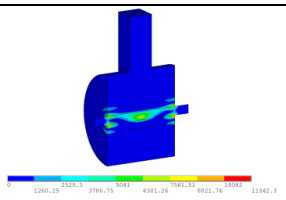	8.5	10.8
48	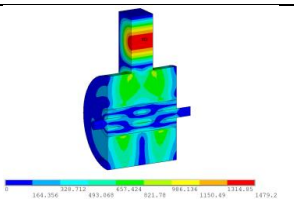	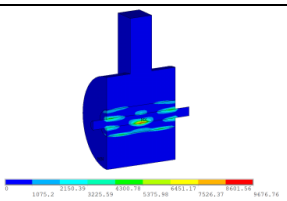	3.6	9.6
56	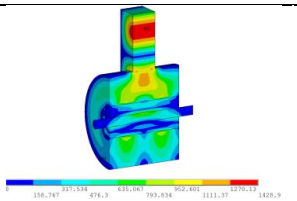	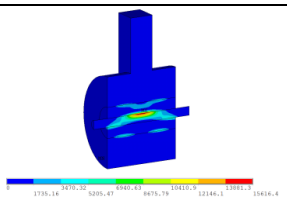	10.1	18.0
64	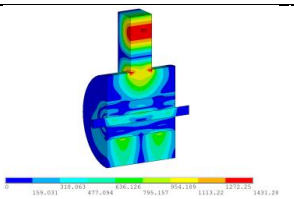	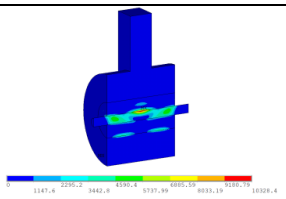	8.6	15.7

Appendix 2

Electric and absorbed energy fields for quartz glass die

Diameter of ceramic die *D*cer, mm	Electric field *E*, V/m	Absorbed energy field *Q*, W/m^3	Energy absorbed in composite %	Energy absorbed in die %
40.9	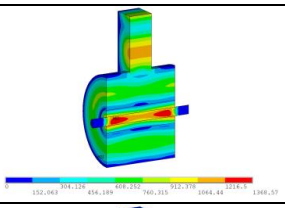	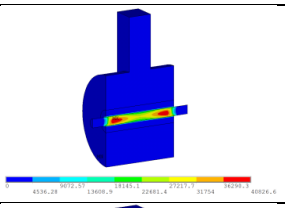	75.5	0.03
33.8	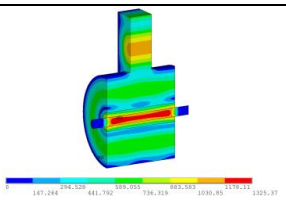	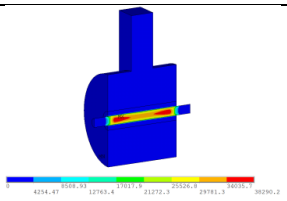	77.2	0.03

Appendix 3

Electric and absorbed energy fields for boron nitride die

Diameter of ceramic die *D*cer, mm	Electric field *E*, V/m	Absorbed energy field *Q*, W/m^3	Energy absorbed in composite %	Energy absorbed in die %
40.9	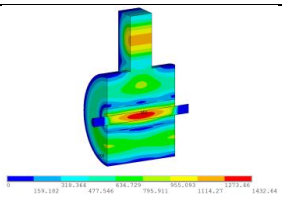	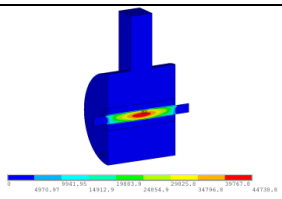	70.6	0.03
29.6	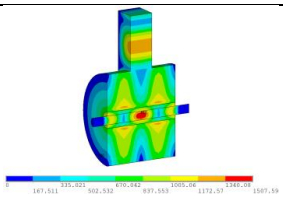	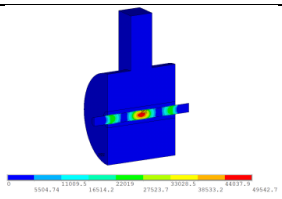	51.8	0.03
60.8	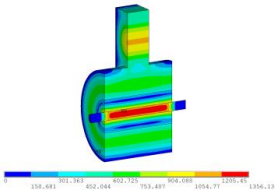	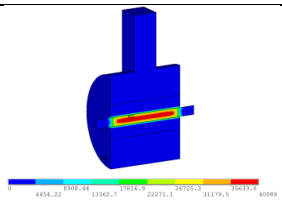	83.7	0.04

Appendix 4

Thermal material properties

Property	Symbol (unit)	Polres 305BV	4800 tex	Composite (lumped)	Air	Zirconium dioxide	Quartz glass	Boron nitride	Steel (die)
Density	ρ (kg/m^3)	1100	2500	1870	1.16	6000	2230	2100	7850
Specific heat	C (J/(kg·K))	1360	1235	1268	1005	418	670	960	460
Thermal conductivity	k_x (W/(m·K))	0.209	11	0.75	0.0267	2	1.4	35	33
Thermal conductivity	k_y (W/(m·K))	0.209	1	0.50	0.0267	2	1.4	35	33

Appendix 5

Different fields intensity for some time steps

Time, min	Temperature T, °C	Degree of cure α	Electric field E_{el}, V/m	Absorbed energy field E_{abs}, W/m^3
0	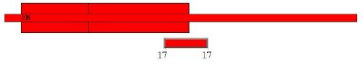	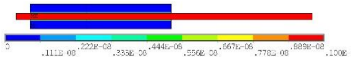	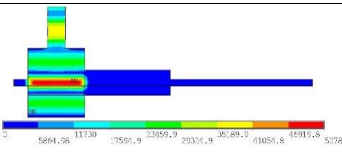	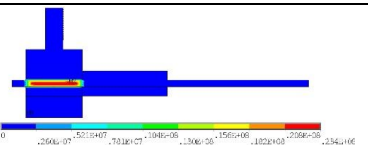
0.07 (4s)	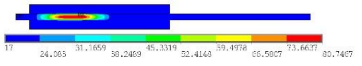	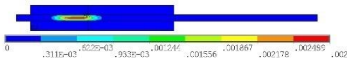	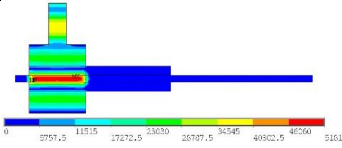	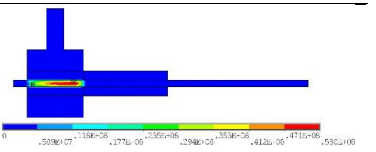
0.17 (10s)	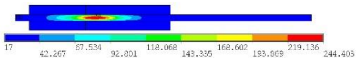	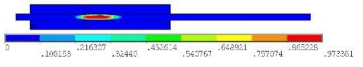	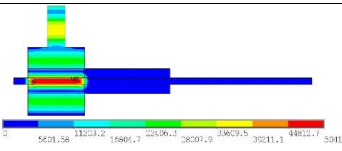	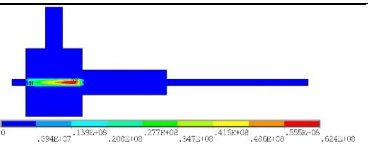
0.5 (30s)	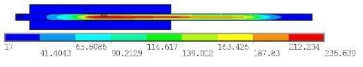	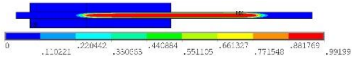	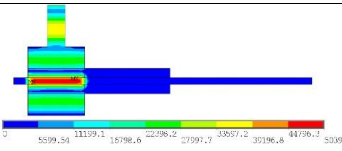	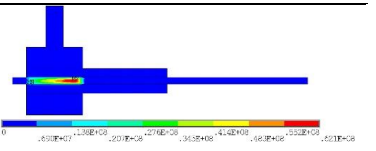

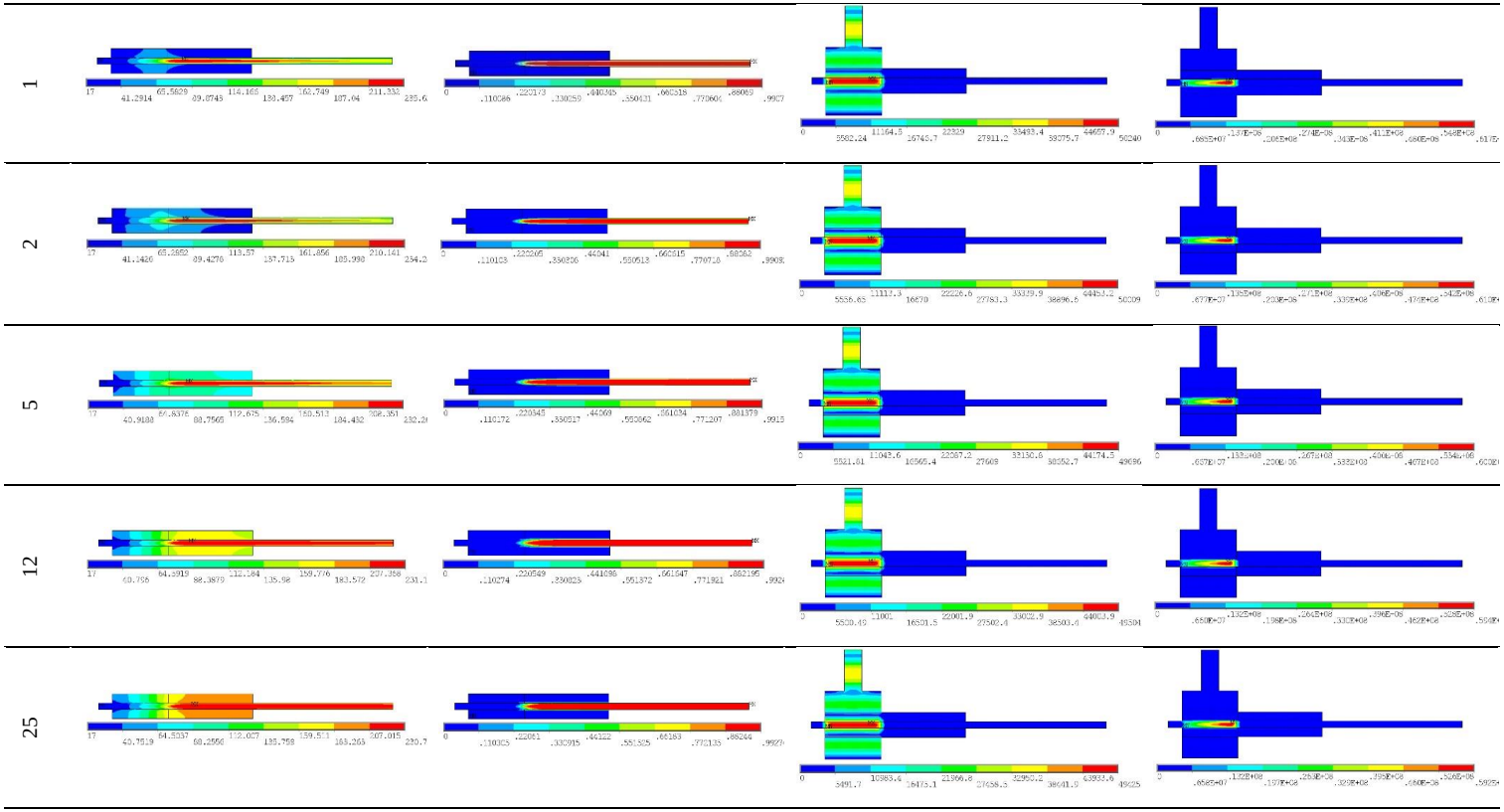
1
2
5
12
25

Results of thermo-chemical analysis for the die made of zirconium dioxide

	T_{room} = 17 °C, V_{pull} = 100 cm/min, P_{MW} = 2.24 kW		T_{room} = 17 °C, V_{pull} = 100 cm/min, P_{MW} = 1.5 kW
	Without dielectric losses in ceramic die	With electric losses in ceramic die	With electric losses in ceramic die
Temperature distribution, °C	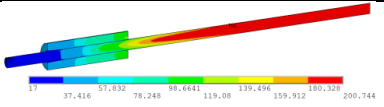	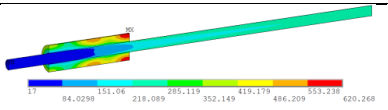	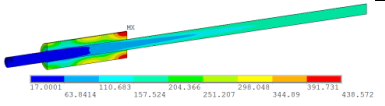
Temperature distribution in composite profile, °C	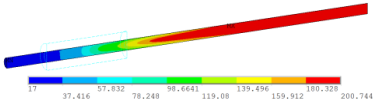	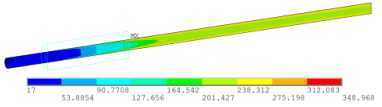	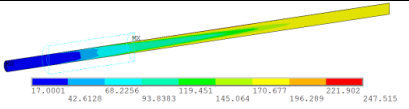
Degree of cure in composite profile	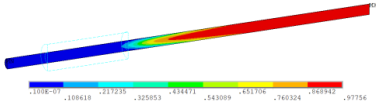	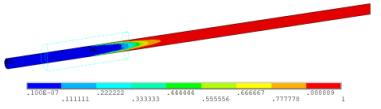	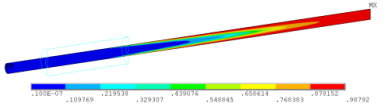
Degree of cure in composite profile at die exit	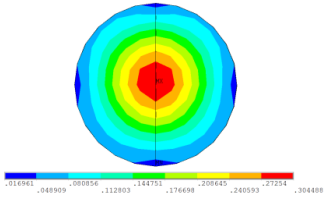	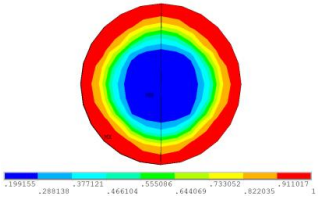	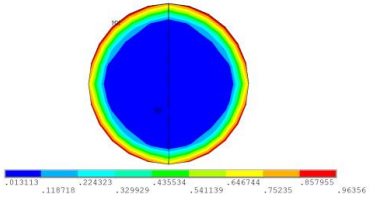

Degree of cure in composite profile at distance of 0.414 m behind die exit	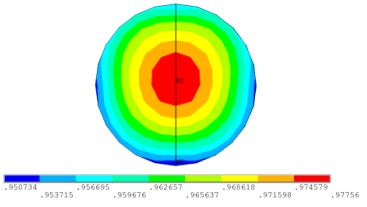	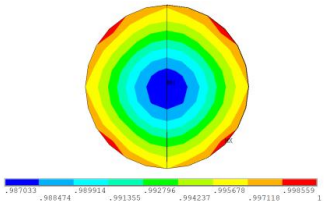	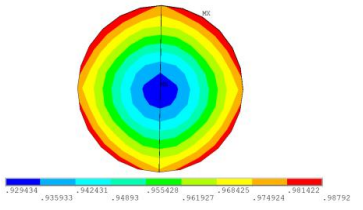
Distribution of temperature along profile	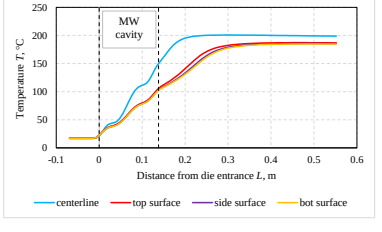	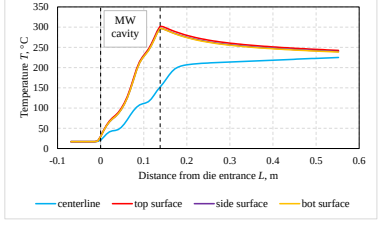	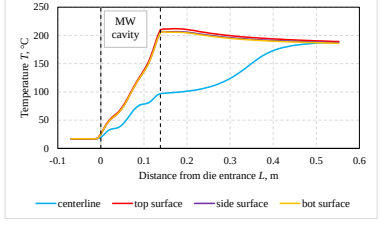
Distribution of degree of cure along profile	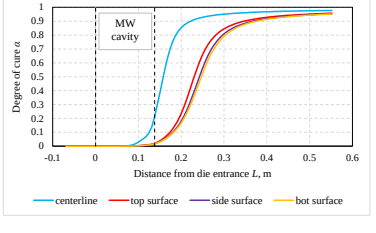	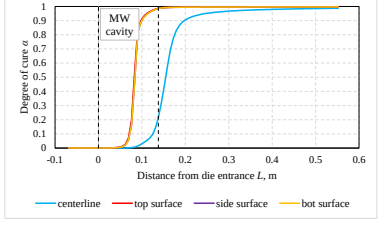	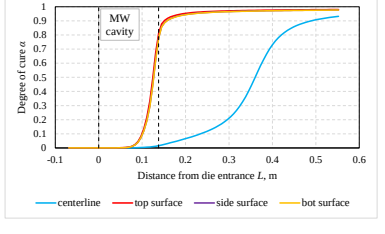

Appendix 7

Results of thermo-chemical analysis

Process parameters	V_{pull} = 100 cm/min, P_{MW} = 6 kW, T_{room} = 17 °C
FE model	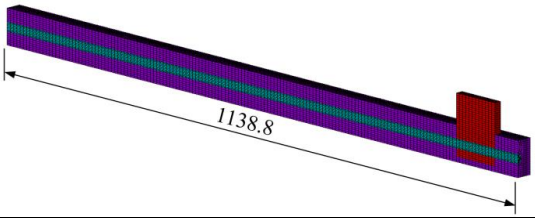
Temperature distribution, °C	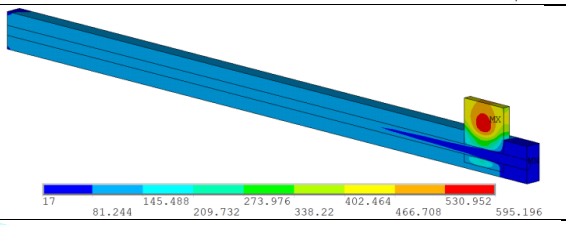
Temperature distribution in composite profile, °C	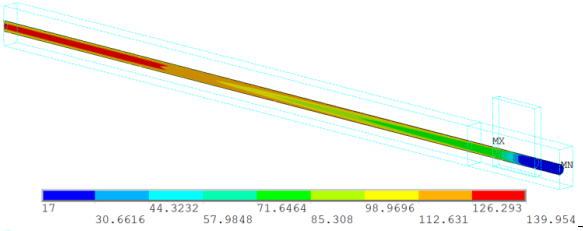
Degree of cure in composite profile	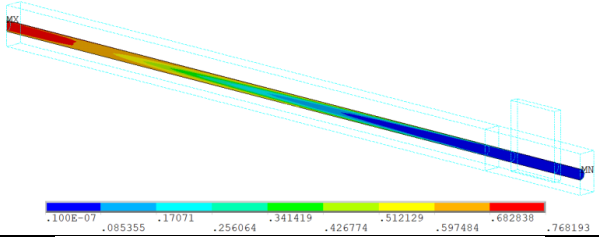
Degree of cure in composite profile at die exit	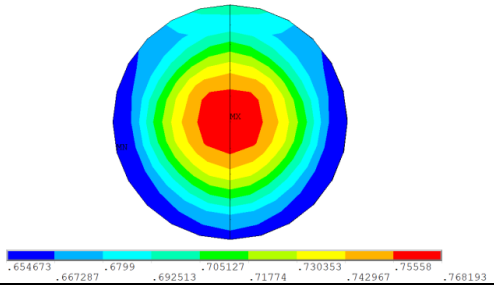

Distribution of temperature along profile	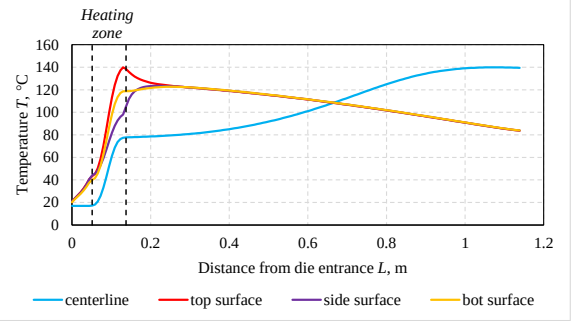
Distribution of degree of cure along profile	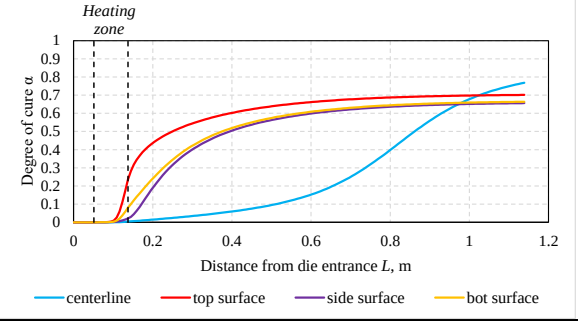

Appendix 8

Results of thermo-chemical analysis for a shorter steel die

Process parameters	V_{pull} = 100 cm/min, P_{MW} = 6 kW, T_{room} = 17 °C	V_{pull} = 59 cm/min, P_{MW} = 5.29 kW, T_{room} = 17 °C
FE model	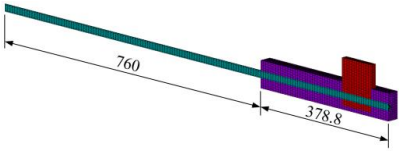	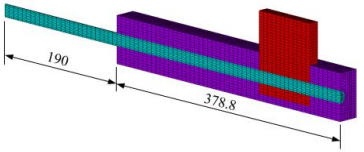
Temperature distribution, °C	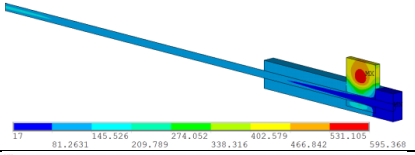	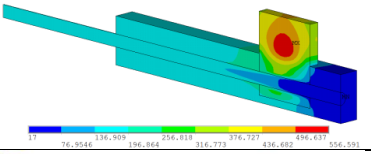
Temperature distribution in composite profile, °C	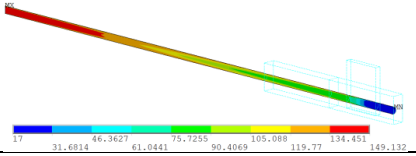	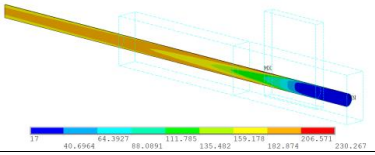
Degree of cure in composite profile	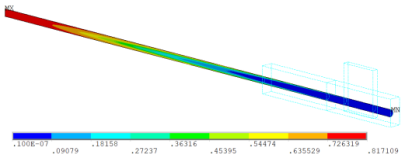	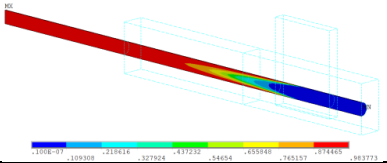

Degree of cure in composite at die exit	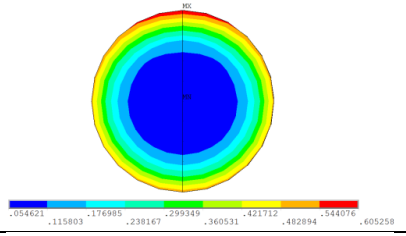	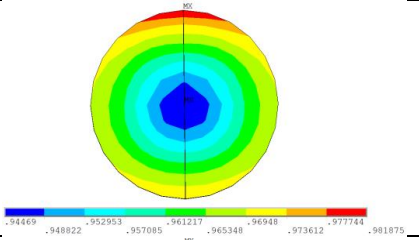
Degree of cure in composite in last modelled cross-section	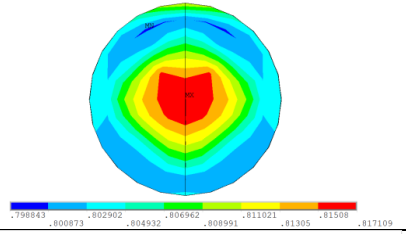	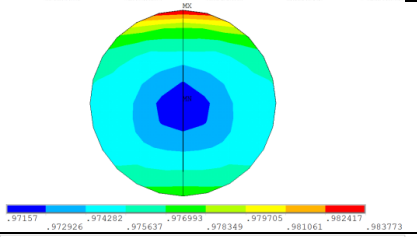
Distribution of temperature along profile	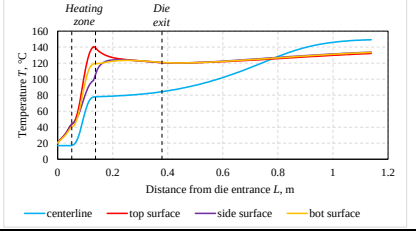	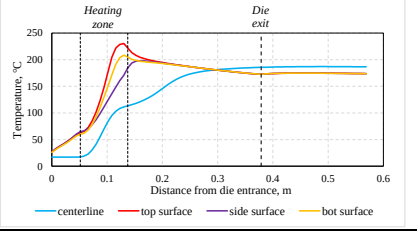

Distribution of degree of cure along profile	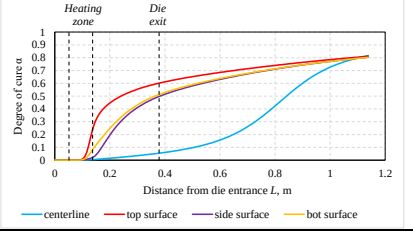	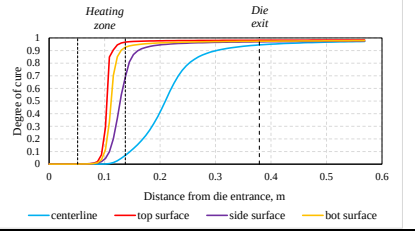

Results of thermo-chemical analysis with the modified ceramic block

Process parameters	V_{pull} = 100 cm/min, T_{room} = 17 °C	
	P_{MW} = 1.0 kW	P_{MW} = 0.85 kW
FE model	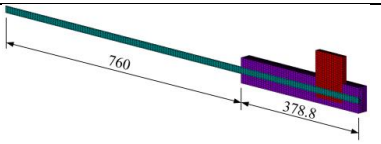	
Temperature distribution, °C	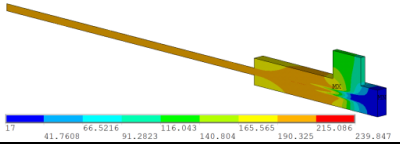	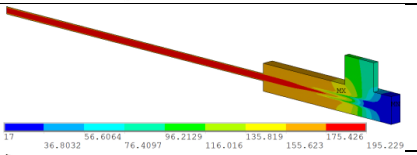
Temperature distribution in composite profile, °C	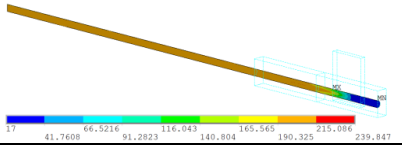	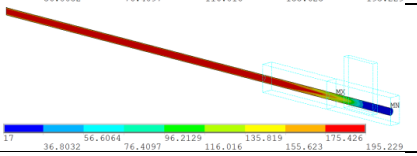
Degree of cure in composite profile	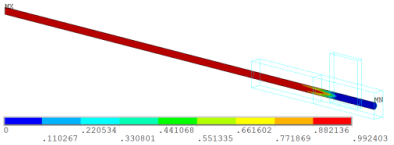	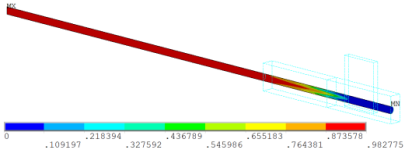

Degree of cure in composite profile at die exit	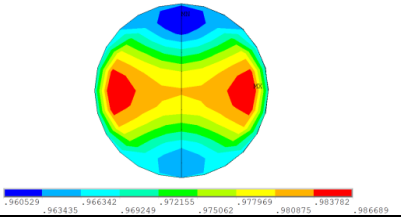	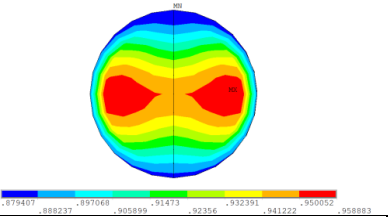
Degree of cure in composite profile at distance of 0.76 m behind die exit	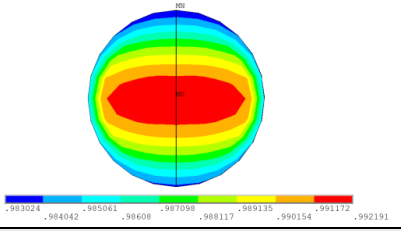	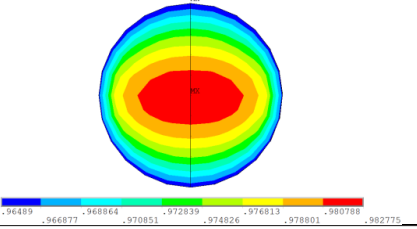
Distribution of temperature along profile	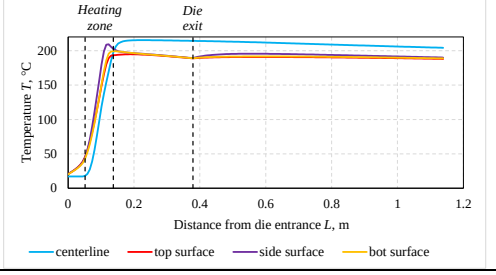	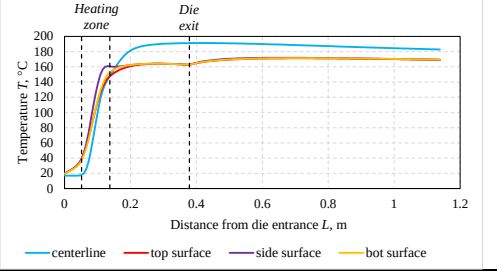

Distribution of degree of cure along profile	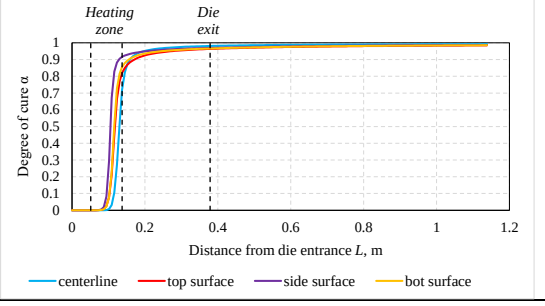	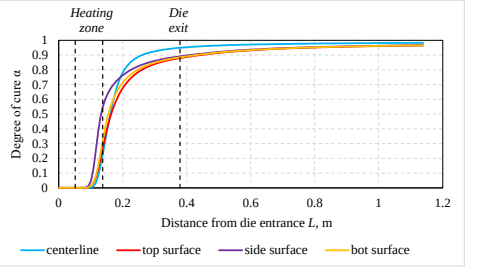

Appendix 10

Results of electromagnetic and thermo-chemical analyses with temperature-dependent dielectric material properties

Process parameters	V_{pull} = 100 cm/min, T_{room} = 17 °C	
	P_{MW} = 0.85 kW	P_{MW} = 0.55 kW
FE model	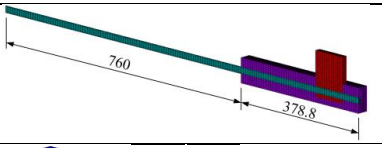	
Electric field, $E_{el,}$ V/m	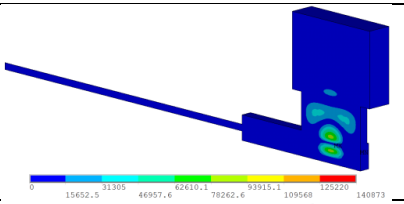	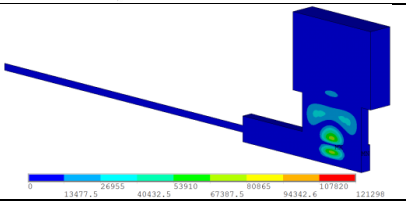
Absorbed energy field, E_{abs}, W/m^3	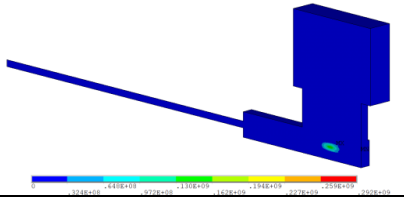	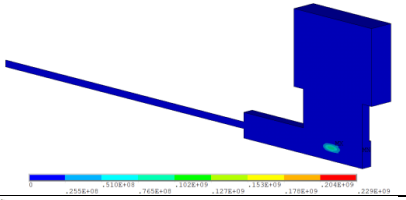
Temperature distribution, °C	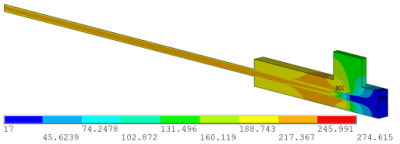	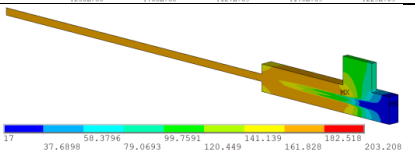

Temperature distribution in composite profile, °C	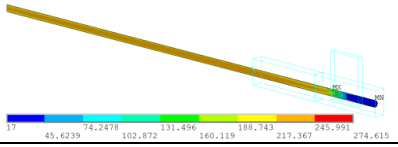	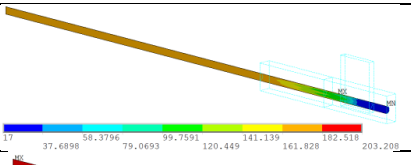
Degree of cure in composite profile	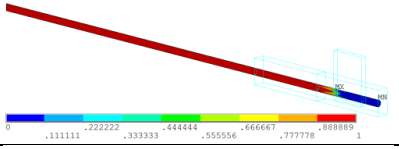	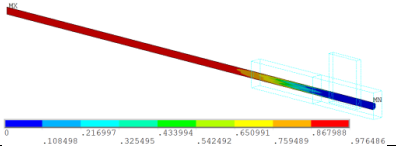
Degree of cure in composite profile at die exit	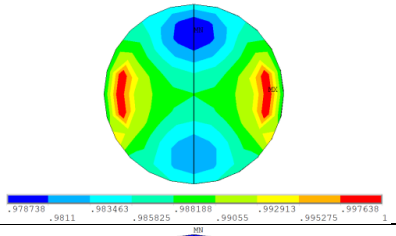	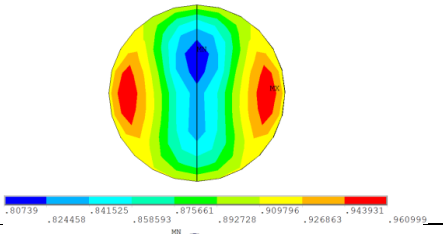
Degree of cure in composite profile at distance of 0.76 m behind die exit	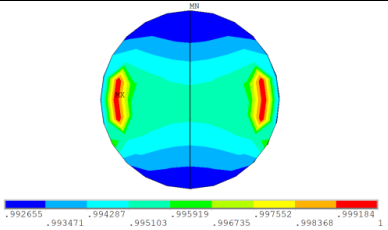	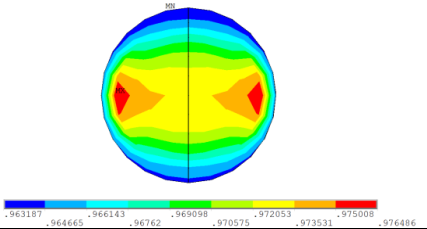

Distribution of temperature along profile	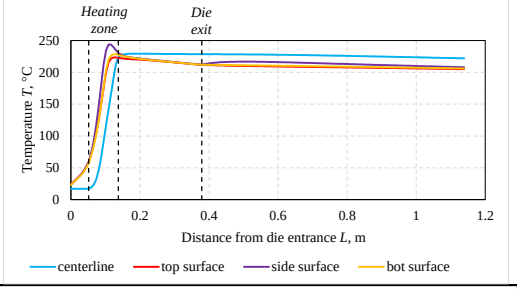	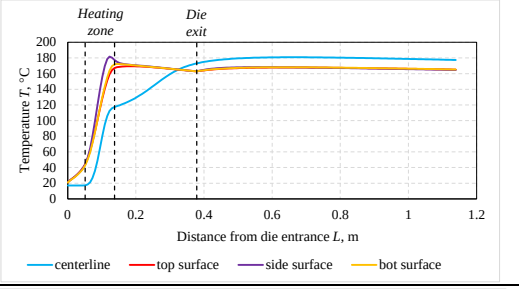
Distribution of degree of cure along profile	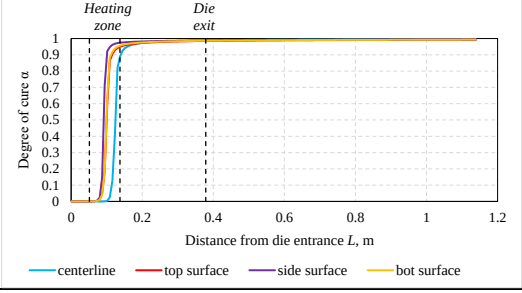	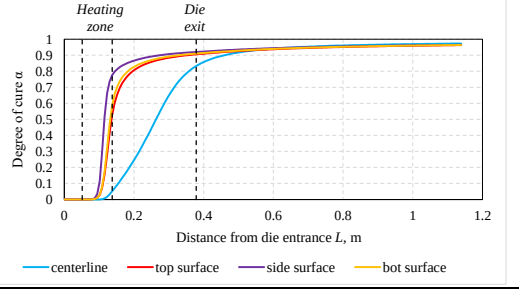

REFERENCES

[1] Safanov A.A., Carlone P., Akhatov I. Mathematical simulation of pultrusion processes: A review, Composite Structures, vol.184, pp. 153-177, 2018.

[2] Howald A.M. Meyer L.S. Shaft for Fishing Rods. US patent US2571717 A, 1951.

[3] Goldsworthy W.B. Apparatus for producing elongated articles from fiber-reinforced plastic material. US patent US2871911 A, 1959.

[4] http://fiberprofil.com/en/pultrusion/que-es/ 15 March 2023.

[5] https://www.oceanfrp.com/frp-profile/ 10 March 2023.

[6] Witten E. The Market for Glass Fibre Reinforced Plastics 2019: Market Developments, Trends, Challenges and Opportunities, 2019.

[7] Barkanov E., Ozoliņš O., Eglītis E., Almeida F., Bowering M. C. and Watson G. Optimal Design of Composite Lateral Wing Upper Covers. Part I: Linear Buckling Analysis, Aerosp. Sci. Technol. 38, pp. 1-8, 2014.

[8] Barkanov E., Eglītis E., Almeida F., Bowering M. C. and Watson G. Optimal Design of Lateral Wing Upper Covers. Part II: Nonlinear Buckling Analysis, Aerosp. Sci. Technol. 51, pp. 87-95, 2015.

[9] Barkanov E., Eglītis E., Almeida F., Bowering M. C. and Watson G. Weight Optimal Design of Lateral Wing Upper Covers Made of Composite Materials, Eng. Optimiz. 48, pp.1618-1637, 2016.

[10] Masarati P., Morandini M., Riemenschneider J., Wierach P., Gluhih S. and Barkanov E. Optimal Design of an Active Twist 1:2.5 Scale Rotor Blade. In: Proceeding of the 31st European Rotorcraft Forum (ERF: Firenze, Italy), 37.1-37.14, 2005.

[11] Barkanov E., Kovalov A., Wierach P. and Riemenschneider R. Optimised Comparative Analysis of an Active Twist for Helicopter Rotor Blades with C and D-Spar Designs, Mech. Compos. Mater. 5 (54), pp. 553-566, 2018.

[12] https://compor.eu/ 15 March 2023.

[13] EN 13706: Reinforced Plastic Composites – Specifications for Pultruded Profiles. Part 1: Designation; Part 2: Methods of Test and General Requirements; Part 3: Specific Requirements, European Committee for Standardization, Brussels, Belgium, 2002.

[14] Starr T.F. Pultrusion for Engineers. Cambridge: Woodhead Publishing, 2000, 303 p.

[15] Han C. D. and Lee D. S. Development of a Mathematical Model for the Pultrusion Process. Polymer Engineering and Science. 26, pp. 393-404, 1986.

[16] Joshi S. C. and Lam Y. C. Integrated Approach for Modeling Cure and Crystallization Kinetics of Different Polymers in 3D Pultrusion Simulation. J. Journal of Materials Processing Technology. 174, pp. 178-182, 2006.

[17] Carlone P., Palazzo G. S. and Pasquino R. Pultrusion Manufacturing Process Development by Computational Modeling and Methods. Mathematical and Computer Modelling. 44, pp. 701-709, 2006.

[18] Valliappan M., Roux J. A., Vaughan J. G. and Arafat E. S. Die and Post-die Temprature and Cure in Graphite/Epoxy Composites. Composites B. 27, pp. 1–9, 1996.

[19] Suranto B. R., Ye L. and Mai Y. W. Simulation of Temperature and Curing Profiles in Pultruded Composite Rods. Composites Science and Technology. 58, pp. 191–197, 1998.

[20] Liu X. L., Crouch I. G. and Lam Y. C. Simulation of Heat Transfer and Cure in Pultrusion with a General-purpose Finite Element Package. Composites Science and Technology. 60, pp. 857–864 , 2000.

[21] Chachad Y. R., Roux J. A. and Vaughan J. G. Three-dimensional Characterization of Pultruded Fiberglass-epoxy Composite Materials. Journal of Reinforced Plastics and Composites. 14, pp. 495–512, 1995.

[22] Liu X. L. Numerical Modelling on Pultrusion of Composite I Beam. Composites A. 32, pp. 663 – 681, 2001.

[23] Batch G. L. and Macosko C. W. A Computer Analysis of Temperature and Pressure Distribution in a Pultrusion Die. Proceedings of the 42nd Annual Conference and Expo (New York: The Composite Institute of the Society of the Plastics Industry), p. 12, 1987.

[24] Sharma D., McCarty T. A., Roux J. A. and Vaughan J. G. Investigation of Dynamic Pressure Behavior in a Pultrusion Die Journal of Composite Materials. 32, pp. 929–950, 1998.

[25] Carlone P., Palazzo G. S. and Pasquino R. Pultrusion Manufacturing Process Development: Cure Optimization by Hybrid Computational Methods. Computers and Mathematics with Applications, 53, pp. 1464-1471, 2007.

[26] Chen C. H. and Wang W. S. The Development of Glass Fiber Reinforced Polystyrene for Pultrusion. II: Effect of Processing Parameters for Optimizing the Process. Polymer Composites. 19/4, pp. 423-430, 1998.

[27] Coelho R. M. L. and Calado V. M. A. An Optimization Procedure for the Pultrusion Process Based on a Finite Element Formulation. Polymer Composites, 23/3, pp. 329-341, 2002.

[28] Chachad Y.R., Roux J.A., Vaughan J.G. and Arafat E.S., Thermal Model for Three-Dimensional Irregular Shaped Pultruded Fiberglass Composites, Journal of Composite Materials, 6 (30), pp. 692-721, 1996.

[29] Baran I., Tutum C. C. and Hattel J. H., The effect of Thermal Contact Resistance on the Thermosetting Pultrusion Processes, Composites Part B: Engineering. 45, pp. 995-1000, 2013.

[30] Barkanov E., Akishin P., Miazza N. L. and Galvez S., ANSYS-Based Algorithms for a Simulation of Pultrusion Processes, Mechanics of Advanced Materials and Structures. 5 (24), pp. 377-384, 2017.

[31] Barkanov E., Akishin P., Miazza N. L., Galvez S. and Pantelelis N. Experimental Validation of Thermo-Chemical Algorithm for a Simulation of Pultrusion Processes. IOP Conf. Series: Journal of Physics: Conf. Series, 991, 012009, 2018.

[32] Akishin P., Barkanov E., Miazza N. and Galvez S. Curing Kinetic Models of Resins for Microwave Assisted Pultrusion. Key Engineering Materials, 721, pp. 92-96, 2017.

[33] Akishin P., Barkanov E. and Bondarchuk A. Finite Element Modelling and Analysis of Conventional Pultrusion Processes. IOP Conf. Series: Materials Science and Engineering, 96, 012012, 10 P, 2015.

[34] Barkanov E., Akishin P., Emmerich R. and Graf M. Numerical Simulation of Advanced Pultrusion Processes with Microwave Heating. In: Proceedings of the VII European Congress on Computational Methods in Applied Sciences and Engineering (Eds. M. Papadrakakis, V. Papadopoulos, G. Stefanou, V. Plevris), Vol. IV (Crete, Greece), pp. 7720-7738, 2016.

[35] Carlone P., Palazzo G.S., and Pasquino R. Pultrusion Manufacturing Process Development by Computational Modeling and Methods, Mathematical and Computer Modeling. 44, pp. 701-709, 2006.

[36] Baran I., Hattel J. H., Tutum C. C. Thermo-Chemical Modeling Strategies for the Pultrusion Process, Applied Composite Materials. 20, pp. 1247-1263, 2013.

[37] Carlone P., Baran I., Hattel J. H., Palazzo G. S. Computational Approaches for Modeling the Multiphysics in Pultrusion Process, Advances in Mechanical Engineering. Article ID 301875, p. 14, 2013.

[38] Chachad Y. R., Roux J. A., Vaughan J. G. and Arafat E. S. Thermal Model for Three-Dimensional Irregular Shaped Pultruded Fiberglass Composites, Journal of Composite Materials. 30/6, pp. 692-721, 1996.

[39] Ding Z., Li S., Lee L. J. Influence of Heat Transfer and Curing on the Quality of Pultruded Composites. II: Modelling and Simulation. Polymer Composites. 23(5), pp. 957-69, 2002.

[40] Khan W.A., Methven J. Determination of the Duty Cycle in Thermoset Pultrusion. In: Hinduja S and Li L, editors. Proceedings of the 36th International MATADOR Conference, London: Springer, pp. 75-78, 2010.

[41] Liu X. L. Numerical Modelling on Pultrusion of Composite I Beam. Composites: Part A, 32, pp. 663-681, 2001.

[42] Li J., Joshi S. C. and Lam Y. C. Curing Optimization for Pultruded Composite Sections. Composites Science and Technology. 62, pp. 457-467, 2022.

[43] Carlone P., Palazzo G. S. and Pasquino R. Pultrusion Manufacturing Process Development: Cure Optimization by Hybrid Computational Methods. Computers and Mathematics with Applications. 53, pp. 1464-1471, 2007.

[44] Lam Y. C., Li J. and Joshi S. C. Simultaneous Optimization of Die-heating and Pull-speed in Pultrusion of Thermosetting Composites. Polymer Composites. 24(1), pp. 199-209, 2003.

[45] Joshi S. C., Lam Y. C. and Tun U. W. Improved Cure Optimization in Pultrusion with Pre-heating and Die-cooler Temperature. Composites: Part A. 34, pp. 1151-1159, 2003.

[46] Coelho R. M. L. and Calado V. M. A. An Optimization Procedure for the Pultrusion Process Based on a Finite Element Formulation. Polymer Composites. 23(3), pp. 329-341, 2002.

[47] Santos L. S., Biscaia Jr. E. C., Pagano R. L. and Calado V. M. A. CFD-optimization Algorithm to Optimize the Energy Transport in Pultruded Polymer Composites. Brazilian Journal of Chemical Engineering. 29(3), pp. 559-566, 2012.

[48] Santos L. S., Pagano R. L., Calado V. M. A. and Biscaisa E. C. Optimization of a Pultrusion Process Using Finite Difference and Particle Swarm Algorithms. Brazilian Journal of Chemical Engineering. 32(2), pp. 543-553, 2015.

[49] Dias R. C. C., Santos L. S., Ouzia H. and Schledjewski R. Improving Degree of Cure in Pultrusion Process by Optimizing Die-temperature. Materials Today Communications. 17, pp. 362-370, 2018.

[50] Wilcox J. A. D. and Wright D. T. Towards Pultrusion Process Optimisation Using Artificial Neural Networks. Journal of Materials Processing Technology. 83, pp. 131–141, 1998.

[51] Chen X., Xie H., Chen H. and Zhang F. Optimization for CFRP Pultrusion Process Based on Genetic Algorithm-neural Network. International Journal of Material Forming, 3(2), pp. 1391-1399, 2010.

[52] Tutum C. C., Deb K. and Baran I. Constrained Efficient Global Optimization for Pultrusion Process. Materials and Manufacturing Processes. 30(4), pp. 538-551, 2015.

[53] Tutum C. C., Baran I. and Deb K. Optimum Design of Pultrusion Process via Evolutionary Multi-objective Pptimization. International Journal of Advanced Manufacturing Technology. 72, pp. 1205-1217, 2014.

[54] Joshi S. C., Lam Y C. and Zaw K. Optimization for Quality Thermosetting Composites Pultrudate Through Die Heater Layout and Power Control. In: Proceeding of the 16th International Conference on Composite Materials, Kyoto, Japan, 2007, 7 P.

[55] Silva F. J. G., Ferreira F., Ribeiro M. C. S., Castro A. C. M., Castro M. R. A., Dinis M. L. and Fiúza A. Optimising the Energy Consumption on Pultrusion Process. Composites: Part B, pp. 57, 13–20, 2014.

[56] Metaxas A. C. and Meredith R. J. Industrial Microwave Heating, IEEE Power Engineering Series 4, Peter Peregrinus Liminited, London, 1983.

[57] Sutton W. H. and Clark D. E. Microwave Processing of Materials. Annual Review of Materials Science. 26, pp. 299-331, 1996.

[58] Thostenson E. T. and Chou T. W. Microwave and Conventional Curing of Thick-section Thermoset Composite Laminates: Experiment and Simulation. Polymer Composites. 22, pp. 197-212, 2001.

[59] Liu L., Yi S., Ong L. S., Chian K. S., Osivemi S., Lim S. H. and Su F. Chemothermal Modeling and Finite-element Analysis for Microwave Cure Process of Underfill in Flip-chip Packaging. IEEE Transactions on Electronics Packaging Manufacturing. 28, pp. 355-363, 2005.

[60] Li Y., Li N., Zhou J. and Cheng Q. Microwave Curing of Multidirectional Carbon Fiber Reinforced Polymer Composites. Composite Structures. 212, pp. 83-93, 2019.

[61] Emmerich R., Graf M., Wendel R. and Reichmann M. Microwave-assisted Pultrusion Process (MAP). 4 pp.

[62] https://www.markommicrowaves.com/wpcontent/uploads/2020/04/Microwave-pultrusion.pdf 20 March 2023.

[63] Lin M., Hawley M. C. Preliminary tests of the Application of Continuous Microwave Technique to Pultrusion in: Proceedings of the 38th International SAMPE Symposium and Exhibition, Anaheim, USA, 1993.

[64] Smith A. C. and McMillan A. M. Microwave Pultrusion of Graphite/Epoxy Composites Using Single Frequency and Variable Frequency Processing Techniques, in: Proceedings of the 30th International SAMPE Technical Conference, San Antonio, USA, 1998.

[65] Methyen J. M., Ghaffariyan S. R. and Abidin A. Z. Manufacture of Fiber-Reinforced Composites by Microwave Assisted Pultrusion, Polymer Composites. 21, pp. 586-594, 2000.

[66] Liang G., Garg A. and Chandrashekhara K. Cure Characterization of Pultruded Soy-Based Composites, Journal of Reinforced Plastics and Composites. 24/14, pp. 1509-1520, 2005.

[67] Liu X. L. and Hillier W. Transfer and Cure Analysis for the Pultrusion of a Fiberglass-Vinyl Ester I Beam, Composite Structures. 47, pp. 581-588, 1999.

[68] Roux J. A., Vaughan J. G., Shanku R., Arafat E. S., Bruce J. L. and Johnson V. R. Comparison of Measurements and Modeling for Pultrusion of a Fiberglass/Epoxy I-Beam, Journal of Reinforced Plastics and Composites. 17/7, pp. 1557-1579, 1998.

[69] Carlone P. and Palazzo G. S. Numerical Modelling of the Microwave Assisted Pultrusion Process. International Journal of Material Form. 1, pp. 1323-1326, 2008.

[70] Kayser T., Link G., Seitz T., Nuss V., Dittrich J., Jelonnek J., Heidbrink F. and Ghomeshi R. An Applicator for Microwave Assisted Pultrusion of Carbon Fiber Reinforced Plastic, in: IEEE MTT-S International Microwave Symposium, pp. 1-4, 2014.

[71] Shannon C. E. Communication in the Presence of Noise. Proceedings of the Institute of Radio Engineers, 37 (1), pp. 10-21, 1949.

[72] COMSOL Multiphysics reference manual, Version: COMSOL 5.5, 2019.

[73] Bogetti T. A. and Gillespie J. W. Process-Induced Stress and Deformations in Thick-Section Thermoset Composite Laminates. Journal of Composite Materials, 26 (5), pp. 626-660, 1992.
[74] Namsone E., Arshanitsa A. and Morozovs A. Analysis of Curing Kinetic Models for Polyester Resin C-L ISO 112 G. Key Engineering Materials, 850, pp. 70-75, 2020.
[75] Barkanov E., Akishin P., Namsone E., Bondarchuk A. and Pantelelis N. In-Line Characterization of Pultruded Profiles. Book of Abstracts of the International Conference on Structural Analysis of Advanced Materials, Ichia, Italy, 14, pp. 12-15, September 2019.
[76] Barkanov E., Akishin P., Namsone E., Bondarchuk A. and Pantelelis N. Real-time Characterization of Pultrusion Processes with a Temperature Control. Mechanics of Composite Materials, 56, pp. 135-148, 2020.
[77] Wu C.F. J. and Hamada M. Experiments: Planning, Analysis and Parameters Design Optimisation. John Wiley & Sons, Inc., New York, 2000.
[78] Myers R. H. and Montgomery D. C. Response Surface Methodology: Process and Product Optimisation Using Designed Experiments. John Wiley & Sons, Inc. New York, 2002.
[79] Barkanov E. Optimal Design of Laser-Welded Sandwich Modules. Schiffbauforschung, 45 (1), pp. 21-33, 2006.
[80] Barkanov E., Eglītis E., Almeida F., Bowering M. C. and Watson G. Weight Optimal Design of Lateral Wing Upper Covers Made of Composite Materials. Engineering Optimization, 48(9), pp. 1618-1637, 2016.
[81] Barkanov E., Kovalov A., Wierach P. and Riemenschneider J. Optimised Comparative Analysis of an Active Twist for Helicopter Rotor Blades with C and D-Spar Designs. Mechanics of Composite Materials, 54(5), pp.553-566, 2018.
[82] Baran I., Tutum C.C., Nielsen M. W. and Jattel J. H. Process Induced Residual Stresses and Distortions in Pultrusion. Composites: Part B, 51, pp. 148-161, 2013.

Endija Namsone-Sīle was born in 1993 in Dobele. She received a Professional Bachelor`s degree and an engineering qualification in Transportation Engineering in 2017 and a Professional Master`s degree in Transportation Engineering in 2018 from Riga Technical University (RTU). From 2019 to 2022, she has been a scientific assistant at RTU, the Institute of Materials and Structures and in the ERDF scientific project "An effectiveness improvement of conventional pultrusion processes". In 2015, she received an outstanding scholarship from "Latvijas Valsts meži". In 2018, she received the Gunta Bole Award for excellent results in studies in the construction speciality. Endija has been twice included in the Golden Alumni Fund of RTU (in 2016/2017 and 2017/2018) and is currently a Transportation Engineer in the Dobele Municipality.